Federal State Autonomous Educational Institution of Higher Education
«Ural Federal University named after the first President of Russia B.N. Yeltsin»

Ural Power Engineering Institute

Department of Automated Electrical Systems

As a manuscript

Mahmoud Mahrous Amery Aref

MODELING OF RENEWABLE ENERGY SOURCES FOR CALCULATION SHORT CURRENT CURRENTS OF LOCAL DISTRIBUTION SYSTEMS OF EGYPT

Specialty 05.14.02 – Electric Power Plants and Systems

Dissertation for the degree of candidate of Electrical Engineering science

Supervisor

Doctor of technical science

Professor V.P. Oboskalov

Yekaterinburg - 2020

List of Contents

ABSTRACT

This thesis presents modeling of DGs (wind, PV, ….etc.) for isolated and grid-connected. The steady state analysis of a grid connected PMSG wind turbine in fixed and variable speed is investigated. The case studied is Zafarana, Egypt. The average values of wind speed of month and day of Zafarana region is obtained from NASA site. Zafarana region has the highest wind speed which is greater than 12 m/sec. The transient analysis is investigated of the grid connected PMSG wind turbine during three-phase-to-ground fault at terminal of grid in different fault time and islanding mode. PMSG wind turbine is based on low-voltage ride-through (LVRT). LVRT is used to protect wind turbine from high fault current as well as to compensate PMSG voltage. PMSG is loaded by converter and capacitor which work as STATCOM. The current protection device is used to limit the fault current where the tripping current of relay is calculated using IEC method. PMSG wind turbine consists of three protection devices, over speed protection, LVRT and point connection circuit breaker. There are three protection zones in terms of the fault of; the protection zone of the fault of wind turbine, the protection zone of the fault of wind farm, the protection zone of the fault of grid.

MPPT of PV system controlled by SPWM which is generated by comparing sinusoidal wave with variable frequency sawtooth wave is investigated. Perturb and Observe (P&O) method is used for MPPT control of PV system. NPC three-phase three-level converter with LCL filter is designed to produce output voltage with minimum Total Harmonic Distortion (THD) and high efficiency. A simple and fast method has been proposed to obtain the maximum power point of PV system with variable irradiation values. This method is based on the use of look-up table employed with microcontroller Arduino Nano. The digital control signal of optimum voltage value from look-up table contributes in obtaining the maximum power from irradiation.

Due to the widespread use of microgrids (MGs), it presents a new challenge problem for MGs to assess supporting electric power network stability. A comparison between transient analysis grid-connected AC and DC Microgrid in case of using Superconducting Fault current limiter (SFCL) at the connection point of Microgrid and grid is investigated. When the three-phase-to-ground fault is applied at connection point of Microgrid and grid, the SFCL minimized the oscillating currents and the active and reactive power of AC and DC microgrid to range 20-30%. The transient analysis of AC microgrid is better than DC microgrid except the values currents and the active and reactive power are very high during the fault.

Fault currents calculations inside a grid-connected and isolated AC microgrid is one of a major challenge due to fault current contributions of inverter-based distributed generators units, which are different according to units' locations and inverter control during the fault. Therefore, the fault current for grid-connected and isolated microgrids is calculated using two methods; virtual impedance and the proposed method. The proposed method is used to calculate the short circuit current contribution of DG under analyze the equivalent model of inverter-based DG. The inverter control limits its current to 2 p.u of the inverter rating. In addition, the static security risk and load shedding are calculated during the fault in different fault locations using operation scenario in which the distribution system will divide into small subsystems, grid-connected and isolated due to remove the faulted bus by the protection devices reaction of the distribution system. The proposed algorithm has been tested on a standard IEEE 33-bus distribution network with 5 DGs using MATLAB code programs. The results show that the impact of DG on the fault current is significant especially when the fault occurs at busses near to the DG location. The calculated fault current value using the proposed method is less than its calculated value using the virtual impedance method by more than 30% for grid-connected microgrid and by

approximately 50% for the isolated microgrid. The load failure and load-shedding need to improve the value of static security risk. After load-shedding, the static security risk decreased its value to about 0.025 %.

Introduction

The relevance of the topic. Clean and renewable electricity generation is main target of the world using different sources while wind energy conversion has been rapidly deployed worldwide. Although the availability of well-designed wind turbines could reach as high as 98% with assistance of fast field service and the cost of maintenance is high. Most wind turbines are operated in variable speed conditions due to the varying wind speeds, and fail more often than other rotating machines [1]. The permanent magnet synchronous generator (PMSG) is used in wind energy applications because it is simple winding structure, ease of control, and the ease of realization of multi-pole machines for low-speed applications [2]. Technical problems (like frequency variations, voltage fluctuations, short circuit current contribution, overall system stability, necessary updating required for power system, power quality…) are expected to accompany high level penetration of wind energy [3-4].

Grid codes are described by the relation between voltage and time to obtain smallest time to be connected during the disturbance of the system. The low-voltage ride-through (LVRT) is used to keep wind turbine PMSG connected and contributed to the grid as well as to improve the voltage profile during low-voltage transients in case of a disturbance such as a voltage dip as low as 15 % retained voltage. The PMSG wind turbine supplies reactive power to help the grid voltage to recover from the voltage dip. Several solutions have been investigated for the LVRT requirements in PMSG wind power systems. Direct-drive wind power system with permanent magnet synchronous generator (PMSG) has lots of advantages over traditional wind systems where its LVRT technology has been paid more and more attention. Fig. 1 shows the LVRT requirements of Germany (E.ON), Great Britain, and Denmark.

Egypt with its large coastal strip, cloudless sky almost year-round and small fossil fuel reserves, to the maximum extent satisfies the conditions for the development of distributed generation (DG) on renewable energy sources. Here, renewable resources make it possible to produce electricity not only individually, but also centrally, with high economic efficiency at power plants (farms) with generating units, of sufficiently large unit capacity. The amount of solar energy incidence per square meter varies between 5 and 8 kWh per day and 2300 kWh/m^2 per year (for 3000-4000 hours per year). The wind speed on the Red Sea coast exceeds 10 m/s with an energy of 400-800 W/m^2 at an altitude of 40 m above ground level. A Zafarana is the one place in Egypt, which has high-speed wind. Zafarana wind farm is the biggest project in Africa and Middle East, which was beginning in 2001 to 2010 by the cooperation protocols between Egypt and other countries (Germany, Denmark, Spain and Japan). The total installed power of this wind farm is 425 MW connected to electric power system. The construction of this wind farm has been realized in few steps (60, 80, 85, 80, 120 MW). Large wind speed value (average 10 m/s at 40 m above ground level) is main advantage of Zafarana location. Table. 1 shows various kinds of wind turbines used in Zafarana wind farm [5].

The motivation of this investigation is that there are around 167000 residents in Egypt according to New and Renewable Energy Authority (NREA) are experiencing need or totally denied from electricity. Such households are distributed around 264 isolated villages in nine towns along Egypt. Among these villages, 211 villages are completely isolated from electricity and the remaining are fed through standalone diesel stations. The vast majority of these isolated villages are situated in desert areas, where rich measure of solar energy and in some places wind energy exists moreover. In Egypt, numerous new projects are being carried out in various areas, for example those in the new valley in the western desert of Egypt and those in the northern coast of Egypt. Worth to

mention that over the past four year, Egypt's electricity sector has confronted it’s most noticeably crisis in production lagging behind consumption resulting in extended periods of rolling blackouts that reaches two to four hours daily in urban areas and sometimes double those in rural areas. The increasing population and increasing comfort demand of households is presenting severe load on the network. One option to handle the electricity crises and diminishing the load on the network is the utilization of both on-grid and off-grid of PV systems. The first integration of renewable sources of energy was in 2011 from the solar thermal part of the power station built in Kuraymat in the south of Egypt with a portion of 20 MW from a total capacity of 140 MW. A 10 MW solar photovoltaic plant has entered service in 2015 in the Siwa Oasis in Western Sahara. Nowadays, Egyptian electricity holding company is planning to find the administrative steps to complete the agreements, which control the process of purchase of the generated energy from the private sector’s projects. The project has a total of capacity of 1000 MW distributed as follow: a wind farm in Suez Golf with an installed capacity of 250 MW, a 200 MW photovoltaic power plant in Aswan (Komombo), and a project in the west of Nile River with a total installed capacity of 550 MW from different renewable sources.

Table. 1. ─ Different types of installed wind turbine

Wind Turbine	Speed	Generator	Power Control	No. of Turbine
Nordex 600kW	11	SEIG	Active Stall	105
ESTAS 660kW	15	SEIG	Opti Slip/Pitch	117
GAMESA 850kW	15	DFIG	Pitch	336

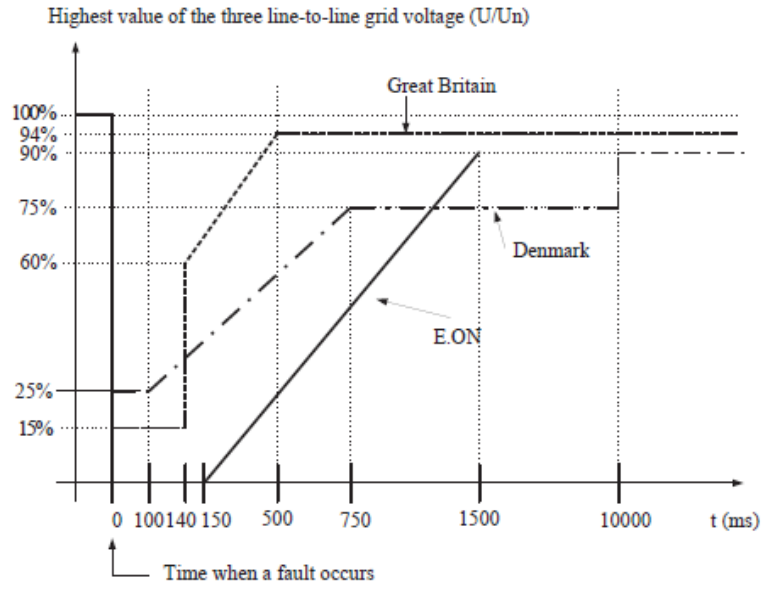

Fig. 1. ─ Limit curves for the voltage generator disconnection

The installation rate of photovoltaic (PV) generated energy into the grid system was increased in worldwide. This increased penetration level offers unique challenges to systems operators. Improving reliability so as to reduce replacement cost during the life of PV array is one of significant challenges [6]. Usually PV plant consists of 3 main parts: large amount of PV units which are combined together to feed inverters. The inverters then are connected to low frequency transformer (medium voltage electric grid) [7].

Converters are main part in PV system to connect with AC loads or electric grid [8]. Nowadays, multilevel converters are widely used and proposed for medium and high voltage applications due to reduce switching losses, low harmonic distortion, high voltage capability and good dynamic response [9]. In general there are six main common multilevel converter topologies; Neutral point Clamped converter (NPC) [10], cascaded H-bridge [11], Y-connected Hybrid Cascaded [12], Capacitor Clamped [13], Z-source [14] and quasi Z-source [15]. The main circuit and control scheme of NPC three-level converter are simple with comparison the conventional two-level topology. The basic benefits of the NPC three-level inverter as follows: 1) reducing the harmonic and the switching

frequency, so that the system loss is small, 2) rising rate of voltage(dv/dt) is lower than the two-level inverter and the rise rate of current (di/dt) is also reduced, 3) reducing the torque ripple and electromagnetic noise with the increase of the number of levels, each amplitude of level will be reduced relatively, 4) reducing the size of the circuit because the voltage which is linked with the absorption circuit is only half of that, the energy flowing into the absorption circuit is small.

The main technical difficulty in any application of the NPC three-level topology is to maintain the two DC-side capacitors' voltages equal and at a pre-specified level, which is more significant for the equipment running safely and reliably. Several methods have been used to retain the capacitor voltages at a desired value; the hardware implementation method including separate DC sources, an auxiliary converter to inject a current in the neutral point is used with additional circuit which adds to the equipment the inefficiency, cost and complexity and the software method is realized by modifying the converter-switching mode according to related control algorithms based on the space vector pulse width modulation (SVPWM) or sine pulse width modulation (SPWM) strategy.

The output power of PV array is depend on irradiation which incident on the PV module surface over the time due to climatic conditions; the output power also varies producing several power-voltage curves for several irradiation levels. The maximum power output of PV array is generated by adjusting voltage or current for irradiation and temperature [16].

To increase the efficiency of PV power generation system, Maximum power point tracking (MPPT) techniques are implemented. Several methods are using to get maximum power point of PV. Perturb-and-observe (P&O) method is dominantly used in practical PV system for MPPT control due to its simple implementation. Look-up table would require large memory storage of the micro-controller as large amount of panel data is stored with high accuracy are implemented.

The converter current is included high order harmonic that flows into the grid causing harmonic pollution. Filters are used to mitigate these harmonics. The most common filter is L-filter while its inductance must be high value to decrease the current ripple. The LC-filter can mitigate these harmonics but it is expensive for medium and high power application and the operation of filter is not better because of uncertainty of grid impedance. Due to the large naturally cut-off frequency and robust powerful capability of LCL filter in low-frequency power systems, the LCL filter is commonly implemented in the inverter. The operation of three-phase inverters of PV system connected to electric network is examined the inductance, the relation of two inductances, choosing the filter capacitor and resonance resistance. The proposal form of LCL filter is having a significant role in the entire system and plays vital role for stability of the system. The designing of LCL filter is necessary to take exceptional attention where the grid impedance plays important role in influence on the performance of the system while any change of the grid impedance occurs the change of the resonance frequency of LCL filter i.e. stiffness of the grid. To mitigate high frequency current harmonics produced from switching of inverter, the electromagnetic interference filter (EMI) is used. In the PV system connected to electric network, L-filter or LC-filter is usually used. From aforementioned cases, the inductance is large value, bulky and costly. In the case of use LCL filter as an EMI filter with two different modes, inductance and differential inductance.

During the past decades, the electric power industry has undergone significant changes in response to the rising concerns of global climate change and volatile fossil fuel prices. For more efficient, reliable, and environmentally friendly energy production, it is critical to increase the deployment of distribution generation (DG). This trend has evolved into the concept of a “microgrid” which can be described as a cluster of distributed energy resources, energy storage managed by an active energy management system. Microgrid (MG) can work

whichever in grid-connected or islanding method of operation. Islanded MGs are viewed as an incredible decision for some applications when the connection to the main network is absurd or not best. For example, islanded MGs are the answer for remote networks situated far from the main grid. AC microgrids are very popular because of easy modeling, simple design and efficient performance

MGs have been significantly deployed during last few years and are anticipated to grow even more in the near future, where future power grids can be pictured as systems of interconnected MGs. The MG is a number loads and renewable energy sources connected together under electrical constraints with only manageable object depending on the grid where it can connect or disconnect from the grid.

In remote and rural area which many people use the electricity service of electric grid, MG is attractive to supply domestic loads as well as many applications like irrigation system. MG is combined distribution system containing small distributed renewables sources and loads capable of operating in islanded as well as grid connected mode [17]. MG is the practical solution to the challenges produced by high DG penetration and makes the large-scale application of DG system possible. The Point of Common Coupling (PCC) is the bus connection between MG and electric network where MG was able to import and export energy from and to the grid flexibly by regulatory of active and reactive power flow. Like all power systems, MGs are not globally stable, which presents unique control challenges. An effective technique is using static synchronous compensator (STATCOM) to increase the stability of AC MG by injection reactive power to support voltage stability. Power electronics, which are used to interface distributed generators and loads to the network, offer new opportunities for decentralized and autonomous control of power supply and demand. They draw constant power from the network to regulate their outputs [18]. The active and reactive power compensation techniques, besides a PID controller

implantation, are used to maintain the constant terminal voltage of constant power load (CPL**)** by using current injection method from the storage system to increase the stability scenario of AC MG [19]. To decrease the size and weight of major system components of AC MG, such as DGs and transformers as well as harmonic filters, High frequency AC MGs are used by multiple high speed generators connected in parallel. They can be lighter, smaller and cheaper than those operating at 50 or 60 Hz [20]. An MG stability controller with energy storage equipment is used to help MG switch operation mode steadily and flexibly and improve transients' characteristics of MG during the fault in distributed network [21].

In contrast with AC MG, the DC MG has drawn many advantages such as higher efficiency, an absence of reactive power and harmonics. The DC MG is already implemented in industrial system, data center, telecommunication system, marine power system and residential applications. DC MGs are very popular in recent time because increasing DC appliances in MGs. The control strategy is essential for addressing the disturbances to maintain DC and AC MGs voltages in grid-connected and standalone operating modes.

Superconducting fault current limiters (SFCL) is one of the applications of superconductors due to the superconducting characteristics. The working of SFCL depends on the unexpected change from the superconducting state to the regular state by surpassing the basic current I_c of the material. An electromagnetic equivalent of resistive SFCL depends on *E-J* power law. To limit the short circuit current in conventional electric power and wind farm networks, The SFCL is implemented in an electric network during the fault [22]. Various strategies for restricting short circuit current by SFCL are studied and the results showed the capability of SFCL to minimize the short circuit current in the range of 20–50% in electric power system. There are many benefits of the SFCL:

• Minimum power loss and voltage drop due to small impedance system in normal state.

• Large equivalent impedance to limit short circuit current during the fault.

• High response to change from normal to emergency operation.

The SFCL is not only used to limit short circuit current, but it is also used to increase temporary stability of generators in the electric network and subsequently the general stability of the electric power system [23].

The DG during the fault makes the equivalent circuit of grouping system not similar to the equivalent of the conventional electric network. In view of the control system and the proportional model of inverter integrated DG under fault, DG can be taken as voltage source or current source in sequence-network. To analyze fault characteristics of DGs with different control schemes and deliver elaborative comparisons among them.

Various approaches have been familiar with controlling islanded MGs. Droop control is generally utilized which is a sort of ward control by which active and reactive powers be shared among DGs. Virtual impedance is used to improve the exhibition of droop control. The adaptive virtual impedance used to improve traditional virtual impedance procedures. The estimation of virtual impedance is not consistent in the adaptive virtual impedance system and fluctuates at any moment by the method which expels impedance imbalance between various DGs. The control innovation of MG is a key to the operation of the MG. Develop control innovations can improve the adaptability of MG activity and improve control quality. The issue of fault current computation in distribution network containing inverter-based distributed generation is underlined by the fault ride-through prerequisite declared in grid codes.

The influence and the potential risk when clean the faults using the relay protection system on power supply in distribution systems are given increasingly

more consideration. The impacts of continuous faults, clean distraction, and absence of reaction of the relay protection systems are analyzed on low electrical energy fed electrical load.

A probability computation method of power source risk incidence because cleaned faults using relay protection system is a probability function of fault of the relay protection systems, the frequency of the cleaned faults happening in operation time and the drop power fed to load. The conventional power distribution grid has recently changed; expanding the portion of distributed power generation systems (DGs) makes it a functioning player in electric power production and supply. Although an expanding DGs penetration might be advantageous, power produced by those devices is influenced by high uncertainty, in this manner may increase system risk, system non-linearity, and overall complexity and propose several challenges for the future grid. Static security risk calculation is one of the important problems in the distribution network due to the influence of surprising and inevitable faults and failures, in which many types of research give more attention.

The degree of development of the research topic. There is a fairly large number of scientific publications devoted to the DG on renewable energy sources. Basically, they are published in foreign publications and are devoted to the issues of conceptual development and organization of microgrid; the design of individual units of generating devices; simulation of the work of sources of DG in normal and emergency modes; analysis of transients arising from failures in the case of parallel operation with the network or during isolated operation of the DG; stability analysis of generating devices; development of protection schemes when the network operates on direct and alternating current at various operating modes of microgrid. At the same time, there are many publications on the calculation of short circuit currents in the most famous foreign journals.

Among Russian scientists, a significant contribution to the development of control theory and the increase in the effectiveness of DGs was made by permanently acting in Ural Federal University under the guidance of Ерохина П.М., Паздерина А.В., Ерошенко С.А. и Самойленко В.О seminar "Problems of connecting and operating small generation in parallel with the electrical power system of Russia", as well as scientists: Воропай Н.И., Дьяков А.Ф, Илюшин П.В., Тарасенко, В.В., Фишов, А.Г. Среди, foreign researchers: Xiaohang Jin, Liyan Qu, J. Yang, J.E., Fletcher, Md, Michael Negnevitsky, Julia A. Belk, Konstantin Turitsyn, Jiahui Zhua, Xiaodong Zhenga, Ming Qiua, Zhipeng Zhang, Mazen Abdel-Salam, Khairy Sayed, Canbing Li, etc.

The objects of study are microgrid with a DG based on renewable energy sources; Wind turbine PMSG; PV connected to a three-phase three-level converter with neutral point; hybrid local electric power stations operating in the climate zone of Egypt, with the allocation of subsystems for AC and DC microgrid.

Purpose and goal of work. The purpose of this study is to develop a methodology and algorithm for calculating short circuit currents in local electrical systems with distributed generation on renewable energy sources.

To achieve this **goal**, the following tasks were solved:

1. Analysis of the specific properties of wind turbines with converters for their consideration in the calculation of short circuit currents.
2. Development of a mathematical model for maximum power point tracking of the PV system under conditions of grid-connected and stand-alone.
3. Testing the feasibility and necessity of using the Arduino Nano microcontroller to analyze the PV control system for short circuit in an external circuit.
4. Development of a Simulink model for modeling generating devices with converters and their control systems with the aim of identifying significant

characteristics for calculating short circuit currents; checking the need to install filters of harmonic components and a selection of their parameters; checks of all developed computational procedures.

5. Development of computational procedures for computer-based calculation of short circuit currents in microgrid with DG based on renewable energy sources.
6. Performing test calculations of short circuit currents with the aim of debugging the proposed computational procedures.
7. Analysis of the balance reliability of subsystems formed as a result of dividing microgrid when short circuits are disconnected.

Scientific novelty:

1. A methodology has been developed for taking into account the current limiting properties of renewable energy generating devices in the calculation of short-circuit currents in local electric power systems.
2. A structural mathematical model of renewable energy sources with converters and control systems for analyzing their operation in the short circuit mode is proposed.
3. A mathematical model of microgrid with distributed generation based on renewable energy sources has been developed.
4. A mathematical model has been developed for maximum power point tracking as the determining function of the PV simulator.

Theoretical and practical significance of the work. The work is fully oriented to solve the main technical problems caused by connection of renewable energy based DGs in the Egyptian energy system. This work was carried out as part of the target program for the development of the electric power industry in Egypt. The developed software procedures for calculating short circuit currents can be used in the educational process and become the basis for the development

of a software package for calculating normal and emergency modes in local EPS with DG based on renewable energy sources

Methodology and research methods of dissertation. During the study, the theoretical foundations of electrical engineering, optimization methods and non-linear programming, as well as various methods for solving system linear equations were used. The C ++ language for the software implementation of programing Microcontroller Arduino Nano is using to detect the irradiation value and control the SPWM. To verify the obtained calculation results, models are created to test networks in an interactive environment for Simulation MATLAB Simulink and MATLAB code.

The main provisions of the dissertation research submitted to the defense:

1. Modeling of DG based on renewable energy sources with the allocation of subsystems that determine short circuit currents.
2. A mathematical model for of the maximum power point tracking of the PV system for grid-connected and stand-alone modes.
3. A modified method for calculating short circuit currents.
4. Assessment of the balance reliability indicators of microgrid based on random divisions of the system into subsystems in post-fault conditions.

The author's personal contribution is the development of mathematical modeling of DGs (Wind, PV) for steady state and transient analysis of the electrical power system. Design the protection scheme devices for wind turbine PMSG as well as a simple protection scheme of the grid-connected wind farm. In addition, it is development of digital control strategy of SPWM MPPT of PV system is designing for two cases; stand-alone and grid-connected using implementation of the cheap and fast digital microcontroller named Microcontroller Arduino Nano 3x is using to detect the irradiation value and control the SPWM. A SFCL investigated to protect the AC and DC Microgrid from high fault current. A method is proposed for the fault current for grid-

connected and isolated microgrids with the comparison with the virtual impedance method. The static security risk and load shedding are calculated during the fault in different fault locations using an operation scenario in which the distribution system will divide into small subsystems.

The reliability of scientific results. The proposed algorithms and methods in the dissertation were used in the calculations of steady-state and transient analyses of PMSG wind turbine connected to grid, PV system for two modes (stand-alone and grid-connected) and hybrid wind-PV-battery bank AC and DC microgrids as well as the fault current calculation of the IEEE 33-bus with 5 DGs distribution system for grid-connected and isolated microgrids. A comparison of the results of the work of these methods with data obtained using other programs and other scientists allows us to judge the proper operation of the developed methods and algorithms, as well as the possibility of their application to solving practical problems within the network of the established modeling conditions.

Testing the results of work. The main provisions of the work were reported and discussed at 8 conferences.

Publications. Based on the research results, 8 works were published, including one in Russian-language publications from the list of the Higher Attestation Commission ("Electricity", "Electrical Systems and Complexes"), 3 articles in publications, indexed in international abstract citation databases Scopus and Web of Science and 4 in other publications.

The structure and scope of work. The dissertation consists of introduction, three chapters, conclusion, and two appendices. It contains 164 pages, includes 95 figures and 20 tables.

Chapter 1. Literature Review

A crisis of reduction of fossil fuels excites the extension of the usage of environmentally friendly renewable energy sources that are effective to meet energy needs. Many problems of power quality in electric power system occurred because of connection renewable energy sources. Nowadays, renewable energy sources energy associated with electric power system through centralization or distribution. The analysis of scientific and financial of renewable energy sources for community and eco-friendly influences is a constricted and clear basis for the analysis. Despite the outline of many improvements in the suitable use of wind energy and photovoltaic energy, further work is necessity to improve the efficiencies of renewable energy sources. Maximum power point tracking control of renewable energy sources is developing to improve the output power for increasing the efficiency to sort renewable energy sources as consistent source of energy in the future.

A serious problem of renewable energy sources, especially for wind and PV energy is voltage dip because the energy of these sources is not constant because of changing of the wind speed and irradiation by interval. The frequency of electric power system must be in normal rang which is supported the continuously the total power generation in accordance with the requirements. However, the inconsistency of the wind speed and irradiation feeding renewable energy sources causes the frequency has nonconformity from the normal value as well as disconnected renewable energy sources due to temporary fault circumstances. Under critical circumstances, renewable energy sources must remain connected to the energy system and make an effective and efficient contribution to maintaining the stability of the energy system.

1.1 Distribution Generator

Distributed generator in the term for generating electricity and storage is completed utilizing different small devices that connected to electric power system called distributed energy resources (DER). The ability of transmit the electrical energy demand to another place is more efficient to use the traditional energy stations like coal, gas and nuclear stations as well as hydroelectric power stations and large-scale solar energy stations. Distributed generators are increasingly reliable and adaptable advances, which distributed in the electric power system near the load. Distributed generators are increasingly significant part in electrical power system where there are many renewable energy sources used as distributed generators for example wind energy system, PV system, etc. Energy storage system considered as distributed generator when connected to electric power system for electrical storage device. The distributed generation is small power plant connected to the electric power system near the electrical load. The distributed generators can be worked at the purpose of utilization with overabundance offered to the electric power system, or by generator units scattered inside the nearby appropriation organize, as shown in Fig. 1.1.

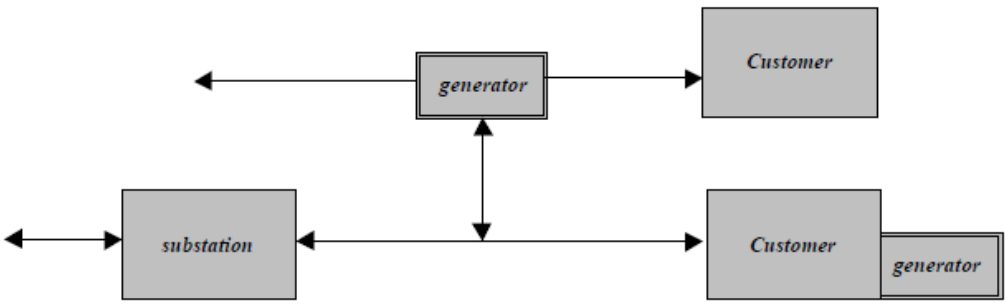

Fig. 1.1─ DG unit connected to consumer

The types of renewable energy sources used as distributed generators are:

- Small gas turbine (Microturbine) is utilized in huge scale power cogeneration plants. It is utilized for army equipment.

- Solar energy source (PV) converts over daylight legitimately into electric power. Advanced industrial technologies must use to make complex semiconductor device of photovoltaic device according to general cost of generator.
- Wind energy source is one of distributed generator. Due to the change of wind speed with time, wind energy source is less reliable source as PV sources. The wind energy source as distributed generator is important generation unit is constrained to the places of large and fixed wind speed that are near or far the main electric power system.
- Fuel cell is one of distributed generator where the electrical power generated by continuing a substance response by move of charged species over a film isolating the fuel and oxidant tributaries. Table 1.1 shows the specification of different distributed generators.

These are many renewable energy sources used as distributed generation but the wind energy and PV sources are more efficient and reliable than other sources. Fig 1.2 shows the rate of distributed generators around the world.

- Table. 1.1. ─ Specification of different distributed generators.

	Engine Generator	*Turbine Generator*	*Photovoltaics*	*Wind Turbine*	*Fuel Cells*
Dispatchability	Yes	Yes	-	-	Yes
Capacity Range	500 kW – 5 MW	500 kW – 25 MW	1kW - 1MW	10 kW - 1MW	200 kW - 2MW
Efficiency	35%	29 - 42%	6 - 19%	25%	40 - 57%
Energy Density (kW/m2)	50	59	0.02	0.01	1.0 - 3.0
Capital Cost ($/kW)	200 - 350	450 - 870	6,600	1,000	3,750
O&M Cost (&/kW)	0.01	0.005- 0.0065	0.001- 0.004	0.01	0.0017
NOx (lb/Btu)					
Natural Gas	0.3	0.1	n/a	n/a	0.003 - 0.02
Oil	3.7	0.17	n/a	n/a	-

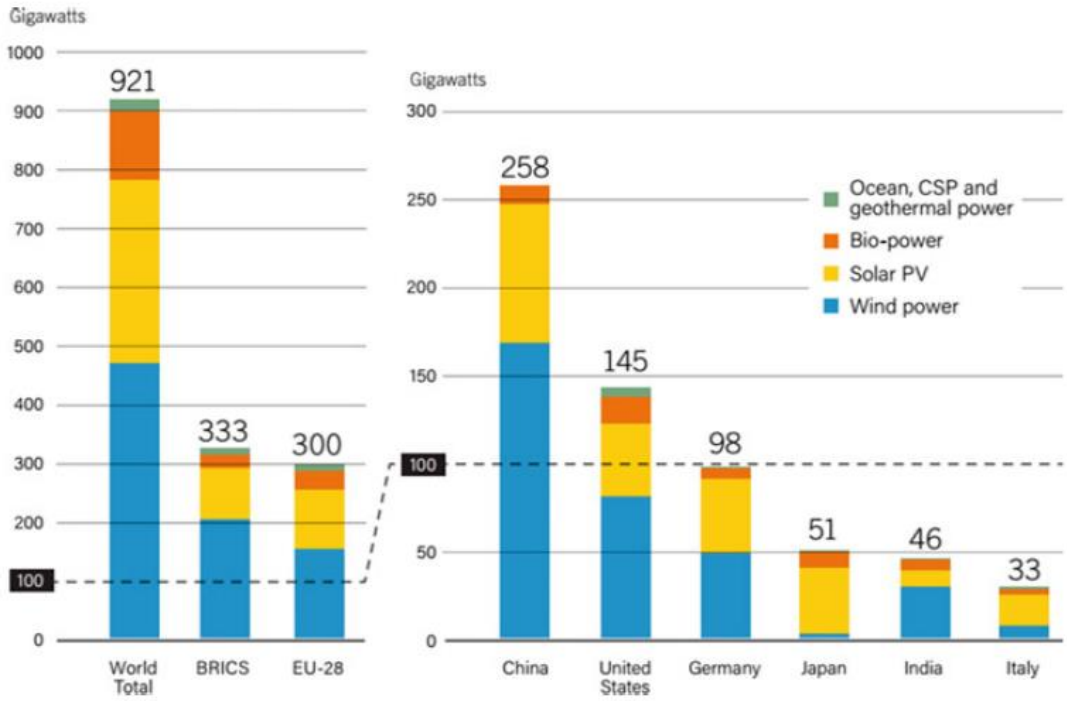

Fig. 1.2 ─ Rate of distributed generators around the world

1.2 DG Control methods

The power losses problem is improved by control system harmonization with controlling the voltage profile. Several studies have been investigated the voltage control in electrical power system. The voltage control of electric power system connected to distributed generator for enhanced the system voltage investigated in [24]. A control method investigated to harmonize the operation of DG and OLTC by controlling the voltage regulator. The method harmonization is expected at keeping the voltage at a suitable value with a number of adaptable strategies, while reducing the number of operations of confrontation between them or removing them [24]. Another system to control microgrids profoundly infiltrated by Voltage Source Converters (VSC) presented in [25]. The theoretical and methodological approach describes the definition of the electric power system parameter, which offers many variations for launching VSC independently. Moreover, VSCs control the sharing electric power by managing voltage of nearby association bus. Volt/VAR control is one suitable solution to

connect DG to electric power system to improve the voltage profile. Volt/VAR control strategy is more reliable when it connected to DG controlling system to accomplish an adaptable and versatile arrangement while limiting unpredictability and necessities for information taking care of ability [26]. A hybrid control strategy for Z-source inverter (ZSI) with LC filter, which utilized in distributed generation described in [27]. Two control strategies are used: a proportional-resonent (PR) regulator in ac-side and proportional-integral (PI) regulator to improve the DC voltage of capacitor. For that, voltage and current regulators are used to increase the effectiveness of operation of converters, which connected distributed generators to electric power system. However, the suitable control strategy for DG connected to main grid is current regulator and voltage regulator is suitable for isolated DG to improve the voltage of loads [28]. A developed DG control technique through LCL filter with limiting current harmonic is investigated to defeat the restrictions of current control and voltage control strategies. With joining droop control and average power sharing strategies, the correct control strategy is used to improve the active and reactive power partaking in microgrid. A low-bandwidth numerical infrastructures to realize correct value of power participation and recovery is used in this technique. The droop control technique is like control traditional power system where the frequency depends on the generation power of distributed generator. The relations between frequency and power and voltage and reactive power characteristics of droop control technique are expressed:

$$f = f^* - m(P - P^*)$$

$$E = E^* - n(Q) \tag{1.1}$$

where $E^*$and f^* are open circuit voltage and nominal frequency respectively. m and n are frequency and voltage coefficients, and P^* is nominal active power.

The voltage of DG can be controlled by ca lculating active and reactive power from active power sharing technique. On the other hand, to overcome the problems of large-scale detecting and infrastructures, the distributed methodology for continuous administration of nearby voltage and thermal requirements is used by controlling the generation active and reactive power [29]. The three components (positive-, negative- and zero -sequence) of voltage at the connection point is controlled by three components voltage and current control technique with controlling the output currents of VSCs to recompense the unbalance voltage of microgrid buses. [30]. To easily change the operation from grid-tied to islanded mode of electric power system integrated to DGs, the droop control technique is investigated with using adaptive virtual impedance to limit the harmonic currents of DG [31]. A self-enhancing technique is investigated to control power and frequency of DG [32].

1.3 Modeling of PMSG Wind Power System

Variable speed generators as doubly fed induction generator (DFIG) and permanent magnet synchronous generators (PMSG) are effective utilized in wind energy plants. PMSG is better than DFIG because it works at low rotational speed, absent of rotor and without gearbox. The efficiency and low operating costs are important factor to choose the generator for the biggest investment problem. The constant electromagnetic field construction is significant requirement of PMSG to a high level of construction in addition to the operating with knowing the variable speed of generator [33]

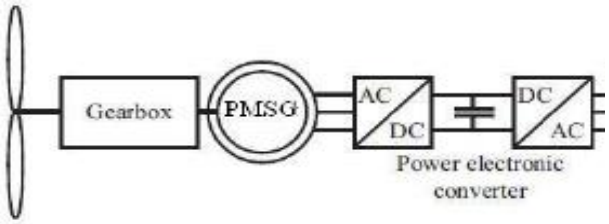

Fig. 1.3 ─ Permanent Magnet Synchronous Generator wind turbine

1.3.1 Wind turbine model

The output mechanical power of wind turbine is given by

$$P_m = {}^{1}/_{2}\,\rho A_r v^3 C_p(\lambda,\beta) \tag{1.2}$$

where ρ is the air density; A_r is the area swept by the blades; v is the wind speed; and C_p is the power coefficient, which is determined by the $\lambda = \frac{\omega_t R}{v}$ and the blade pitch angle β which is always constant during MPPT control, where ω_t is the turbine rotating speed [34].

1.3.2 Modeling of PMSG

A synchronous generator with full AC/DC/AC converter is another variant generator to the asynchronous machine, which is used to a large extent by electrical excitation system or by permanent magnets. The interface converter is used to couple the synchronous generator to electric power system by controlling the voltage and frequency. This converter control the active power fed to DC capacitor and output reactive power using IGBT switches in two back-to-back VSCs. Due to the multi-pole synchronous generator structure, the rotational speed of generator is small and allowed to couple with wind turbine without gearbox. Fig. 1.4 shows the equivalent circuit model of balanced three-phase PMSG. For neglecting the losses of generator as magnetic saturation, eddy current and slot effect, the PMSG voltage equations are expressed as:

$$\begin{aligned} v_a &= e_{af} - R_a i_a - L_s \frac{di_a}{dt} \\ v_b &= e_{bf} - R_b i_b - L_s \frac{di_b}{dt} \\ v_c &= e_{cf} - R_c i_c - L_s \frac{di_c}{dt} \end{aligned} \tag{1.3}$$

where L_s and R are the equivalent reactance parameters and e_{af}, e_{bf}, e_{cf} are excitation electromotive force.

$$e_{kf} = p\omega_r \Psi_f \sin\theta \ (k= a, b, c) \tag{1.4}$$

where ω_r is the angular speed of the rotor and Ψ_f is the rotor flux.

The transformation form of PMSG model from three-phase static coordinate to synchronous rotating frame are:

$$u_d = R_s i_d + p\Psi_d - \omega\Psi_q$$

$$u_q = R_s i_q + p\Psi_q - \omega\Psi_d \tag{1.5}$$

$$T_{em} = \frac{3}{2} p(\Psi_d i_q - \Psi_q i_d)$$

$$\Psi_d = L_d i_d + \Psi_f \tag{1.6}$$

$$\Psi_q = L_q i_q$$

where Ψ is excitation component and T_{em} is torque component

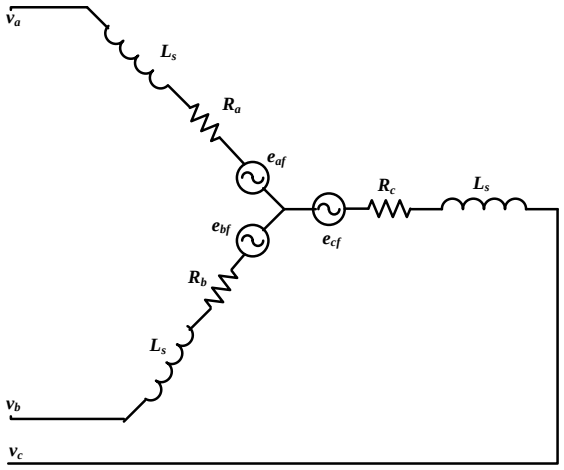

Fig. 1.4 ─ Open circuit equivalent model of PMSG

1.3.3 Modeling of back-to-back PWM Converter

Based on the equivalent model of PMSG, the generator-side converter is modeled in Fig. 1.5. The mathematical model of the generator-side converter is:

$$L_s \frac{di_a}{dt} + Ri_a = e_{af} - (v_a + v_{NO})$$

$$L_s \frac{di_b}{dt} + Ri_b = e_{bf} - (v_b + v_{NO}) \tag{1.7}$$

$$L_s \frac{di_c}{dt} + Ri_c = e_{cf} - (v_c + v_{NO})$$

$$C \frac{dv_{dc}}{dt} = \sum_{k=a,b,c} i_k s_k - i_l$$

The transformation form of three phase static coordinate to synchronous rotating frame is:

$$C \frac{dv_{dc}}{dt} = \frac{3}{2}\left(i_q s_q + i_d s_d\right) - i_L$$

$$L_s \frac{di_q}{dt} + \omega_e L_s i_d + Ri_q = e_q - v_q \tag{1.8}$$

$$L_s \frac{di_d}{dt} + \omega_e L_s i_q + Ri_d = e_d - v_d$$

Where v_{NO} is the voltage of three phase midpoint, i_L is the load current, i_d and i_q are the dq component of the output current of the generator-side converter respectively.

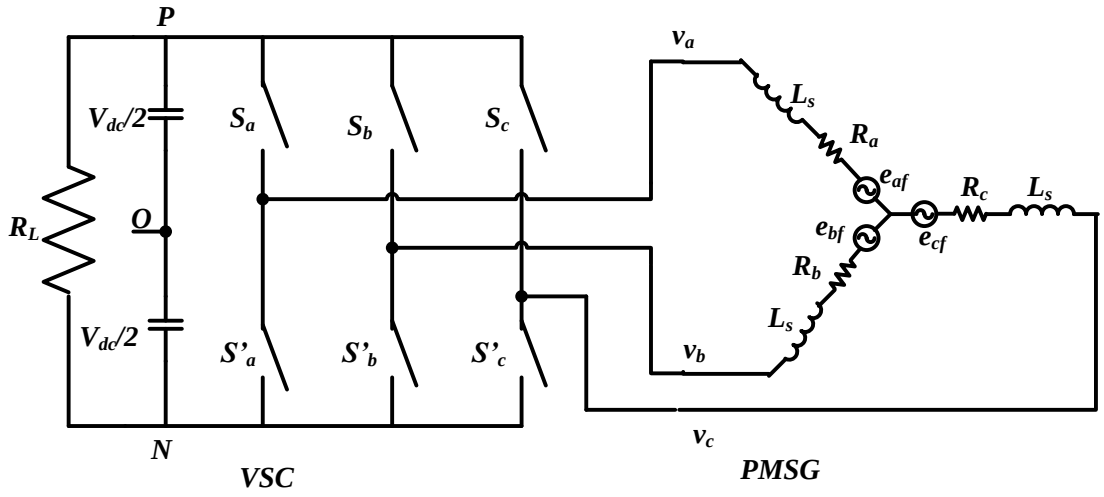

Fig. 1.5 ─ Generator-side converter and its equivalent model

Dynamic dq model of the grid-side converter based on grid voltage orientation is given in (1.7).

$$u'_d = u_{id} - R'i'_d - L\frac{di'_d}{dt} + \omega L i'_q$$

$$u'_q = u_{iq} - R'i'_q - L\frac{di'_q}{dt} + \omega L i'_d \tag{1.9}$$

where *L* and *R* are the grid connected inductance and resistance, u'_d and u'_q are the dq component of grid voltage, u_{id} and u_{iq} are the dq component of inverter output voltage, i'_d and i'_q are the dq component of grid current, ω is the fundamental frequency respectively. The active and reactive output powers are:

$$P = \frac{3}{2}u'_d i'_d$$

$$Q = \tfrac{3}{2}u'_q i'_q \tag{1.10}$$

1.4 LVRT control strategy

There many techniques are used to achieve the operation of low voltage ride-through. One of these techniques is a sliding mode controller (SMC) technique. This techniques has two principle features; the choice of switching function can improve dynamic manner of the system where the control system reaction is completely nonsense to a specific type of vulnerability. But the drawback of SMC technique is using the quasi-continuous process to regulate the DC voltage for PMSG wind turbine [35]. To improve the performance for unbalanced voltage sags of electric power system, the dc-link voltage controller is used depending on a feedback linearization theory. Through the voltage sag of electric power system, a DC chopper absorbed additional energy in DC-link to maintain constant DC voltage. To maintain balancing mode, energy storage methods are used. A hybrid mechanical an electrical LVRT technique is used for high moment inertia of generator, storage inertia of rotor and the connection power features. Nonetheless, the LVRT capability of PMSG wind turbine is developed in different degrees by

these techniques, these is no connection between PMSG and electric power system because the additional energy must transmit to DC-link and generator-side through FCL then for predisposed [36-37]. Another technique namely different field orientation control is studied for converters [38]. The ability of fault ride-through (FRT) is improved to increment operational dependability and producing proficiency utilizing MATLAB/SIMULINK by coordinating control procedure between lattice side converter (GSC) and bidirectional Buck-Boost converter (BDBBC) has been examined to improve the ability of shortcoming ride through (FRT) to increment operational dependability and producing proficiency utilizing MATLAB/SIMULINK [39]. Regulating dc-link voltage and transmitting additional undesirable energy to the kinetic energy of generator wind turbine concluded to power conversion provided to increase the ability of LVRT. The best strategy is just utilizing control systems to accomplish LVRT of PMSG [40]. To limit the output current of inverter within its limit value during the fault while the input power stifled to recover the balance power, The LVRT of PMSG based on Z source is studied in [41]. In ref. [42], the new control technique is studied to settle dc-link voltage and obtain maximum power. Different control techniques with testing LVRT capability for single wind turbine and wind farm in some fundamental standards of DFIG and PMSG generators have been investigated in [43]. The extra energy can be saved in the mechanical inertia through the fault in electric power system where the mechanical reaction of direct drive wind turbine is slowly compared to reaction of electrical [44].

1.5 PV System Modelling

Friendly environment renewable energy source is PV generator, which generate electrical energy from sunlight without burning fuel. PV generator can be utilized in many applications like solar cars, lighting of buildings, UPS systems and isolated region. PV system connected to electric power system or worked as stand-alone mode in the region so far from main grid. The PV system is contained

the solar photovoltaic array, converters, filters and control system. Fig. 1.6 shows the PV system.

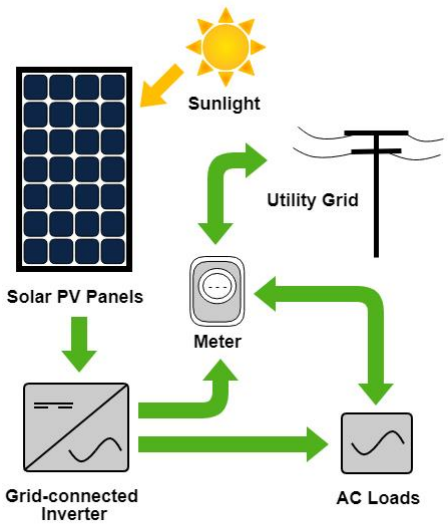

Fig. 1.6 ─ PV system

1.5.1 Photovoltaic Cell (PV)

Photovoltaic Cell is mainly a p-n junction with P-type silicon at the bottom and diffused thin layer of n-type on the top. PV cells produce current when photons incident on its surface [45]. The open circuit voltage of single solar cell is in range 0.5-0.7 according to the various strategies and prototypes reference of solar photovoltaic array system. PV array module consists of number of series and parallel connected cells as per the required rating of PV array [46]. The electrical model of a PV cell has a current source (I_{pv}), a diode connected in anti parallel (D), a series resistor (R_s) and a parallel resistor (R_p) as shown in Fig. 1.7 [47].

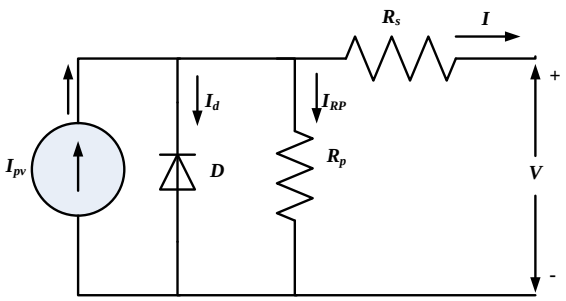

Fig. 1.7 ─ Electrical model of PV cell

The equivalent resistances of PV array are:

$$R_{se} = R_s(\frac{N_s}{N_p})$$

$$R_{pe} = R_p(\frac{N_s}{N_p}) \quad (1.11)$$

where N_s = No. of series-connected modules per string, N_p= No. of parallel strings. The output current of the PV cell is expressed as,

$$I = I_{pv} - I_s\{\exp\left(\frac{q}{A_k T_c N_s} V + IR_s\right) - 1\} - \frac{V+IR_s}{R_p} \quad (1.12)$$

where I_{pv} denotes light generated current, I_s is the saturation current of the diode, q is the electron charge which is 1.60 x 10^{-19} C. V and I denote the output voltage and the output current of the PV cell respectively. The ideality factor of the cell is defined as A_k in the equation is Boltzmann constant (1.38x 10^{-23} J/K). The number of series connected cells in a PV module is denoted by N_s. The light generated current (I_{pv}) in equation (2) is expressed as,

$$I_{pv} = \left[I_{sc} + K_f\left(T_c - T_{ref}\right)\right].G \quad (1.13)$$

where K_f is the temperature co-efficient of short circuit current of the cell. T_c and T_{ref} are the cell's operating temperature and reference temperature respectively. G is the solar irradiation level in W/m^2.

1.5.2 Maximum power point tracking

Maximum Power Point Tracking (MPPT) is a technique to obtaining maximum probable instant power of PV system. Various MPPT strategies have been utilized for various arrangements dependent on the system. The relation between power and voltage or current of PV array is shown in Fig. 1.8. The issue of MPPT methods is to fasting obtain the values of voltage VMPP or current IMPP of maximum point for specific value of irradiation and temperature.

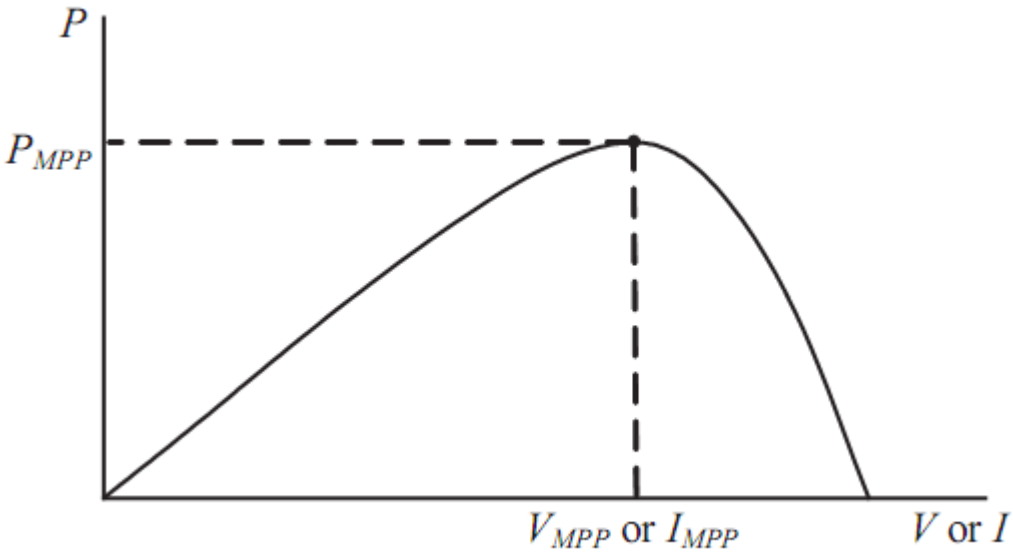

Fig. 1.8 ─ Characteristic PV array power curve

There are many methods of MPPT, which are intensive on hill-climbing [48] and perturb and observe (P&O) [49] methods. Hill-climbing method depended on the disconcertion change of the power converter duty ratio of the power converter and P&O method depended on the disconcertion change of the voltage of the PV array. The incremental conductance method [50] is mathematical method which is used the derivative of slope at maximum power point is zero. In this method, the MPP can be obtain by matching instant conductance (I/V) with incremental conductance (dI/dV). In the past, the efficient and fast method to get MPP is fuzzy logic control technique employed by microcontroller. The benefits of fuzzy logic technique is not necessity to know exact mathematical equations and works with inexact input data. The neural network technique which also employed by microcontroller, created from fuzzy logic technique to obtain MPP. Alternative method of MPPT is Ripple correlation technique which is used of ripple to implement MPPT. The current sweep technique is obtained MPP by far-reaching waveform of the PV array current like that the characteristics of PV array is gotten and reorganized at regular value of time. With helping of digital devices such as DSP and microcontroller, it is easy to work with compound

calculations to get MPP by calculating slope (dP/dV or dP/dI) of the PV characteristics and employing it to control of power converter to get MPP. Due to the climate changes, the MPPT techniques have incorrect value of current efficiency where the commercial PV system has not been obtained MPP. From above, the MPPT methods can be classified based on a reconfigured array. The MPPT techniques are once cycle control (OCC), best fixed voltage (BFV) algorithm and slide control method [51], look up table method [52], hill climbing [53], perturb and observe (P&O) method [54], incremental conductance [55], fractional open circuit voltage [56], fractional short circuit current [57], ripple correlation control (RCC) [58], load current maximization [59], load voltage maximization [60], linear current control [61], dP/dV and dP/dI feed back control [62], current sweep [63], DC link capacitor drop control [64], fuzzy logic control [65], and neural network-based control [66]. Best fixed voltage (BFV) algorithm is designed based on the annual history of the temperature and irradiance data [51]. The most widely used method is the Perturbation and Observation (P&O) because it is easy to implement. A new MPPT method is particle swarm optimization (PSO). This method executed in field-programmable gate array is investigated to obtain MPP under partial shading circumstances. This MPPT method has been tested on various configurations of photovoltaic arrays in order to estimate the behaviour of photovoltaic array under irregular radiation [67]. A mathematical method is provided for tracking the maximum power point of a photovoltaic array by calculating the theoretical value of the MPP voltage [68]. To overcome the disadvantage of conventional P&Q technique, the advanced P&Q technique is used to obtain MPP by estimating the short circuit current value I_{sc} with calculating value of voltage and current in each step of perturbation and observation [69]. Many methods are used to obtain MPP partial shading circumstances such as a transfer reinforcement learning (TRL) [70], the modified firefly algorithm (MFA) [71] and two stage PSO [72]. Flower pollination technique is a new method for obtaining MPPT [73].

1.6 Modeling of a battery energy storage

Batteries are electrochemical cells that store energy in the form of a chemical substance to convert it into electrical energy when the battery is discharging. Standalone PV system must integrate with energy storage system because the output energy of PV system is not constant due to the instantly change of irradiation. The main function of energy storage system is charging the surplus energy during the day and discharging to the load during night.

Energy storage system used in photovoltaic systems must have certain characteristics to reduce the cost of the system, and meet the strict reliability requirements related to the structures of the photovoltaic system.

Staggered inverters can work at high voltage levels utilizing gadgets with low force voltages, delivering low consonant substance at the yield waveforms, when contrasted and the waveforms acquired with two-level inverters

The battery model is shown in Fig. 1.9. The terminal voltage of a battery can be modeled as the sum of constant, exponential and polarization zones given by

$$V_b = V_0 - k\frac{C}{C-q}q - Ri + Ae^{(-B.q)} \tag{1.13}$$

The equivalent scheme of the lead acid battery (LAB) consists in a controlled voltage source (E_b) in series with the internal resistance (R_{int}) and the LAB voltage (V_b), as shown in the Fig. 1.10. It is known that the E_b voltage depends on the charging state, battery type, temperature and is expressed by the following relationship:

$$E_b = E_{b0} - \frac{K.Q}{Q - \int_0^t i_b dt} \tag{1.14}$$

where *Q* is the charge of battery

The input of the charging/discharging controller is used as parameter the SOC of LAB, defined as follows:

$$SOC_{[\%]} = SOC_{0[\%]} + \left(1 - \frac{Q_n}{Q - \int_0^t i_b dt}\right).100 \quad (1.15)$$

where SOC is state of charge

If the LAB is fully charged, SOC = 1 and if the battery is discharged at the maximum value, SOC = SOC_{min}. The SOC block diagram is shown in Fig. 1.10 [74].

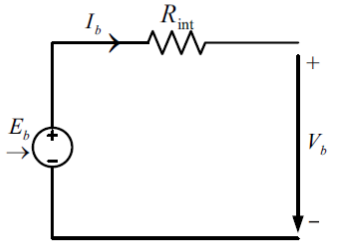

Fig. 1.9 ─ Battery Model

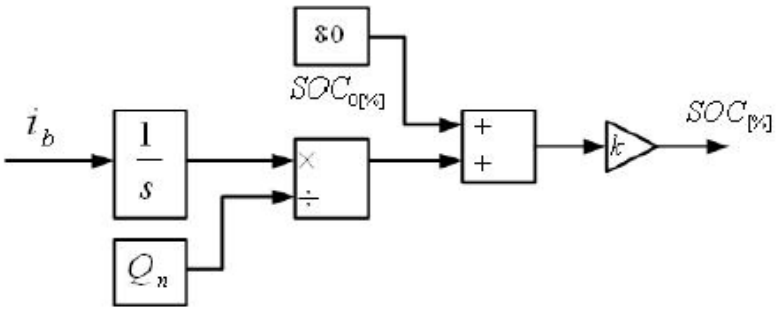

Fig. 1.10 ─ The SOC block diagram

1.7 Multi-level converter

Multi-level inverter can work at high voltage levels with low power devices which leads to a low harmonics of waveform with the comparison with the harmonics of waveform of two-level inverter. By increasing the levels of multi-level inverter, the harmonics level of output waveform is decreased but the price and difficulty of inverter will be increased. There are three main types of multi-level inverters; Neutral Point Clamped (NPC) Inverter, the Flying Capacitor Inverter and the Cascaded H-Bridge Inverter.

The output voltage of neutral point clamped inverter consisted a low harmonics where the semiconductor devices can be able to use in the minimum threshold voltage compared with devices of two-level inverter. The multi-level NPC inverter has the ability to working as a source to move energy from the DC side to the AC side, or working as a rectifier, moving energy from the AC side to the DC side.

In contrast, the multi-level flying capacitor inverter isn't as regular inverter as different structures, it has some particular preferences over the diode-braced topology with disappear the clamping diodes the capability to control the flying-capacitor voltages through excess state choice, regardless whether the quantity of voltage levels is more than three.

The cascaded H-Bridge multi-level inverter has different structure where it comprises of at least two single-phase full bridge converters series coupling at the AC side to produce three altered voltage levels. The high rating of power, modular index and price efficiency are the features of cascaded H-Bridge multi-level inverter. By reducing the switching frequency of multi-level cascaded H-Bridge inverter, the harmonic of output waveform is decreased.

From the above literature, the multi-level NPC inverter is better other multi-level inverter where its control system is simplest comparison with multi-level flying capacitor inverter which needs a complexity voltage control. In contrast, the multi-level cascaded H-Bridge inverter is used two distinct DC sources for that it has restricted application. Multi-level flying capacitor inverter has complex control and large losses when it is used in power transmission [75]. To obtain minimum THD and MPP tracking, the multi-level cascaded H-Bridge inverter is used with LeBlanc transformer with constructing of two single-phase inverters, a four-wire voltage source inverter [76]. The new topology of multi-level inverter contains fewer switches with accumulating the benefits of H-bridge and MLI construction to increasing the global performance of inverter [77]. Ref [78] has

been investigated multi-level 11-level cascade inverter. To increase the power efficiency of PV application, the modular multi-level inverter is used by producing the maximum output power from PV array without adding extra DC-DC converter and feed these power to electric power system [79]. Multi-level inverter can be used in the manufacturing part such as multi-level T-type clamped inverter because small THD and large efficiency [80].

1.8 Microgrid

Distributed generators like those that wind energy sources, PV source, small gas turbine and fuel cells have been connected to electric power system on account of eco-friendly and advanced technical operation sources [81]. Subsystem "Microgrid" is a best method to achieve the possible emergent of distributed generation and loads. Microgrid has many advantages like improving the reliability of system, decreasing the line losses, improving the voltage profile, ensuring greater efficiency through the usage of excess hotness from joint heat and power (CHP), correcting voltage sags and correcting UPS functions [82 and 83]. MG is working in two different mode: grid-connected mode (MG connected to electric power system) and islanding mode (MG under abnormal conditions) [84]. The interfacing converters is needed to connect MG to grid or load are AC/DC or AC/ DC/ AC depending on the DG type. Inverter control is thus the important basic in MG operation. The process of a small MG consisting of small wind power generator and a solid polymer membrane-type fuel cell (PEM-FC) feeding a house composed of 12 apartments was presented [85]. The MG operations under normal and emergency conditions have been investigated under different load fluctuations conditions. The performance of PV generator in a MG System installed in Thailand to feed an academic center was introduced [86]. The MG consists of PV generator, diesel generator, and batteries storage. The MG is operating in grid connected mode. An integrated prototype MG with an elastic and robust structure containing many DG systems with storage energy system

was presented [87]. Coordination a diesel generator and flywheel energy storage constructed MG to improve the operation of uninterrupted power-supply in assistance with diesel generator. The control system of MG is to allow to easily transfer between two modes grid-connected and isolated. The MG control, protection, and other technologies have been carried out. Control and process of a grid-connected and isolated DC micro-grid have been investigated [88]. In contrast with AC microgrid, DC microgrid contains distributed generators such as wind power, PV system or DC load and connects to electric through converter. In grid-connected mode, a constant DC voltage must be a fixed value using active power fed to the electric power system under normal condition. The load shading technique is used for isolated MG to guarantee feeding the power to the maximum critical loads. The input switching control signal depends on DC voltages under normal and emergency conditions. A helpful control technique of micro-sources and battery system of islanded microgrid has been introduced [89]. The MG comprises of PV, wind, diesel engine, gas engine, micro turbine, and an ESS as support system to fulfill the stable operation of a facility. A control strategy for a stand-alone photovoltaic-diesel MG without energy storage element has been proposed [90]. Control technique and dynamic model of hybrid wind-PV microgrid was presented [91]. While the wind power and PV generators are emerged to DC bus using interface DC-DC converter. Dynamic models of renewable energy sources such as wind power, PV source, hydro source and storage energy source using EMTP/ATP program has been investigated [92]. The analysis of operation and control techniques of DC microgrid contained PV system and battery has been proposed [93]. Microgrids are modern, localized, small-scale grids, which can operate in isolated mode as well as they used to reinforce main grid flexibility and minimize the fluctuations of main grid.

1.8.1 The Microgrid Concept

The main grid operates by connecting residential, commercial or industrial areas to a central power source and allows consumers to use electrical appliances. The structure of the microgrid is the same to the structure of electric power system but operates at a smaller scale. It is a power distribution system which consists of electrical components such as renewable energy sources and loads. The microgrid loads are generally electronic loads but in some cases, rotating or resistive loads are used instead. Fig 1.11 shows microgrid with sources and control structure.

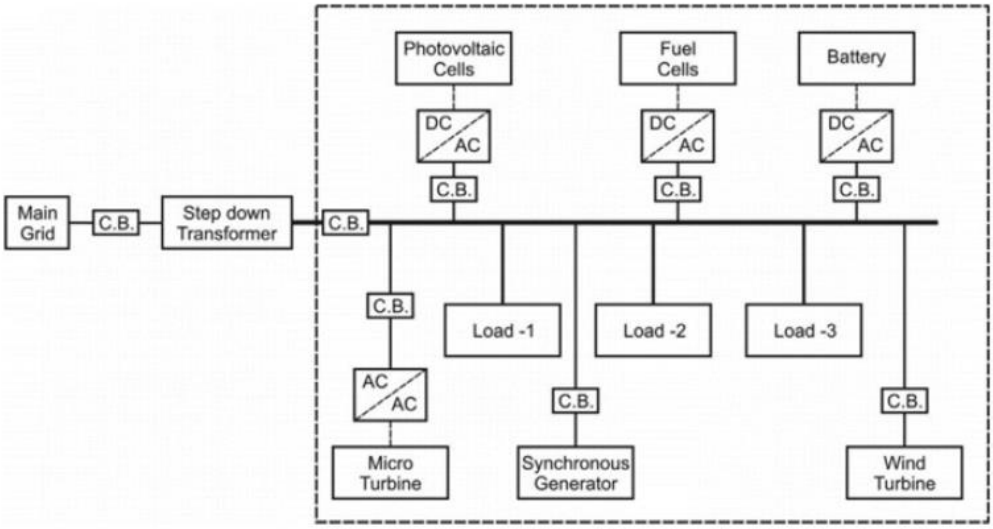

Fig 1.11 ─ Microgrid with sources and control structure

Microgrids generally have two modes of operation, normal mode and islanding mode. During the normal operations, the main grid and microgrid are connected at a point of common coupling (PCC) in which the voltage from both grids are synchronized and maintained at the same magnitude. During a disturbance on the main grid, Microgrids go into an islanding mode. During islanding operations, microgrids are capable of detecting faults in electric power system then disconnecting itself automatically or manually from the electric power system. In a sense, microgrids work as a backup for the main grid during emergencies and there are many distinct advantages of implementing microgrids, such as improved

efficiency and cost reduction. Installing a microgrid can also improve reliability of the system during generation and consumption.

1.8.2 Control of Microgrids

A microgrid may have several DG unit connected or disconnected from the grid, intentional or unintentional islanding may occur, or there is less power generation which further leads to a frequency instability due to higher power demanded by the loads. The main responsibility of microgrid control system under any condition mentioned above is to ensure continuous supply of electrical energy to the loads and to increase the reliability of the network. Fig. 1.12 shows control system of microgrid with active distribution network. The controllable variables are frequency, voltage, reactive and active power. These control methods are implemented through guiding control that contain centralized control and decentralized control. Both control scheme includes (i) Microgrid Central Controller (MCC), (ii) Market Operator (MO), (iii) Local Controller (LC) linked with (a) storage unit, (b) load and (c) DG units (LCDG).

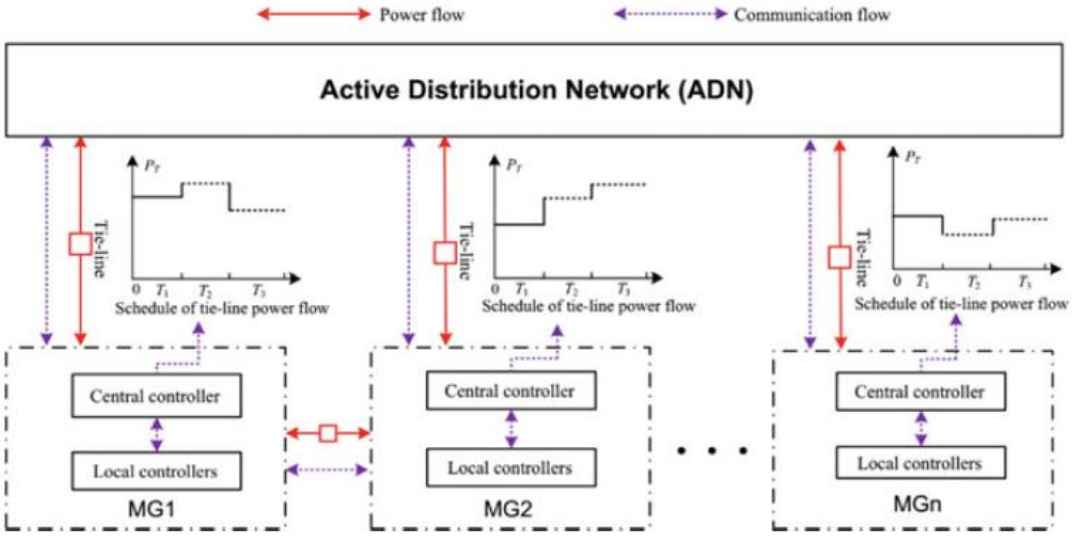

Fig. 1.12 ─ Control system of microgrid with active distribution network

1.8.2.1 Centralized control

The basic aim of the centralized control is islanding detection and fault current measurement. After this appropriate protection, settings should apply by PCM to stable the microgrid network and utility grid.

The central controller performs the following operation during grid-connected mode:

• Monitoring of above discussed system parameters from bus, load, DG unit whichever needed for specific control.

• The energy management in most economic way of the DGs.

• Ensure secure and reliable operation of the network and maintain synchronism with the host grid.

The task of central controller is different than before in case of islanded mode and is listed below:

• Voltage and frequency controls command issue for master DG unit and, active and reactive power controls command for other operating DG units.

• A tripping signal issue for load controllers to disconnect the loads except critical loads based on the backup reserves and load criteria.

The implementation of centralized supervisory control scheme requires a comprehensive communication between local controllers and microgrid central controllers. This large communication architecture is sometimes infeasible for massive areas.

1.8.2.2 Decentralized Control

It is impractical to employ centralized control scheme in remote areas due to large distance between DG sources. In addition to this, it requires extensive communication structure which demands higher cost. These decentralized control

system enables to connect more number of DG units which are owned by different service providers. Local controllers are more responsible and must perform more functionality in decentralized control schemes compared to centralized control scheme. Due to this, DGs and loads have more autonomy to operate. The hierarchical structure of the decentralized control scheme is the same as centralized control scheme, which includes LC, MCC and DNO. The DG is modeled with droop control for load sharing which is most popular control scheme. In grid-connected mode, the main concern is to provide active and reactive power to the main network. Hence, reactive power sharing is controlled by voltage droop and similarly real power sharing is control by frequency droop. The main limitation of decentralized control system is that microgrid central controller is not general used in all actions taken by local controller as more emphasize is given to local controllers.

1.9 Power flow of isolated microgrid

The power flow analysis of isolated microgrid is different from grid-connected microgrid where there is no slack bus. DG units are for the most part worked in droop mode amid the isolated mode of operation of microgrid. The droop technique largely gives a superior alternative to authority over the load to be shared by the various generation units because in droop strategy, power sharing is relative to the rating of the distinctive DG units. In the droop method of operation, the settings of the droop coefficient of distributed sources ought to be picked with the end goal that the loads are partaken in extent to their ratings. The electrical energy shared by the DG units is constrained by P–f droop and Q–V droop attributes, separately. For grid-connected operation, DGs by and large work in the (P–Q) or (P–V) mode. Generally the problem of non-linear equations of load flow program are unraveled utilizing the Newton Raphson (NR) calculations Many researches were solved the power flow of isolated microgrid using modified newton Raphson [94] and a Newton-Trust region method [95].

1.10 Fault current calculation

There are four types of faults which can happen in electric power system, three-phase-to-ground, one-line-to-ground, line-to-line, double-line-to-ground shown in Fig. 1.13. These types can be divided into symmetrical and nonsymmetrical faults. Each fault even symmetrical or nonsymmetrical has three components, positive, negative and zero components. These three components are independent and their values depend on the type of fault.

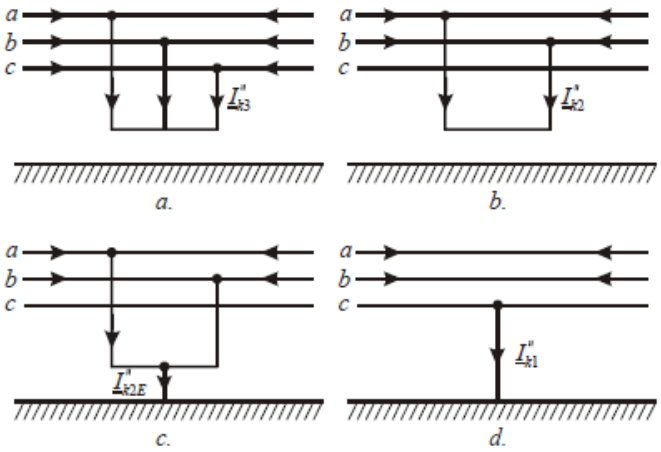

Fig. 1.13 ─ Four types of fault

In distribution networks with DG, the requirement of not surpassing the design short-circuit capacity be fulfilled at each purpose point of the network, under maximum fault current conditions. The fault current condition of distributed system connected HV/MV (or MV/LV) substation must be verified at MV or LV bus because the main electric system gives the prevailing contribution, which quickly lessens downstream the network because of the series impedances of the lines. The short circuit current of DG is very small value at the connection with the main network because the equivalent impedance of power electronic device is greater than the feeder impedance. For that, the short circuit current must be calculated at the substation buses without taking into account the connection method. The fault current value is summation of the short circuit currents

contribution from the main network, through transformer and different type of generator (and probably motors) which associated to distributed power system.

1.11 Electromagnetic Coupling Mathematical Model of SFCL

Figure 1.14 shows the model of Resistive SFCL limiter [96].

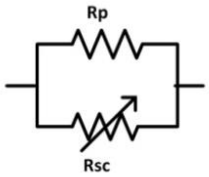

Fig. 1.14 ─ Resistive SFCL limiter

As shown in Fig 1.14, resistive SFCL limiter contains two parallel resistors and it can be considered a variable resistor connected to electric power system. Therefore, the construction of resistive SFCL is variable resistor R_{sc} and constant resistor R_p to minimize the short circuit current in electric power system during the fault. The characteristic of superconductor depends on factor n. The large value of n is increased the speed the superconductor state.

$$E = E_0 \left(\frac{J}{J_c(T_{op})} \right)^n \tag{1.16}$$

where E is electric field , J and T_{op} are superconducting current density and optimum temperature respectively. Fig. 1.15 shows Matlab/Simulink model of Resistive type SFCL.

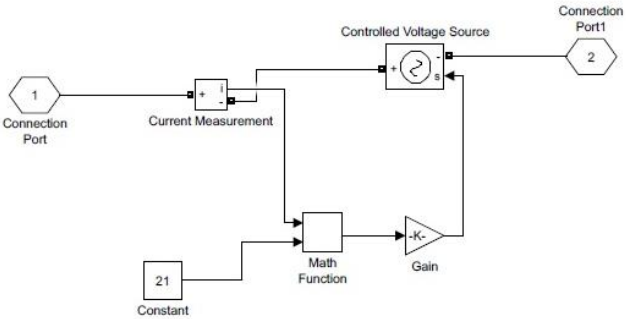

Fig. 1.15 ─ Resistive type SFCL model based on Matlab/Simulation

1.12 Inverter current control during fault

A voltage-source-converter control method under unbalanced short circuit power arrangement is looked into in two groups, power-characteristic-oriented technique and voltage-support-oriented technique. Considering semiconductor capabilities, the converters curent should be restricted during the fault current inside to secure operation limits that converters can only give 1–2 p.u of its limit during fault [97]. This current is critical to help grid voltage and activate protective relays contingent upon their semiconductor capabilities. So as to restrict the phase current, converter current limit should be specifically analyzed for each control strategy. Considering the way that a very high fault current may be required to keep active power level unchanged during severe voltage dips, the current limit is forced by limiting dynamic power. The control technique is moved to adjusted current operations under this situation.

A bouncy control utilized a changeable disturbance parameter, to upgrade or decrease the power of converter during fault described in [98]. The power of converter is restricted by the nominal power of converter during the fault. Fig. 1.16 shows the construction of VSG system depending on the dq-axis with similarity between the angular grid frequency and the dq-axis. The dq-axis technique has the advantage to take independently influences of active and reactive power components. The 3-Φ voltages are measured by abc-axis then transferred to dq-axis. Pulse width modulation signal got from voltage and current control then feed it to VSG to control voltage in specific value

To increase the stability of microgrid, power control technique is used to improve the required time to recover pre-fault values of voltage and current during disturbance. The definition of system stability depends on the reaction of VSGs control during the disturbance. The change in active power ‘ΔP’ and the derivative of it (equal to dP/dt), is utilized to stabilize a microgrid; without altering the control parameters of the VSG control. The active power attempts to

move toward its steady state after cleaning fault. The parameters of VSG technique depend on the state of stability, droop coefficient for static and droop coefficient and inertia for dynamic. Subsequently, a new stability state of VSGs arguments can obtain from P-ω droop control like power and angular frequency. The transient condition of inverter control technique has been examined and analyzed in light of the recently issued Italian connection grid codes for active users [99]. The DG units connected through inverters are required to share with the voltage regulation, using a local control. Fig. 1.17 shows control scheme. The currents are transformed from the abc reference frame to the dq synchronous frame, then the output power of the inverter is regulated using id and iq current components by suitable PI controllers. Voltage and frequency controls are used to regulate the output power of converter which feeding to load to ensure stable operation of isolated microgrid. The park transformation harmonize the terminal voltage bus with inverter reference.

Another control method of inverter depends on the cascaded control construction is established [100]. The control system creates a firing pulse for inverter according to the specified control strategy, shown in Fig. 1.18. The commonly used constant P-Q control technique based on dq synchronous reference frame is embraced. Two different control modes are intended for various operating circumstances. For steady state operation, DGs feed the normal output power to distributed network. Nevertheless, during fault conditions, additional reactive power feeds to the connection between DGs and distributed network to improve the voltage profile. As well as the reactive current component will be modified depending on the disturbance with, constrain its value not more than 2 times of nominal.

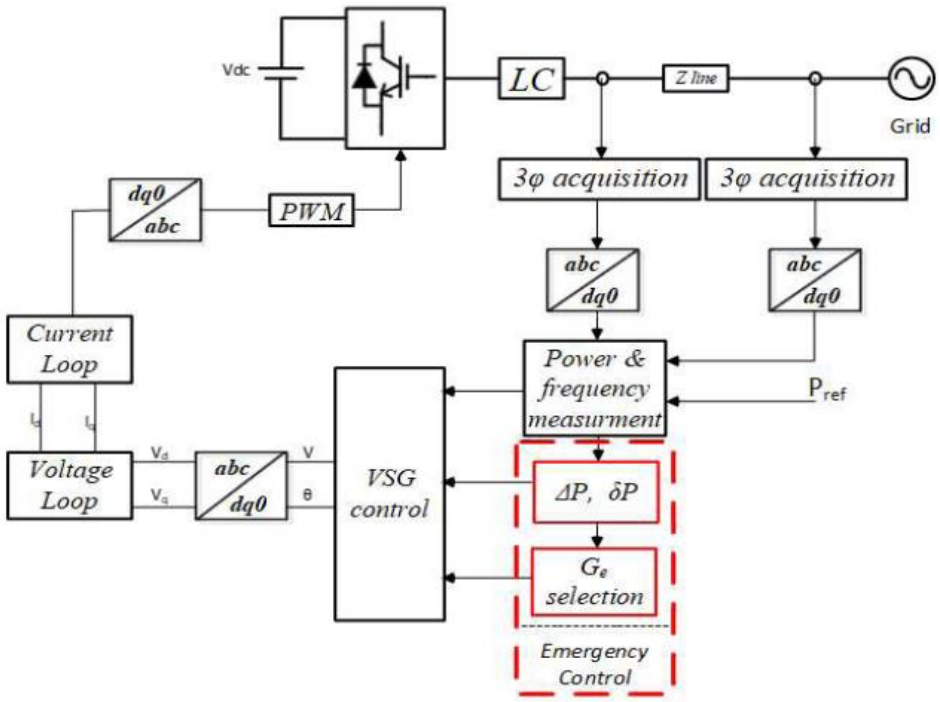

Fig. 1.16 ─ Control of grid-connected VSG [98]

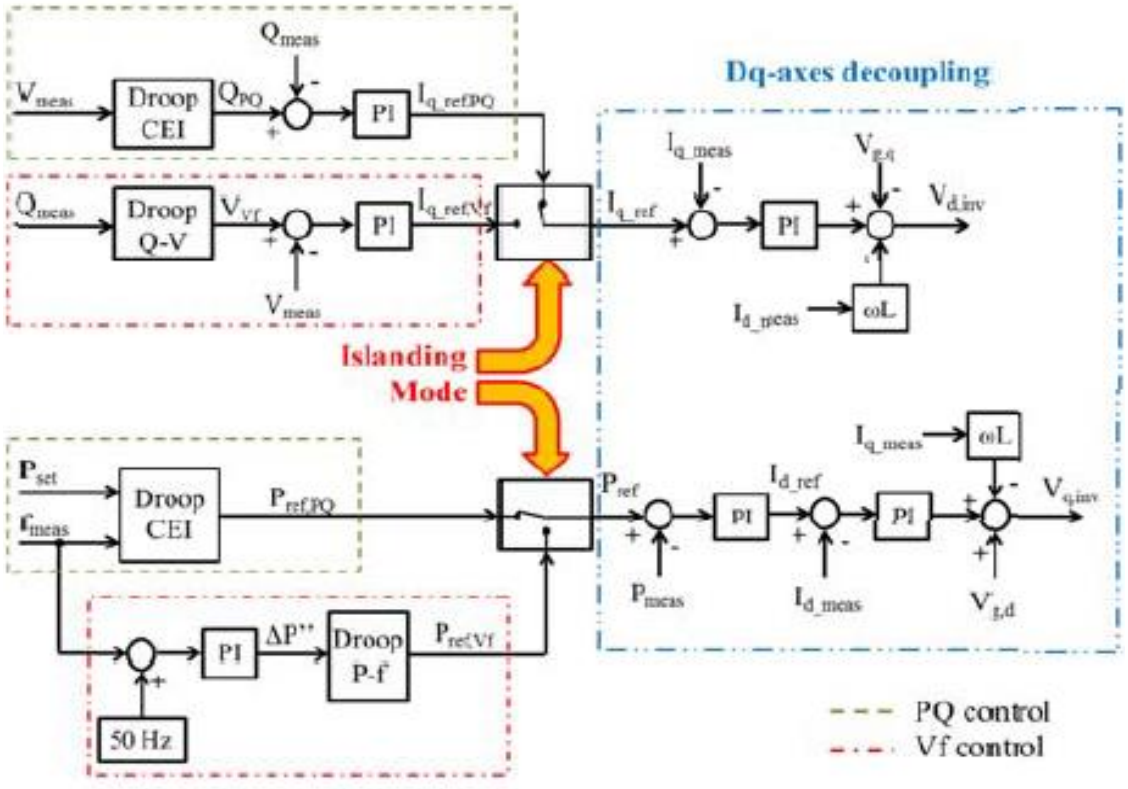

Fig. 1.17 ─ Control scheme [99]

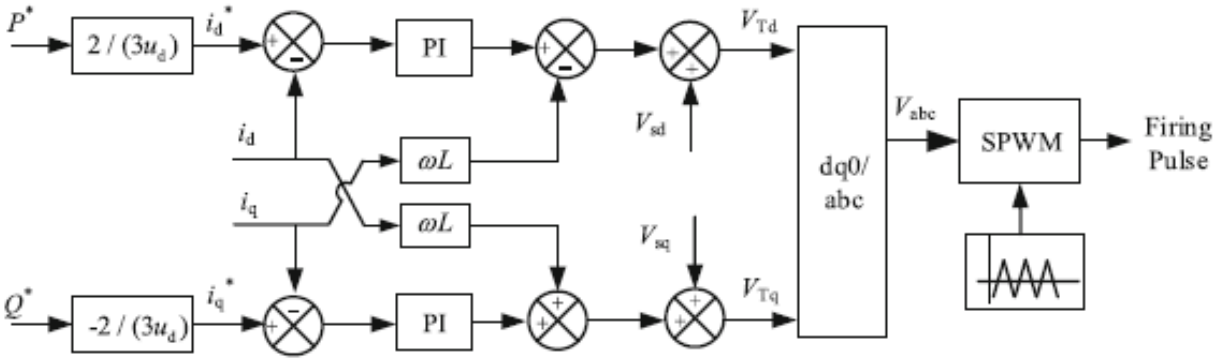

Fig. 1.18 ─ The structure of control system [100]

1.12 Smart Grid

The smart grid is subsystem incorporating of conventional power sources produced in 20th century and intelligent techniques produced in 21th century. The intelligent techniques provide to increasing the output power efficiency and control the power sources to obtain maximum power. There are two method to control smart grid using wire coupling or wireless like WIFI or power line transporter, etc... Many programs are created and upgraded to support and the executives control of smart grid, for example, SCADA system [101]. The main features of smart grid are improving system efficiency, increasing stability and enhancing the system operation. A hybrid PV source and wind power emerged to construct smart grid has been investigated [102]. Ref. [103] gives another type of smart grid with intelligent meters to improving the output load without any additional communication. A prototype of smart grid with smart technologies are furnished to increase the power quality of the system and secure the financial aspects [104]. The construction of smart grid is three parts: body of system part, control scheme part and load part. Analysis of microgrid contain PV source and wind power in detail presented in [105]. A real structure of smart grid contained to intelligent meter such as SCADA to collect and review the waveforms values during the day and give numerical description has been investigated [106].

Chapter 2. Protection Design Scheme of Grid Connected PMSG Wind Turbine

Due to the lack of electrical energy worldwide and the related environmental challenges, the penetration of wind energy is increasing quickly to reduce this lack. Wind turbine driven permanent magnet synchronous generator (PMSG) system is used for power generation, as a direct-driven application. PMSG has the advantages of ease of control, ease of realization of multi-pole machines and simple winding construction for low-speed applications, along with the capability to generate high power. Hence, PMSG has been found highly useful for wind power applications. Inverse-definite minimum time (IDMT) type overcurrent relay (OCR), and differential frequency relay (DFR) are the protection devices using for wind energy conversion system. These protection devices are mainly used for PMSG and utility system/ loads. The operational time of this relay is more or less inverse to the values of current and voltage, causing the relay to operate early when operating quantity is large and vice-versa. Thus, a definite minimum time is set to protect an electric system. OCR is widely used to limit the over-current flow in the power system; when faults occur in the power system, decreasing the impedance of faulty sections, resulting in massive output current from the supply. This is causing insulation damage, failure of electric equipment/ components and tripping the relays. For that, suitable fault protection systems are needed. Due to the widespread using PMSG for wind turbines of high rates several MW systems, this thesis focuses on studying the steady-state and transient analysis of wind turbine PMSG with the influence of low voltage ride-through technique to design the suitable protection system. Many types of researches focus on investigating the LVRT technique for wind turbine PMSG system under emergency condition.

2.1 Control Strategy

A. System Control Strategy

The system control block diagram of the control strategy is shown in Fig. 2.1. PMSG is connected to the grid through a full power back-to-back converter consisting of generator-side and grid-side VSCs, which matches the power capacity of the wind turbines. The generator-side converter controls the rotor speed of the PMSG to achieve a variable-speed operation with MPPT control. To regulate the wind turbine-generator rotational speed to guarantee the continuous operations at optimal tip speed ratio, the generator-side converter regulates the q-axis element of the stator current to adjust the electromagnetic torque when changing of wind speed. By controlling power factor, the grid-side converter feeds the produced active power from wind turbine generator to electric power system. Cascade PI control loops are implemented to control DC-link voltage and reactive power regulation by outer control loops and grid-side current regulator by inner control loops. Dual closed-loop control is implemented to control d-axis where the DC-link voltage loop feed the reference current to inner current loop and keep fixed value of DC-link voltage during steady-state conditions. Under fault conditions, the active and reactive current references of the main GSC are determined by the LVRT control strategy. The voltage drops due to the fault restrict the power output of the GSC. The output power of wind turbine PMSG must be adjusted to limit surplus power which causes DC-link overvoltage and effects on the operation of converters. The pitch control system is to maintain the speed of the wind turbine rotor at nominal value in strong winds. When the rotor speed is higher than the nominal speed, each blade will be rotated about its axis to reduce the angle.

B. LVRT control strategy

The control diagram of the braking resistor is illustrated in Fig. 2.2. When wind turbine speed or DC voltage reaches their limitations during the regulation process of LVRT, the braking resistor would be paralleled to DC-bus. DC capacitors and the PMSG are protected from over voltage in a quick response.

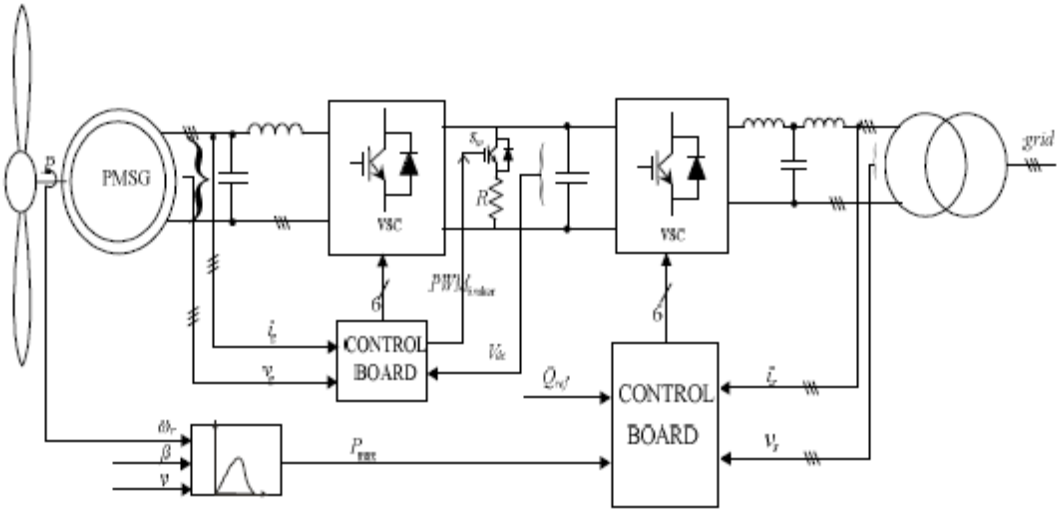

Fig. 2.1 ─ Control block diagram of PMSG

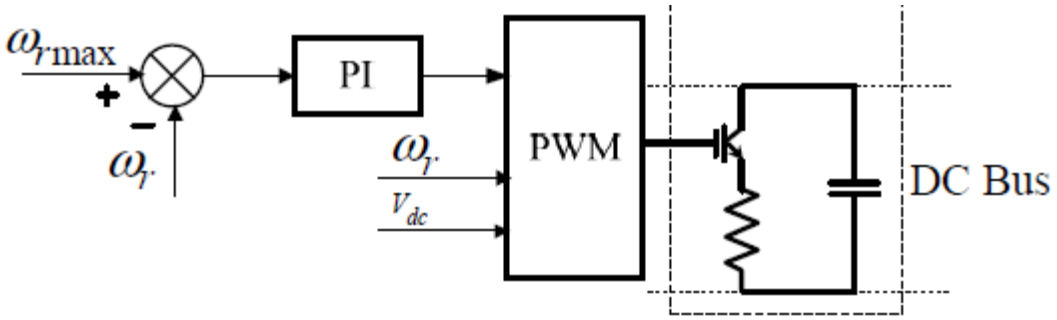

Fig. 2.2 ─ Control diagram of the braking resistor

Additionally, when the rotor speed reaches its limitation, the propeller pitch angle can be regulated to store the redundant energy. As is the common case propeller pitch angle varies 5~10 grade per second. It responses slowly compared with the LVRT request. Therefore variable propeller pitch control only operates as auxiliary method of the rotor speed regulation and the braking resistor ones.

2.2 IEC Method

The tripping current of relay which represents the thresholds for relay operation is calculated using the IEC 60909 method. It introduces impedance correction factors for transformers (K_T):

$$K_T = 0.95 \frac{C_{max}}{1+0.6x_T} \tag{2.1}$$

where x_T is the relative reactance of the transformer and C_{max} = 1.1 [107].

The tripping current of relay which represents the thresholds for relay operation is calculated:

$$I_{relay} = K_T I_{Fault} \tag{2.2}$$

2.3 Zafarana wind speed

Zafarana is the one place in Egypt which has high speed wind. Fig. 2.3 shows hourly variations of wind speed of Zafarana region in day. Table 2.1 shows Monthly Averaged Wind Speed at 50, 100, 150 and 300 m above the Surface of The Earth (m/s).The average values of wind speed of month and day of Zafarana region got from NASA site.

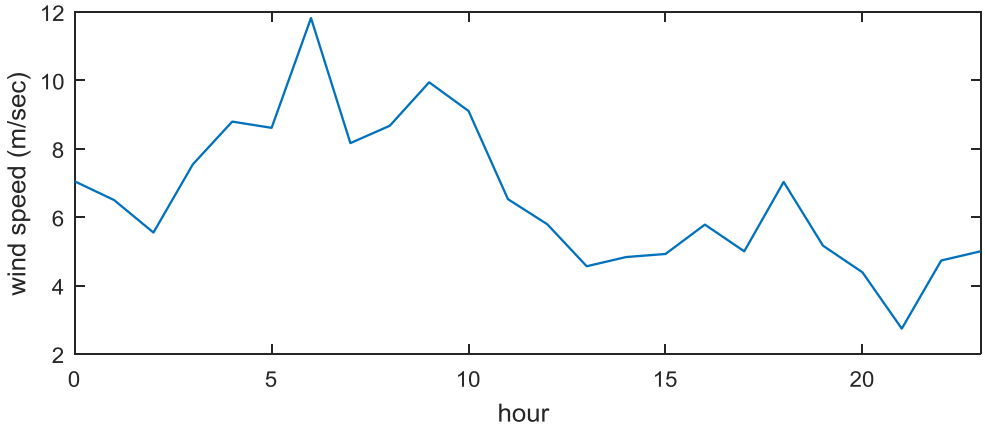

Fig. 2.3 ─ Hourly variations of wind speed of Zafarana region in day

Table. 2.1. ─ Monthly Averaged Wind Speed at 50, 100, 150 and 300 m above the Surface of the Earth (m/s)

Lat. 28.75 Long. 32.75	Jan	Feb	Mar	Apr	May	Jun	Jul	Aug	Sep	Oct	Nov	Dec	Annual Average
50m	4.22	4.33	4.78	4.86	4.97	5.11	4.93	4.83	4.86	4.75	4.11	4.13	4.66
100m	4.68	4.80	5.30	5.39	5.51	5.66	5.48	5.35	5.39	5.27	4.56	4.59	5.17
150m	4.97	5.10	5.63	5.73	5.86	6.02	5.82	5.69	5.73	5.60	4.84	4.88	5.49
300m	5.52	5.66	6.25	6.35	6.50	6.68	6.46	6.31	6.35	6.21	5.37	5.41	6.09

2.4 System description

Figure 2.4 shows PMSG wind turbine connected to grid.

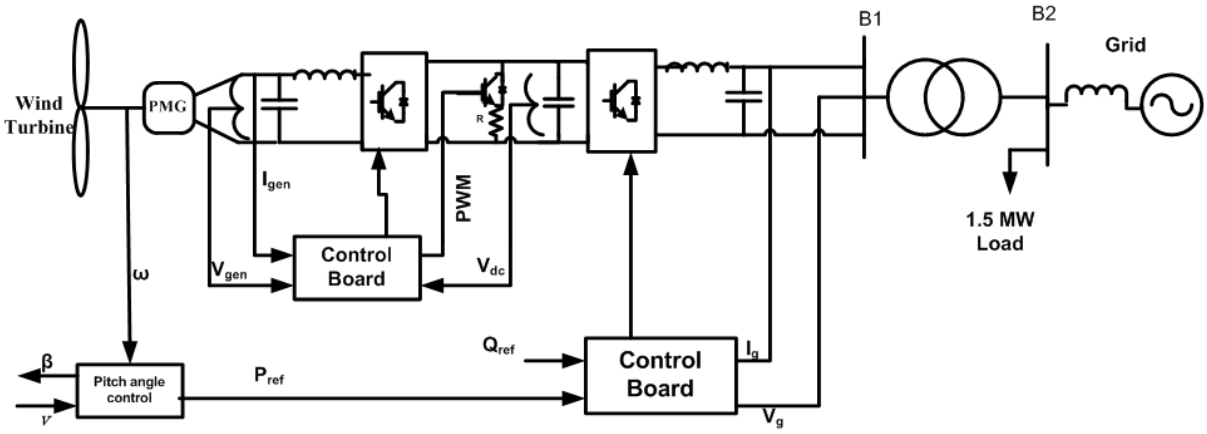

Fig. 2.4 ─ PMSG wind turbine connected to grid

As shown in Fig. 2.4, the wind turbine of 1.5 MVA, 575 V is connected to the electric grid. The wind turbine includes a power station transformer, rated to 2 MVA, 0.575/25 kV. The short circuit power of 25kV grid at point common connection is 300 MVA. The 2 MW load is connected to grid by bus B2.

2.5 Simulation studies

In the simulation studies, the steady state analysis was investigated in fixed and variable wind speed as well as the transient analysis in different time fault 140

m sec, 1 sec and islanding mode was investigated. Simulated circuit is given in appendix A.1.

2.5.1 PMSG wind turbine connected to grid

A. The steady state behaviour

1. Fixed speed:

The circuit shown in Fig. 2.4 was simulated in fixed wind speed, 12 m/sec which is the maximum value wind speed in Zafarana. Generator speed, terminal voltage, grid power, output power of wind turbine generator devices at B1 and load power values as given in Table. 2.2.

Table. 2.2. ─ The generator speed, voltage, grid power, turbine power and load power

The speed (p.u)	The voltage (p.u)	The grid power (kW)	The wind turbine power (kW)	The load power (kW)
1.06	0.98	85	1330	1415

2. Variable speed

The circuit shown in Fig. 2.4 was simulated in variable wind speed which is the wind speed during the day in Zafarana, shown in Fig. 2.3. Fig. 2.5 shows the temporal variation of (a) the generator speed and (b) turbine power. As shown in Fig. 2.5, the corresponding dependence of the output power of wind turbine PMSG , which varies in the range from 0 kW at a wind speed lower 2.7 m/s (minimum than cut-in wind speed) up to 1200 kW at wind speed 11.7 m/s.

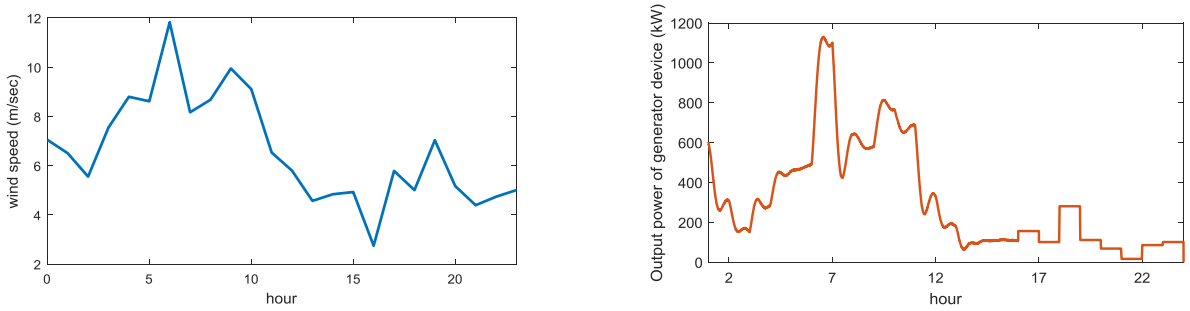

(a) (b)

Fig. 2.5 ─ (a) Temporal variation of wind speed and (b) Output power of wind turbine PMSG at B1

Functional Characteristics.

Fig. 2.6 shows P-V characteristic of 1.5 wind turbine PMSG. Fig. 2.7 shows I-V characteristic of 1.5 wind turbine PMSG. From Figs. 2.6 and 2.7, output power and current increase with increasing output voltage of converter.

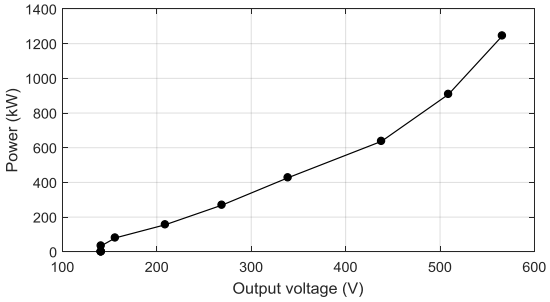

Fig. 2.6 ─ P-V characteristic of 1.5 wind turbine PMSG

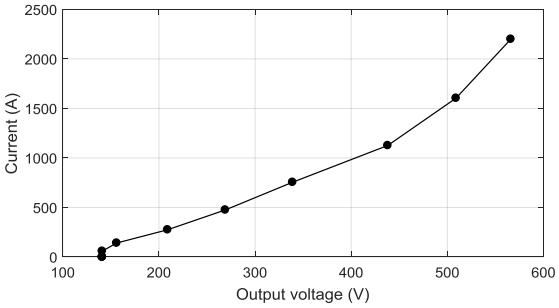

Fig. 2.7 ─ I-V characteristic of 1.5 wind turbine PMSG

B. Three- phase- to- ground fault:

A three-phase-to-ground fault is applied to the connection point between the wind turbine and the grid at t =7 sec for duration of 140 msec (detection time and operation time of the breakers is 140 ms) [108], 1 sec and islanding mode, in Fig. 2.4. Figure 2.8 shows the results of simulation of three-phase-to-ground fault behind the transformer for the Figs of the generator speed (Fig.2.8.a) and the current at the output of the wind turbine converter (Fig.2.8.b) with and without LVRT. The generator speed increases in the range from 1.065 at the time of the occurrence of short-circuit to 1.1 at t = 7.4 s; decreases from 1.1

to 1.055 in the interval t = (7.4–8.6) and is oscillatory, with a period of 2.4 s. converges to an initial speed of 1.065. With LVRT, the amplitude of the oscillations decreases to the level (1.08-1.065). As shown in Fig. 2.8 (b), after clearance fault, the output current of the converter with LVRT decreases almost instantly and, with a small range of oscillations, quickly enough recovers to a steady state, while without LVRT transients are more severe Figure 2.9 shows the temporal variation of the generator speed, grid power, turbine power and load power of time fault of 1sec. During the fault, the PMSG is isolated with the converter and DC voltage capacitor using LVRT control, which is working as STATCOM, DC chopper, is connected in DC-link to consume extra energy for keeping DC voltage in constant value. Fig. 2.10 shows PMSG during fault, temporal variation of the crowbar pulses of LVRT in different fault time 140 msec and 1 sec. The grid power is oscillated to -10000 kW where grid feeds the fault current to 2000 A. The wind turbine power and load power reached to zero and recovered pre-fault values when fault cleaned. Table. 2.3 shows voltage and current during the fault and time required recovering pre-fault values. From Table. 2.3, the voltages and currents recovered the pre-fault values within small time less than 0.1 sec except wind turbine within 1 sec.

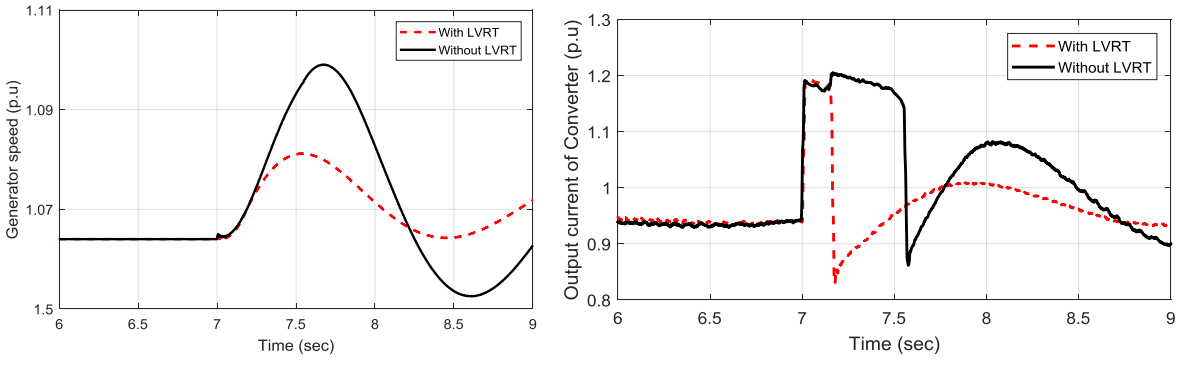

(a) (b)

Fig. 2.8 ─ The temporal variation of (a) the generator speed and (b) Output current of wind turbine PMSG converter of time fault 140 m sec with and without LVRT

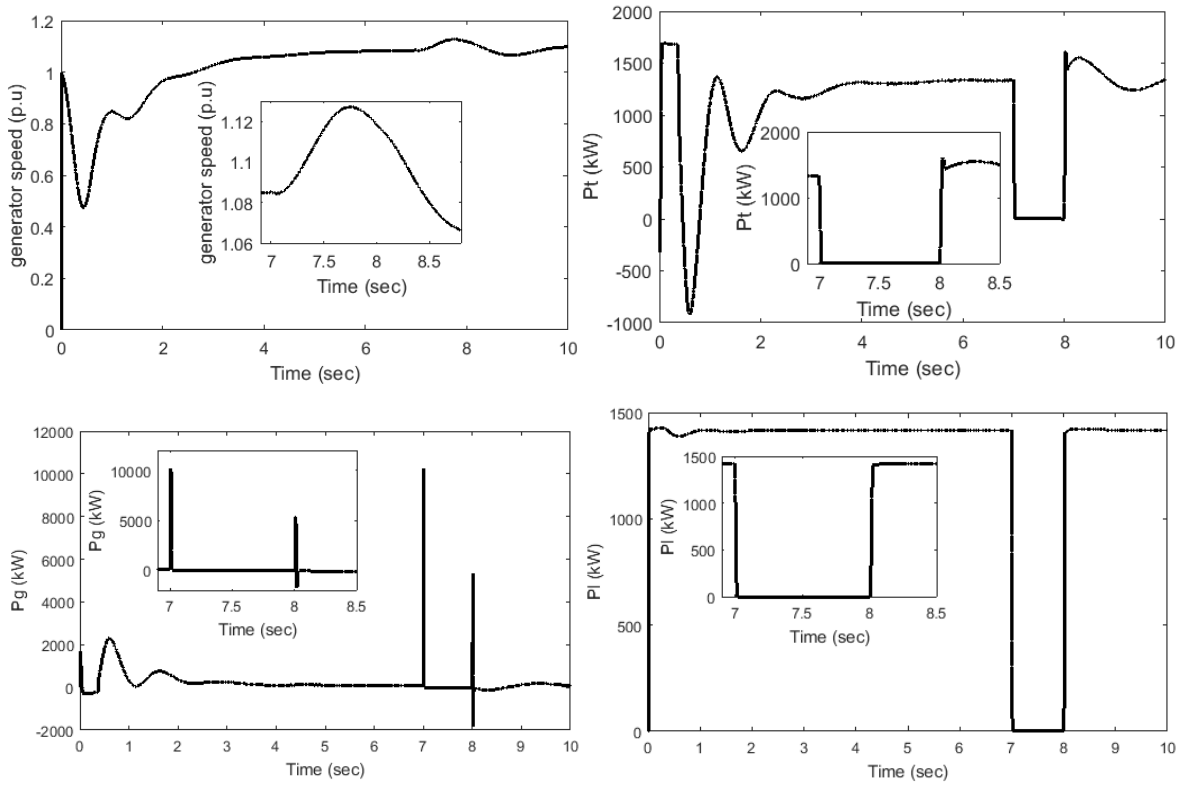

Fig. 2.9 ─ Temporal variation of the generator speed, grid power, turbine power and load power of time fault 1 sec

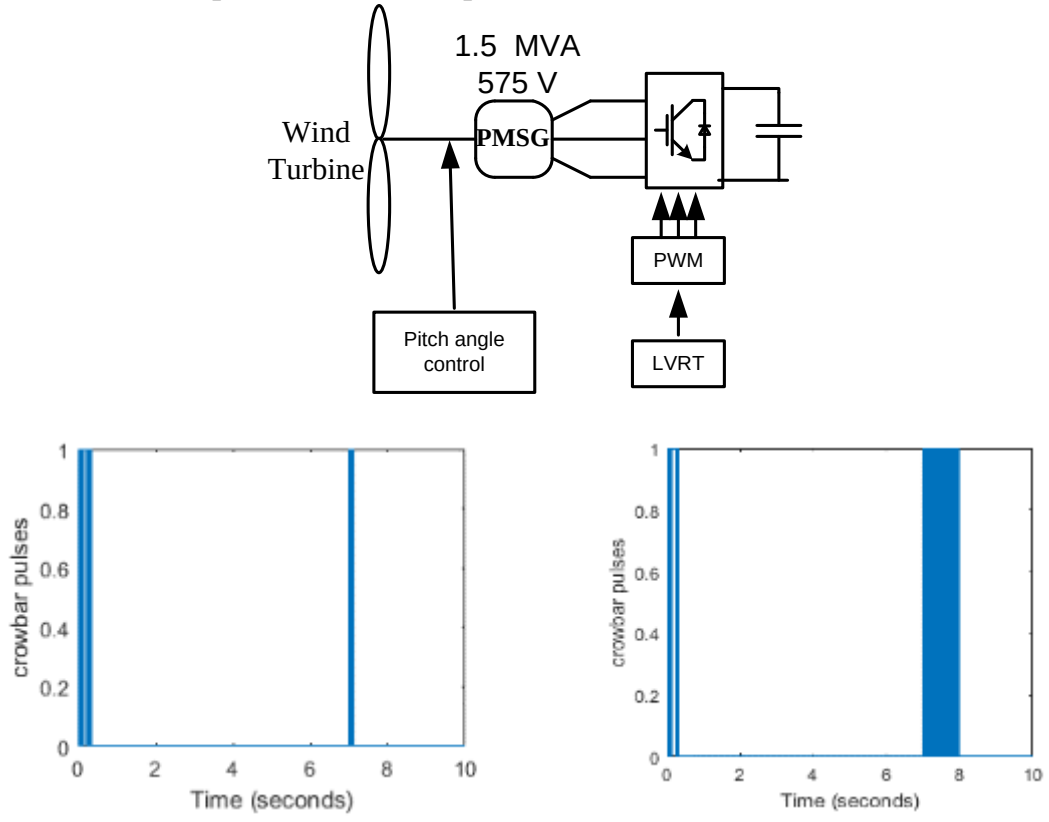

Fig. 2.10 ─ PMSG during fault, temporal variation of the crowbar pulses of LVRT in different fault time 140 msec, 1 sec

Table. 2.3. ─ Voltage and current during the fault and time required to recover pre-fault values

The time of fault	pre-fault value				During the fault				Pre-fault recovery after fault			
	Voltage (kV)	Current (A)			V (kV)	Current (A)			Time to recovery voltage value	Time to recovery current value (sec)		
		I_g	I_l	I_t		I_g	I_l	I_t		I_g	I_l	I_t
140 msec	24.49	8.5	48	46	0	2000	0	58	0.08	0.1	0.1	1
1 sec	24.49	8.5	48	46	0	2000	0	58	0.02	0.12	0.09	1
Islanding mode	24.49	8.5	48	46	0	2000	0	58				

Transient analysis of grid connected wind turbine PMSG with distributed loads.

Fig. 2.11 shows grid connected wind turbine PMSG with two feeders. As shown in Fig. 2.11, the load divided into two feeders 1 and 2. The maximum load is connected to feeder 1 (1.499 MW) and small load is connected to feeder 2. A three-phase-to-ground fault is applied at terminal of small load with different length (5 km and 0.5 km) of feeder 2 to investigate the effect of location of fault near or far from wind turbine PMSG (DG). Fig. 2.12 shows (a) output current of inverter of wind turbine and (b) grid current. As shown in fig. 2.12 (a), the output current of inverter of wind turbine increased to 63 A where the control of inverter limit the current in two cases 5 km and 0.5 km feeders. As shown in fig. 2.12 (b), the grid current of 0.5 km feeder is greater than 5 km feeder. After clear the fault, the output current of inverter of wind turbine oscillated to reach pre-fault value.

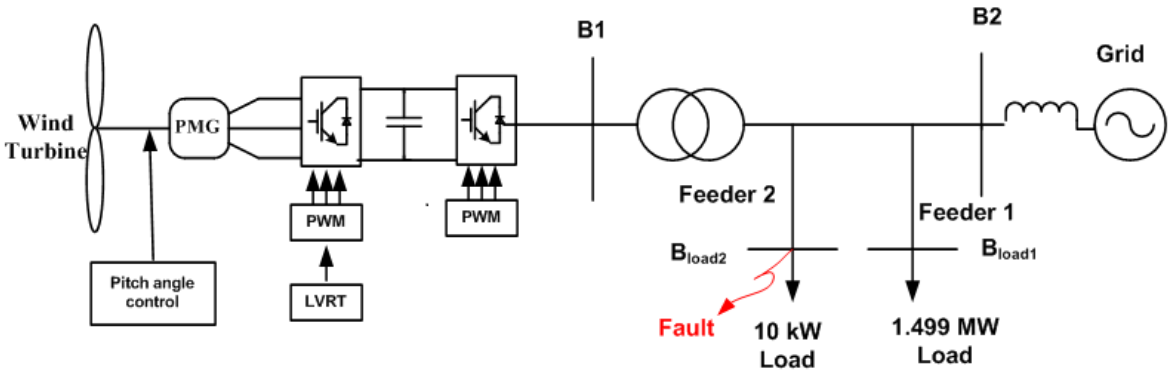

Fig. 2.11 ─ Grid-connected wind turbine PMSG with two feeders

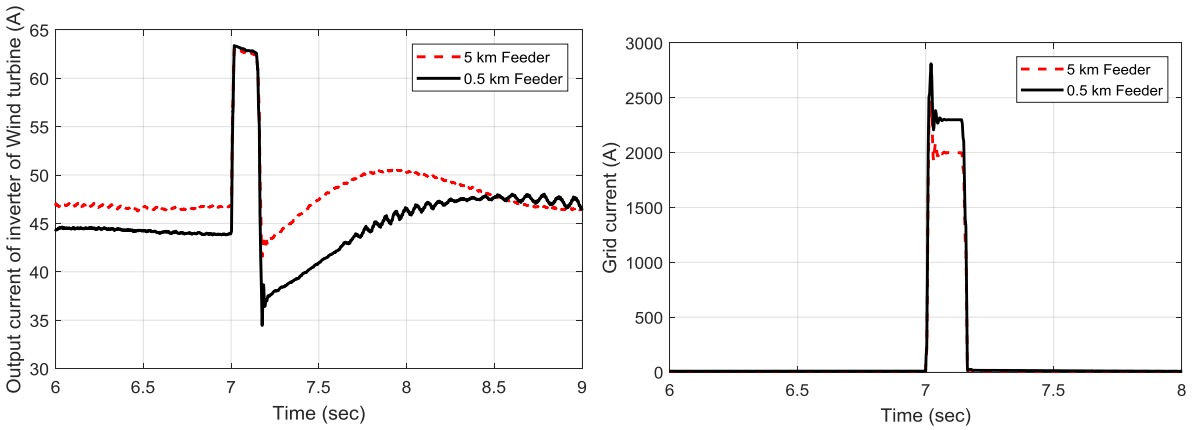

(a) (b)

Fig. 2.12 ─ (a) output current of inverter of wind turbine and (b) grid current

Equivalent circuit during fault.

During the fault wind turbine PMSG considers as source in series different reactances depending on the case of current peak currents (in the interval (0–0.02) sec, ultra-transient currents and voltage (in the interval (0.02–0.1) sec and steady-state short-circuit currents, shown in Fig. 2.13. Table 2.4 shows sub-transient, transient and steady state reactance values of 1.5 MVA wind turbine PMSG with values of current. Fig. 2.14 shows the terminal voltage. Fig. 2.15 shows the output current with DC component during fault. From table 2.4, DC component can be plotted by the equation: $(4671-3552)*e^{(-t/0.02)}+3552$. DC component is different from Synchronous generator because the control limit current during fault.

Table 2.4 Sub-transient, transient and steady-state reactance values of 1.5 MVA wind turbine PMSG with values of current

E(V)	I(A)	I'(A)	I''(A)	x (ohm)	x' (ohm)	x''(ohm)
500	1470	3552	4671	0.34	0.14	0.11

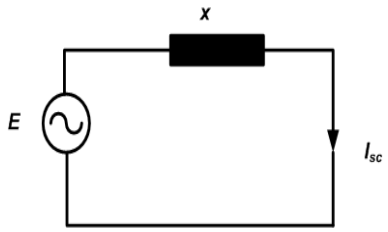

Fig. 2.13 ─ Equivalent circuit of DG during fault

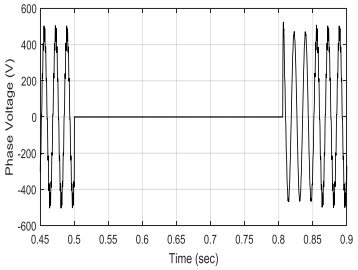

Fig. 2.14 ─ Terminal voltage during fault

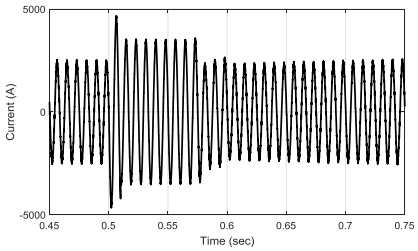

Fig. 2.15 ─ Output current

C. Relay design of PMSG wind turbine:

The tripping current of relay, which represents the thresholds for relay operation, is calculated using IEC method. The relative reactance of the transformer, x_T=0.08, C_{max}=1.1: $K_T = 0.95\frac{C_{max}}{1+0.6x_T} = 0.95\frac{1.1}{1+0.6*0.08} = 0.997$

From Table. 2.3 $I_{Fault} = 2000\ A$. The adjustable relay current of circuit breaker CB1: $I_{relayCB1} = K_T I_{Fault} = 0.997 * 2000 = 1994\ A$

Figure 2.16 shows the overcurrent relay of PMSG wind turbine

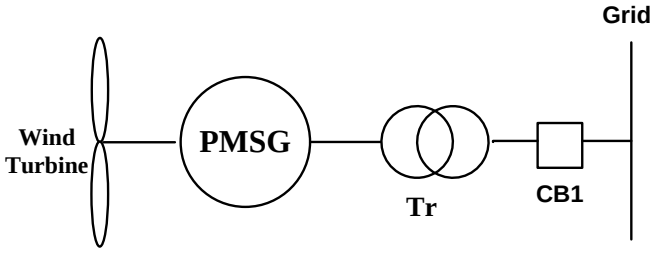

Fig. 2.16 ─ Overcurrent relay of PMSG wind turbine

2.5.2 PMSG wind farm connected to grid

For the wind farm consists of 75 units each of 1.5 MVA PMSG wind turbines which connected to the electric grid. A power station transformer is rated to 0.575/25 kV. The tripping current of relay which represents the thresholds for relay operation, is calculated using IEC method. Figure 2.17 shows the simple protection scheme of the grid-connected wind farm where the circuit breaker is using every 10 units. The fault current of 10 units wind turbines which is calculated using Matlab Simulink, is $I_{Fault} = 3.6\,kA$. The adjustable relay current of circuit breaker CB_{WF}:

$$I_{relayCBWF} = K_T I_{Fault} = 3.59\,kA$$

The 8 circuit breaker are using for wind farm. The total fault current of wind farm which is calculated using Matlab Simulink, is $I_{Fault} = 7.5\,kA$. The adjustable relay current of circuit breaker CB_{grid}:

$$I_{totalrelay} = K_T I_{Fault} = 7.48\,kA.$$

$$I_{relayCBgrid} = I_{relayCBWF} * transformer\ ratio = 7.48 * \frac{0.575}{25} = 1720\,A$$

As shown in Fig. 2.17, the protection system at the wind farm is a combination of 4 hierarchically redundant blocks: the wind turbine block - protection of the wind turbine from exceeding the permissible rotation speed, PMSG from internal damage, electronic keys of inverters, and the power unit as a whole (the block is switched off by CB1 relay); sectional block - protection of a block set of wind turbines against damage and failures of power switches and directly to the section to which the wind turbines are connected (section disconnection is carried out by CB_{WF} relay); transformer protection (shutdown by an appropriate high voltage circuit breaker); High voltage switchgear, to which a power line is connected connecting the wind farm with the main high voltage distribution network. Power line disconnection is carried out by CB_{grid} relays. The coordination of switching

by relays depends on the zone of occurrence of the fault: each subsequent zone reserves the previous one.

Relay protection kits for all zones except the first one does not have specific features and can be implemented with standard panels. Wind turbine protection includes not only electrical but also mechanical and electronic protection principles, including protection against overcurrent of converters.

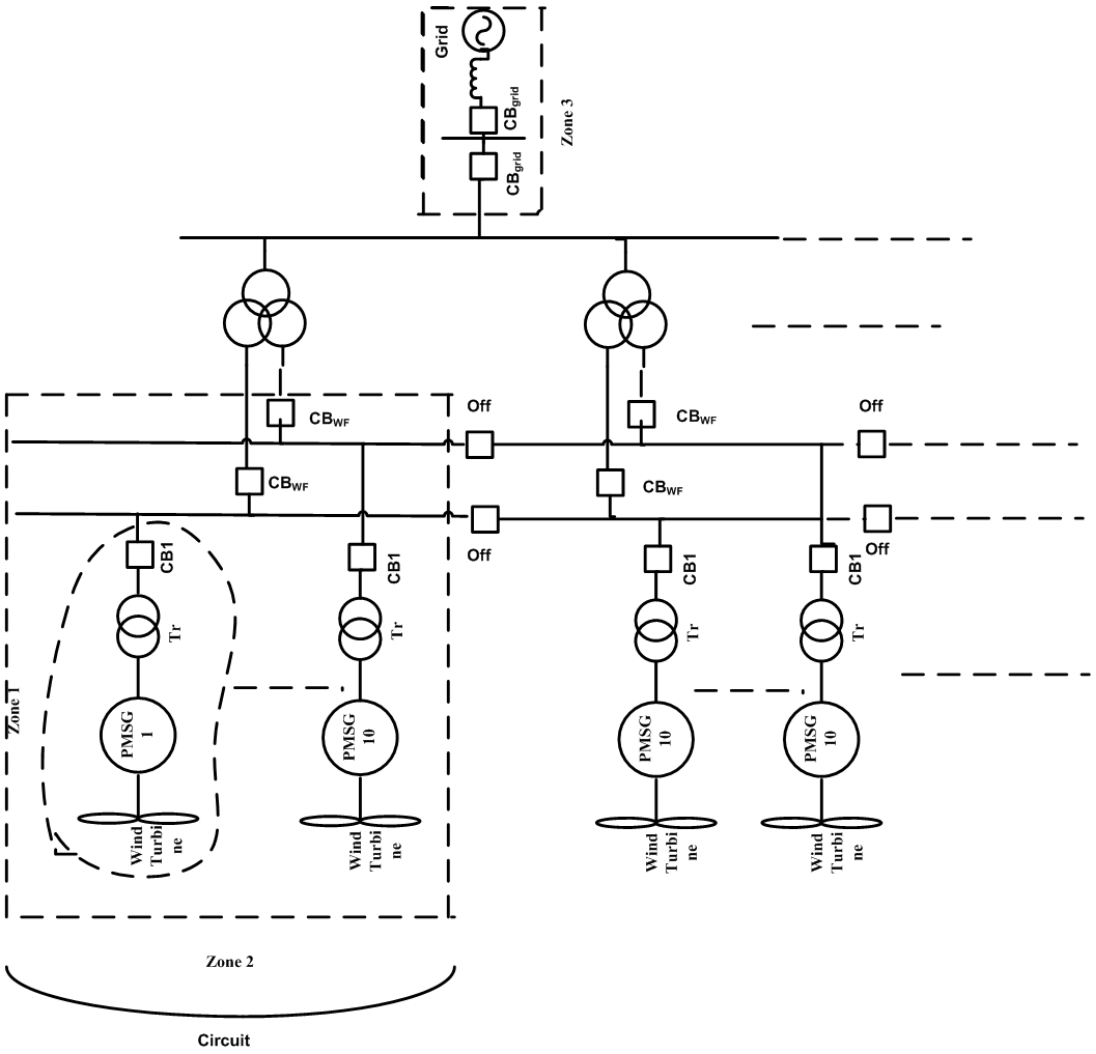

Fig. 2.17 ─ Simple protection scheme of grid connected wind farm

Chapter 3. Digital Control strategy for SPWM MPPT of PV System with Three-Phase NPC Three-Level Converter

Photovoltaic (PV) systems have been used in remote applications as low cost for example wireless highway call boxes, and standalone power generation units. PV generation is gaining importance as distributed generator causing its advantages, like disappearing of fuel price, simple maintenance, quiet, and nonappearance of rotating parts. The actual energy conversion efficiency of the PV module is slightly small and depends on climate circumstances and output load. For that, many techniques are used to obtain high possible efficiency by designing all parts of the PV systems are working in optimized mode. To get high efficiency and maximum power point, the PV system must be operated at the maximum point of PV system. For that, MPPT technique is important for PV system. The MPPT control is complex issue because of the maximum power point changes with irradiation and temperature. Many MPPT methods are implemented to overcome this problem as perturb and observe methods. Interfacing converter between DC side (PV) and AC side (electric network or load) is responsible to feed power to AC side. To connect PV system to electric power system, it is needed to achieve the requirement of grid codes.

3.1 System Modelling

Figure 3.1 shows the block diagram of PV system

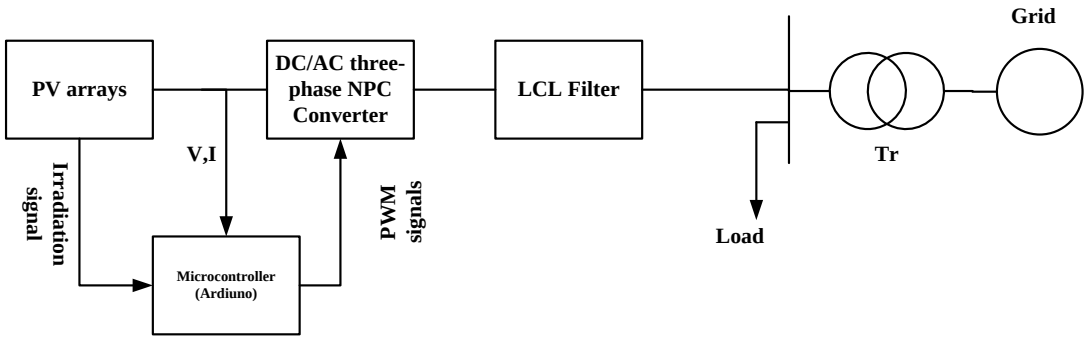

Fig. 3.1 Block diagram of PV system

3.2 Maximum Power Point Tracking (MPPT)

In this model, Perturb-and-Observe (P&O) method is used.This method works by calculating the current output power for step (*P (k)*) for the current values of voltage ($V_{ph}(k)$) and current ($I_{ph}(k)$), then compare it with the previous output power values (*P (k-1)*). In case of power increases, change the voltage in the same direction as the previous change. Otherwise, change the voltage in the opposite direction of the previous one [45]. Fig. 3.2 shows the flow chart of the P&O method.

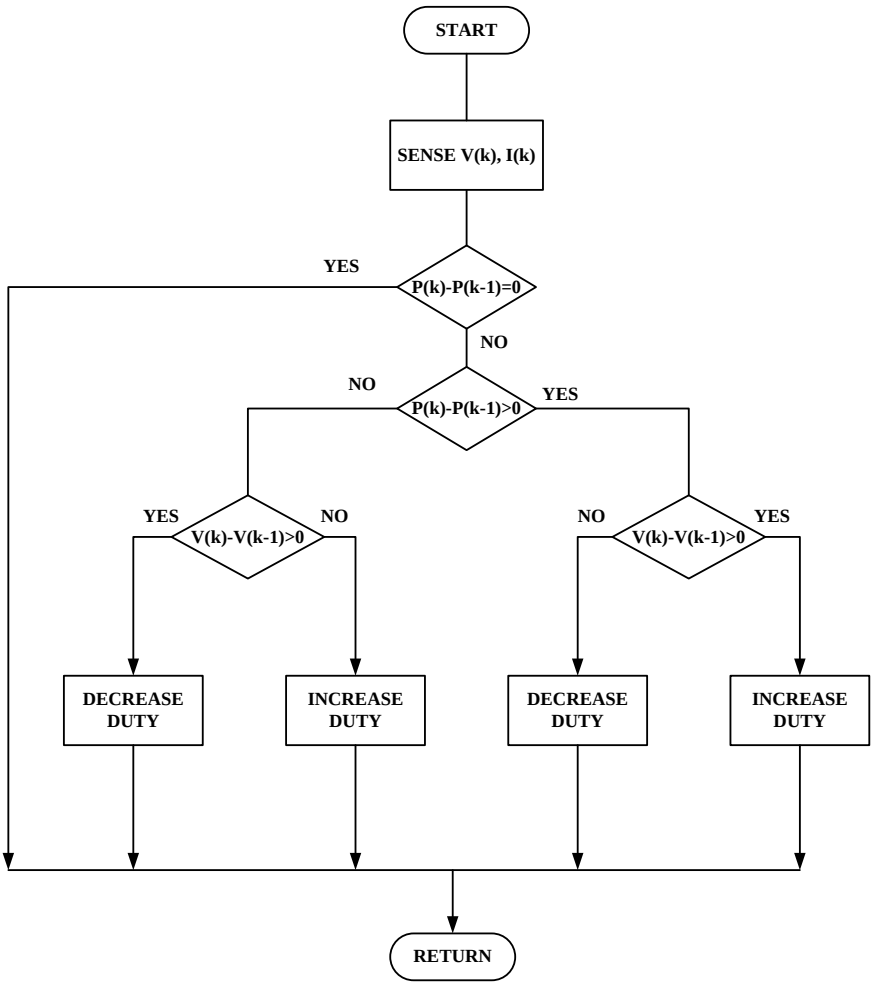

Fig. 3.2 ─ The flow chart of the P&O method

The power-voltage (P-V) characteristics of a photovoltaic module operating under different intensities of global solar radiation ranging from 100 W/m^2 to 1000 W/m^{2}is shown in Fig. 3.3. I_{sc} increases in proportion with increasing insulation, and V_{oc} slightly increases with increasing insulation, Fig. 3.3a.

Maximum power P_{max} increases highly with insulation, Fig. 3.3b. As shown in Fig. 3.3b, there is a unique point on the characteristics at which the photovoltaic power is maximum. This point is termed as the maximum power point (MPP). Due to high cost of solar cells, it must be ensured that the photovoltaic array operates at all times to provide maximum power output.

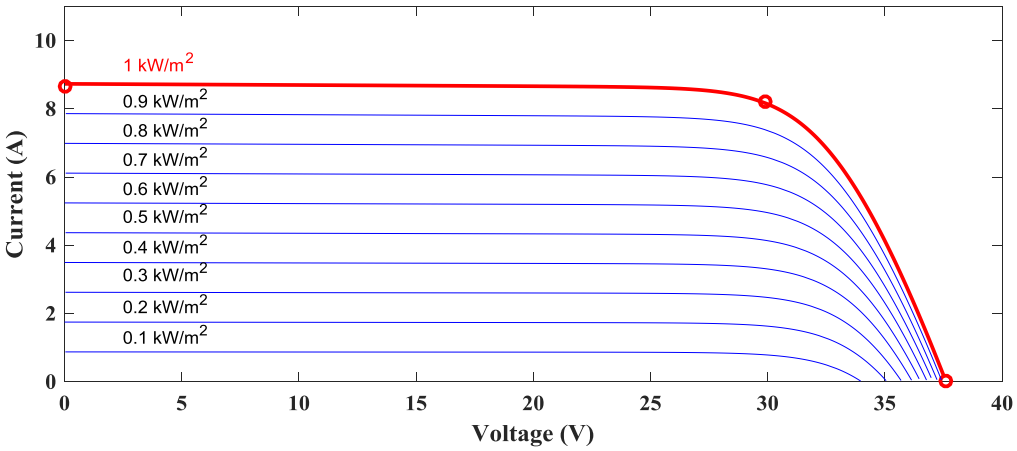

Fig. 3.3a ─ I-V characteristics of a photovoltaic module

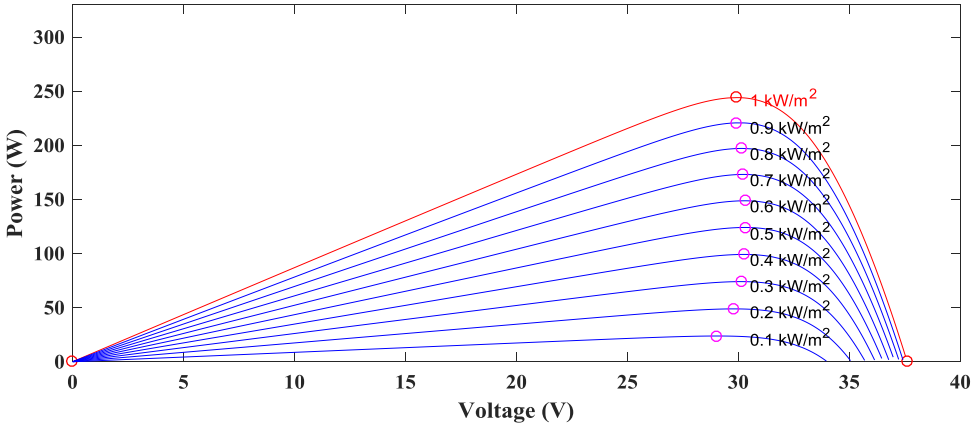

Fig. 3.3b ─ P-V characteristics of a photovoltaic module

3.3 Three-level Neutral point Clamped converter (NPC)

The number of levels of a converter is the number of steps in the voltage of the output terminals with respect to any arbitrary internal reference point. Three level NPC characterized by obtaining the lowest THD (36.22%) and very high efficiency (98.93%) in comparing with other multilevel converters topologies mentioned before [109]. The voltage and current waveforms for every part as

IGBT switches and diodes can be obtained by designing three-phase inverters to treat the losses. Fig. 3.4 shows a simple 3L-NPC. As shown in fig. 3.4, there are three legs which are denoted by a, b, c.

Each leg has four switches and two diodes. For ideal switch, V_a is the output voltage for phase a, $V_L$and I_L are the inductor voltage and current, L is the AC-side filter inductance, r_L is the winding resistance related to the inductance L, R_{Load} is the load resistance and V_N is the neutral point voltage. Starting from V_j=a, b, c, a KVL can relate $V_j$to V_N as below [110].

$$V_j = L\frac{dI_{Lj}}{dt} + I_{Lj}r_L + I_{Lj}R_{Load} + V_N, \quad (j = a, b, c) \tag{3.1}$$

The neutral point voltage can be related to phase voltages in three-phase systems.

$$V_N = (V_a + V_b + V_c)/3 \tag{3.2}$$

Combining (2.3) with (2.4) as well as doing further rearrangement for getting two independent inductor currents leads to

$$\frac{dI_{La}}{dt} = -\frac{I_{La}(r_L + R_{Load})}{L} + \frac{1}{3L}(2V_a - V_b - V_c)$$
$$\frac{dI_{Lb}}{dt} = -\frac{I_{Lb}(r_L + R_{Load})}{L} + \frac{1}{3L}(2V_b - V_a - V_c) \tag{3.3}$$

In order to avoid the inner switches suffering from high voltage, the outer two switches are not allowed to be in on state at the same time. Therefore, there are three different voltage outputs, and this is the reason why it is called three-level [111].

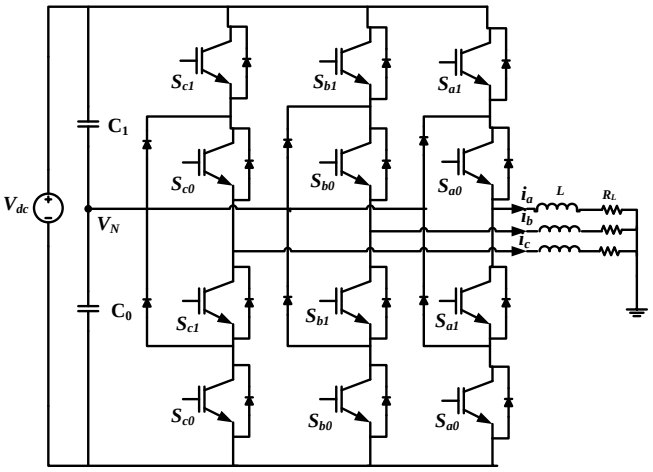

Fig. 3.4 ─ Topology of the Three-phase Three-level NPC converter

3.4 Design of LCL filter

The LCL filter designing is considered into two parts. First part deals with the design of inverter side inductance (L_i) and the second part deals with the design of grid side inductance (L_g) and capacitance (C_f) which is considered as L_gC_f second order low pass filter. Fig. 3.5 shows the circuit diagram of LCL filter. The grid side inductance designs using the relation with inverter side inductance where the ratio between grid side inductance and converter side inductance depends on the ripple current attenuation. The simplified equations for the designing of LCL filter are expressed as following [46]:

$$L_i = \frac{V_s}{2\sqrt{6}f_s i_{ripple}} \tag{3.4}$$

$$C_f = \frac{0.05}{\omega_n Z_{base}} \tag{3.5}$$

$$Z_{base} = \frac{V_{sll}^2}{P_n} \tag{3.6}$$

$$L_g = L_i \tag{3.7}$$

where V_s is grid r.m.s. phase voltage, f_s is inverter switching frequency, i_{ripple} is expressed as a percentage of the inverter current I_{inv} which lies in the range 5%-25%, L_g is grid side inductance, L_i is inverter side inductance, C_f is capacitance of LCL filter, P_n is inverter rated power and ω_n is operating frequency.

Splitting the total filter inductance L_T into L_i (inverter-side inductance) and L_g (grid-side inductance) follows the relationship:

$$L_g = r * L_g \tag{3.8}$$

where r (0.4<r<2) is the inductance index [112-114].

However, the following limitations on the filter parameters have been taken into account [112]:

- The total inductance (L_T=L_i+L_g) should be less than 0.1 (p.u) because it results in ac voltage drop during operation. Otherwise, a higher dc-link voltage will be required and this results in higher switching losses. However, for high power levels, the main aim is to avoid the saturation of the inductors L_i and L_g.

- The capacitance is limited by the reactive power limit (normally this limit is less than 5%).

- To avoid resonance problems, the resonance frequency ω_{res} of the filter should be higher than 10 times the grid frequency ω and smaller than half of the switching frequency ω_{sw}.

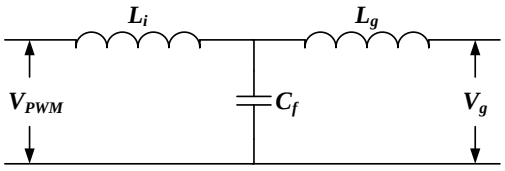

Fig. 3.5 ─ The circuit diagram of LCL filter

3.5 Sinusoidal pulse width modulation

The generation of a sinusoidal PWM signal are used in more applications in industries, which can be generated by comparing a sinusoidal reference signal with a sawtooth carrier wave. The width of each pulse is varying proportionally to the amplitude of a sine wave that evaluated at the center of the same pulse. The output frequency of the inverter can be calculated by using the frequency of the reference signal. The rms output voltage can be controlled by modulation index, which is controlled by peak amplitude. The gating signal can be produced by using the variable frequencies unidirectional sawtooth carrier wave [115]. Fig. 3.6 shows one signal SPWM generation of specific frequency of sawtooth. The frequency of PWM represents the amount of time taken by PWM to complete one cycle. In order to produce variable values, the sawtooth frequency can be changed In order to make the analysis of control PWM it is necessary to define some parameters. The index of amplitude modulation m_a and index of frequency modulation m_f.

$$m_a = \frac{V_{ref}}{V_{saw}} \quad , \qquad m_f = \frac{f_{saw}}{f_{ref}} \tag{3.9}$$

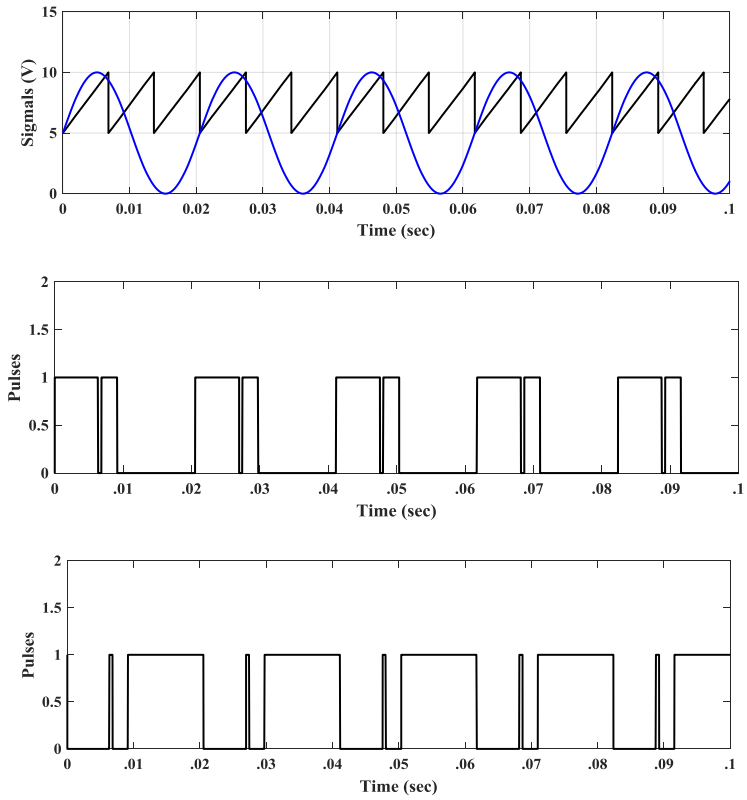

Fig. 3.6 ─ One signal SPWM generation of specific frequency of sawtooth

3.6 Microcontroller

The Arduino Nano 3x microcontroller is a small, complete, and breadboard-friendly board based on the ATmega328. Fig. 3.7 shows Microcontroller Arduino Nano Chip. This microcontroller has similar functions of the Arduino Duemilanove, but in a different package. the drawback of this microcontroller is absence of DC power jack where it works with a Mini-B USB cable instead of a standard one. Table. 3.1. shows Ardino specifications.

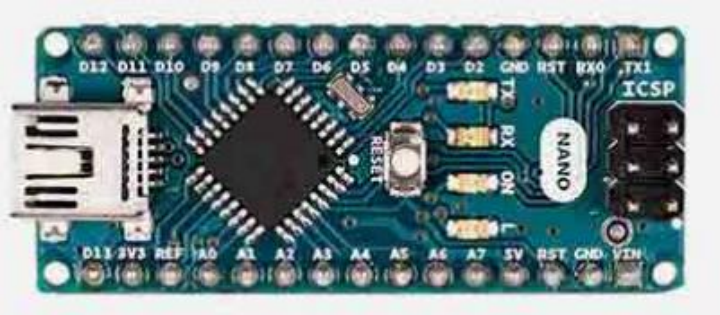

Fig. 3.7 ─ Micro-controller Arduino Nano Chip

Table. 3.1. ─ Ardino specifications

Specifications	Values
Microcontroller	ATmega328
Operating Voltage	5V
Power Consumption	19 mW
clock speed	16 MHz

The Arduino clock frequency is 16 MHz that a pulse-width-modulated (PWM) signal, using the hardware timers on the ATmega328 might be the way to go. This gives very precise and consistent timing and allows to toggle a pin as fast as f_{PCU}. The delay time response of Arduino and its effect on simulation based model are negligible.

3.7 Control strategy

MPPT curve of PV array is obtaining using P&O method. In this method, the RMS value of output voltage of inverter is changing using SPWM. SPWM is controlled by amplitude of sine wave signal that compares with saw tooth signal. To get MPP of PV array in the variable irradiation, we are using the following steps:

1) Irradiation is changing from 100 W/m^2 to 1000 W/m^2 by step 100.

2) Micro-controller Arduino Nano is changing the amplitude of sine wave signal of SPWM to get MPP in specific irradiation using P&O method.

3) Recording MPP with the amplitude of sine wave signal of SPWM.

From the above steps, we are obtained MPPT curve with the amplitude of sine wave signal of SPWM. This curve is used as look-up table of Micro-controller Arduino Nano with curve fitting.

Digital control strategy is using to PV system by Micro-controller Arduino Nano as the following:

1) Measure the value of irradiation to Micro-controller Arduino Nano.

2) Using Look-up table of MPPT, Micro-controller Arduino Nano is adjusting the amplitude of sine wave signal of SPWM.

3.8 System Description

Figure 3.8 shows grid connected PV system. As shown in Fig. 3.8, PV array is 800 modules, each module peak power is rated 250 W at 35 V and 5 A, the number of Series-connected modules per string is 20 and the number of parallel strings is 40. PV array connected to three-phase three-level NPC converter controlled using SPWM of MPPT control. Three-phase LCL filter is used to connect the inverter output voltage to Three-phase load (stand-alone mode) or the grid (grid-connected mode). Digital micro-controller (Arduino Nano) controls the output voltage of inverter at maximum power point by generating SPWM signals. Digital micro-controller measures the signals of PV voltage and current to calculate maximum power point by P&O method.

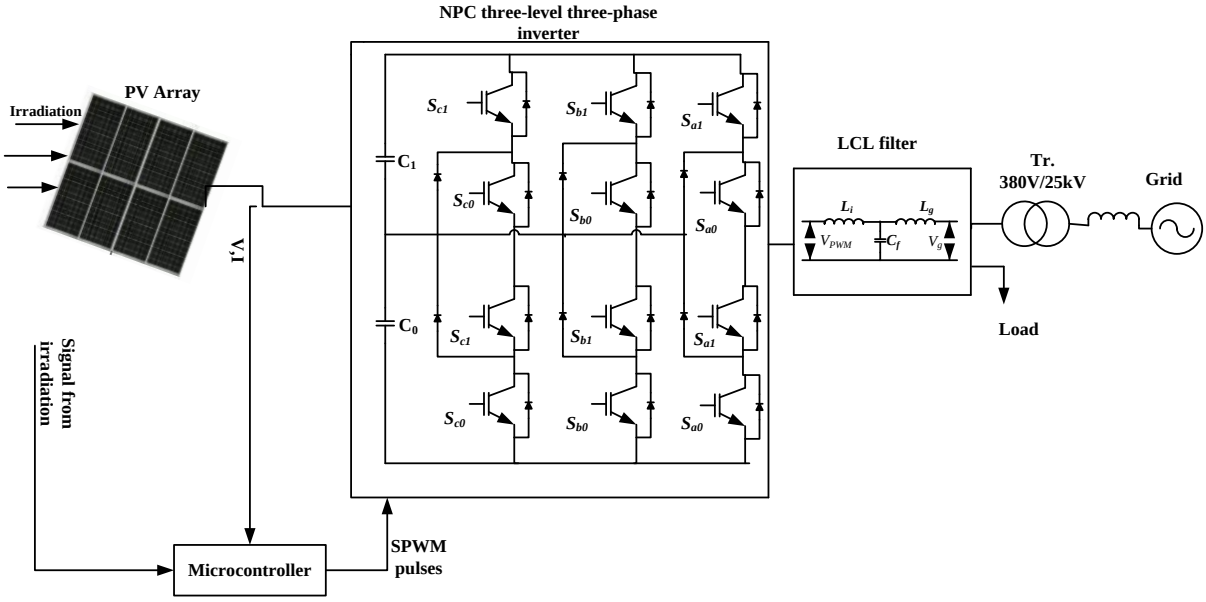

Fig. 3.8 Grid connected PV system

3.9 Simulation Results

Stand-alone and grid connected PV system is simulated using MATLAB/SIMUINK with coupling Micro-controller Arduino Nano. Arduino Nano is coupling with MATLAB/SIMUINK using USB cable. Fig. 3.9 shows MATLAB/SIMUINK of PV system connected Arduino Nano using USB.

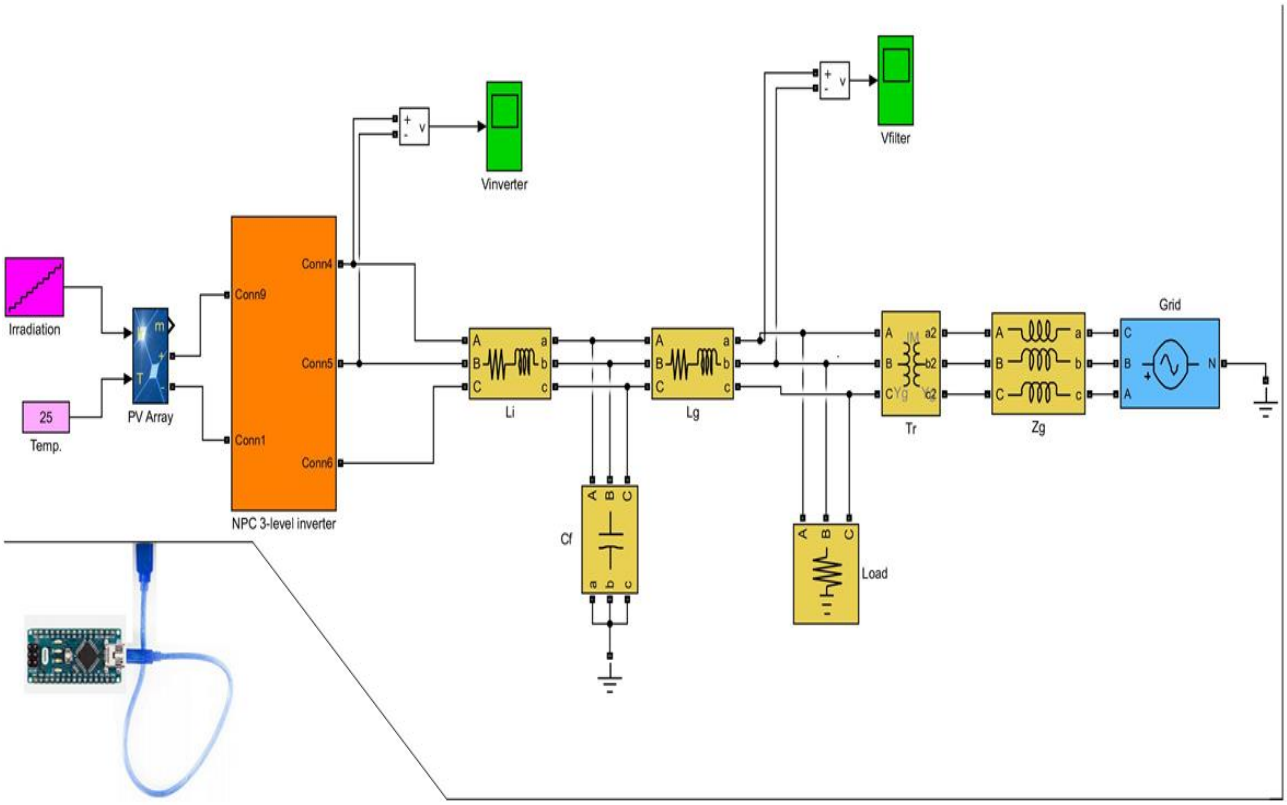

Fig. 3.9 ─ MATLAB/SIMUINK of PV system connected Arduino Nano using USB

3.9.1 LCL filter design

The design of inverter side inductance (L_i) and the second part deals with the design of grid side inductance (L_g) and capacitance (C_f) which is considered as L_gC_f second order low pass filter:

where $V_s = 220\,V$, $V_{sll} = 380\,V$, $f_s = 50Hz$, $P_n = 800 * 250\,W = 200\,kW$, $\mathrm{I}_n = 5\,A * 40 = 200\,A$, $i_{ripple} = 0.15 * I_n = 30\,A$,

$$L_i = \frac{V_s}{2\sqrt{6}f_s i_{ripple}} = \frac{220}{2 * \sqrt{6} * 50 * 30} = 0.0299\,H \approx 30\,mH = L_g$$

$$Z_{base} = \frac{V_{sll}^2}{P_n} = \frac{380^2}{200000} = 0.722\,\Omega$$

$$\omega_n = 2\pi f_n = 2 * \pi * 50 = 314\,rad/s$$

$$C_f = \frac{0.05}{\omega_n Z_{base}} = \frac{0.05}{314 * 0.722} = 2.2 \times 10^{-4} F$$

3.9.2 Maximum power curve

Matlab/Simulink is using to simulate controlled three-level three-phase NPC converter gate switching using variable modulation indices with carrier signal sampling frequency 100 KHz and reference signal frequency 50 Hz, with irradiation of 1000 w/m^2 and temperature of 25 ^oC. To obtain the maximum power-voltage curve of PV array, the peak value of sinusoidal wave of controlling SPWM is changing to get the inverter voltage value of maximum power in different irradiation (100 W/m^2 to 1000 W/m^2). Fig. 3.10 shows the P-V maximum power curve. The proportional relation between rms output voltages of filter is increasing with the output power of the solar panel while increasing the modulation index of the SPWM controlled by MPPT. This curve with curve fitting in different points is using as look-up table of microcontroller.

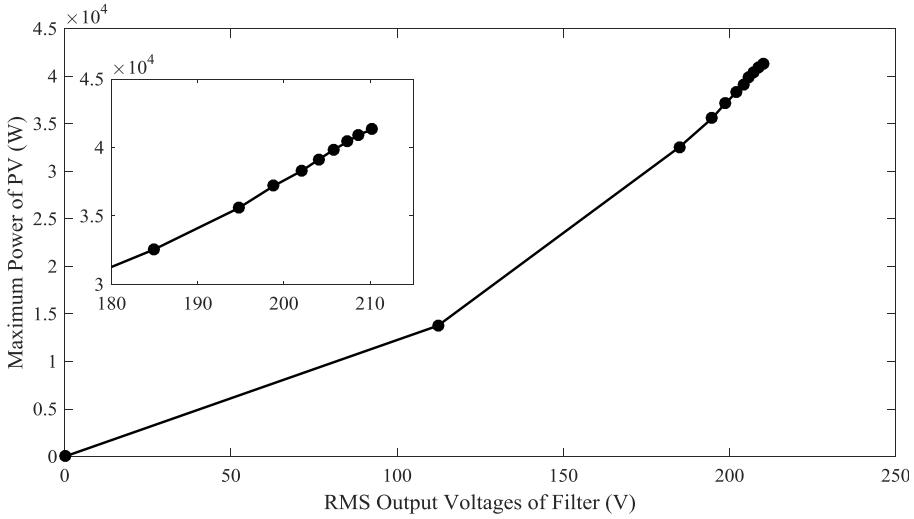

Fig. 3.10 ─ P-V maximum power curve

3.9.3 Case 1: Stand-alone PV system

The PV system connected to three-phase load, in Fig. 3.8, was simulated in irradiation of 1000 W/m^2 and temperature of 25 ^oCusing Matlab/Simulink. Fig. 3.11 shows the output voltages of the inverter before and after the filter and their harmonics. As shown in Fig. 3.11, the THD is very small approximately 22 % using to control SPWM of three-level three-phase converter. The LCL filter is used to reduce THD to 4.9% within IEEE limit of medium and low voltage (5%).

Stand-alone PV system with three-phase load, in Fig. 3.8, was simulated in variable irradiation from 100 to 1000 W/m^2 and temperature of 25 ^oCusing Matlab/Simulink. Fig. 3.12 shows DC output voltage and power of PV array. Fig. 3.13 shows output voltages of inverter and filter. Fig. 3.14 shows output power of inverter and load.

As shown in Fig. 3.12, DC voltage of PV array is changing from 420 V at 100 W/m^2 to 620 V at 200 W/m^2. DC voltage of PV array is changing with small from 620 V to 782 V with irradiation change from 200 to 1000 W/m^2. As well as DC power of PV array is changing from 15 kW at 100 W/m^2 to 36 kW at 200 W/m^2. DC power of PV array is changing with small from 36 kW to 39 kW with irradiation change from 200 to 1000 W/m^2. Output voltage of filter is approximately sine wave and constant frequency (50 Hz) where it has small THD due to LCL filter in different values of irradiation, shown in Fig. 3.13. As shown in Fig. 3.14, the load power is variable from 2500 W at 100 W/m^2 to 6000 W 1000 W/m^2 where it depends on voltage and irradiation. The power loss of LCL filter is approximately zero which is the difference between the output power of inverter and output power of filter.

3.9.4 Case 2: Grid connected PV system

The Grid connected PV system with three-phase load, in Fig. 3.8, was simulated in irradiation of 1000 W/m^2 and temperature of 25 ^oCusing Matlab/Simulink. Fig. 3.15 shows the output voltages of the inverter before and after the filter and their harmonics. As shown in Fig. 3.15, the THD is very small approximately 22 % using to control SPWM of three-level three-phase converter. The LCL filter is used to reduce THD to 3.51% within IEEE limit of medium and low voltage (5%). The Grid connected PV system with three-phase load, in Fig. 3.8, was simulated in variable irradiation from 100 to 1000 W/m^2 and temperature of 25 ^oCusing Matlab/Simulink. Fig. 3.16 shows DC output voltage and power of PV array. Fig.

3.17 shows output voltages of inverter and filter. Fig. 3.18 shows output power of inverter, filter, load and grid.

As shown in Fig. 3.16, DC voltage of PV array is changing from 300 V at 100 W/m^2 to 620 V at 200 W/m^2. DC voltage of PV array is changing with small from 620 V to 782 V with irradiation change from 200 to 1000 W/m^2. As well as DC power of PV array is changing from 10 kW at 100 W/m^2 to 36 kW at 200 W/m^2. DC power of PV array is changing with small from 36 kW to 42 kW with irradiation change from 200 to 1000 W/m^2. Output voltage of filter is approximately sine wave where it has small THD due to LCL filter in different values of irradiation, shown in Fig. 3.17. As shown in Fig. 3.18, the load power is constant value (=22 kW). The PV system and grid is feeding load in different values of irradiation. The power loss of LCL filter is approximately zero which is the difference between the output power of inverter and output power of filter.

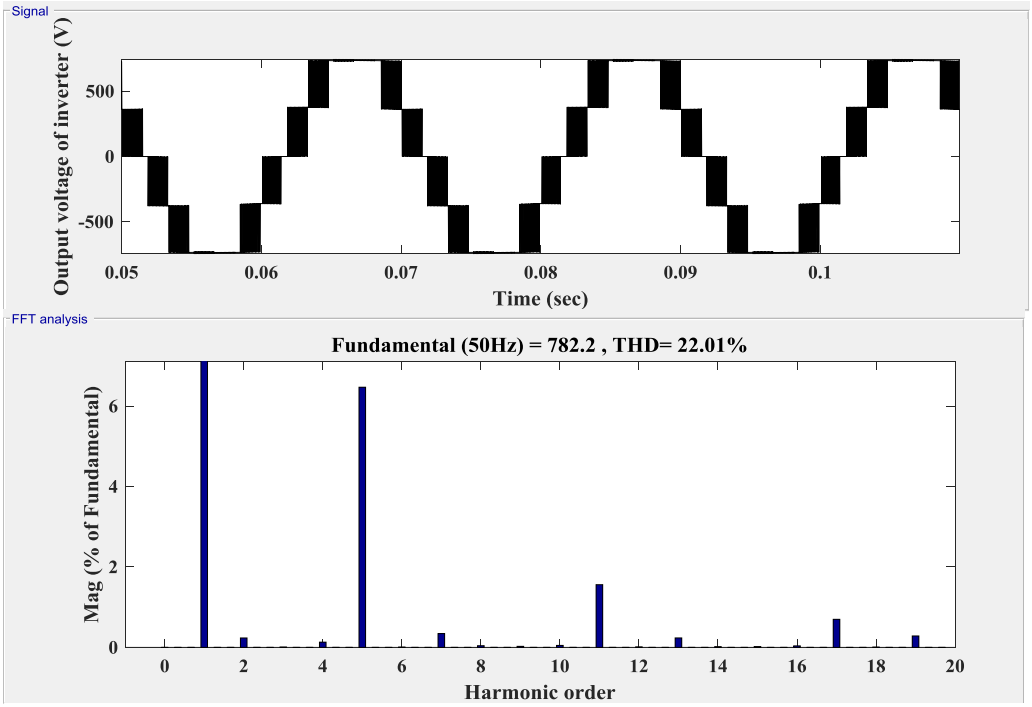

Fig. 3.11a ─ The output voltage of the inverter and harmonics

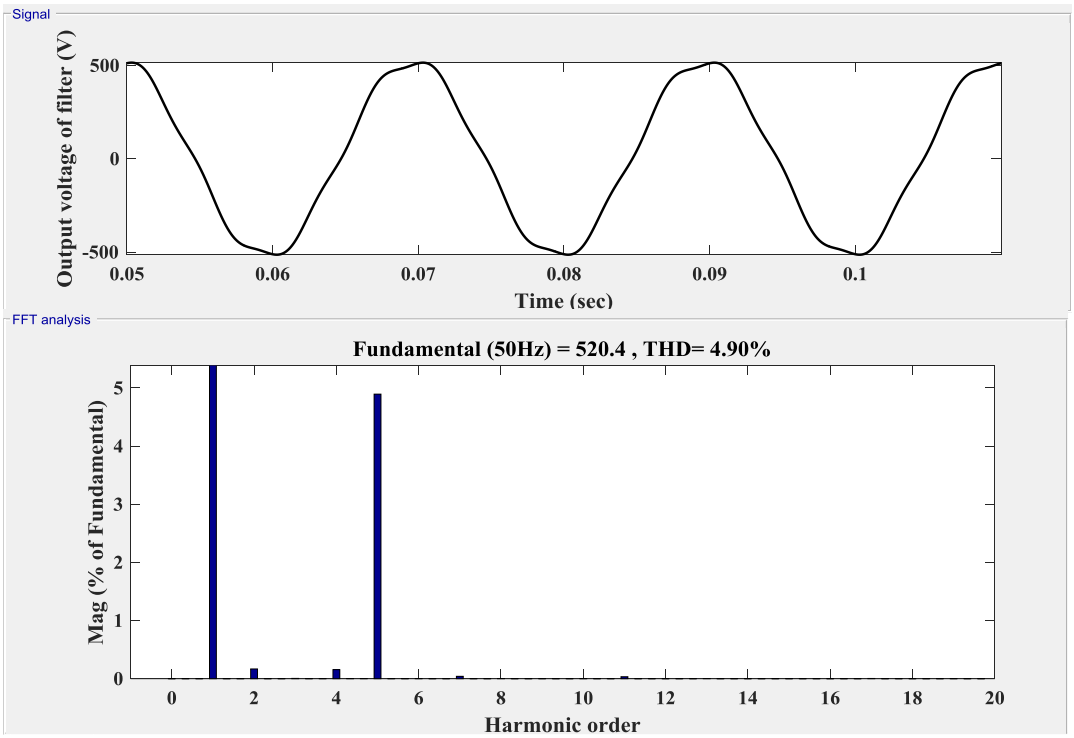

Fig. 3.11b ─ The output voltage filter and harmonics

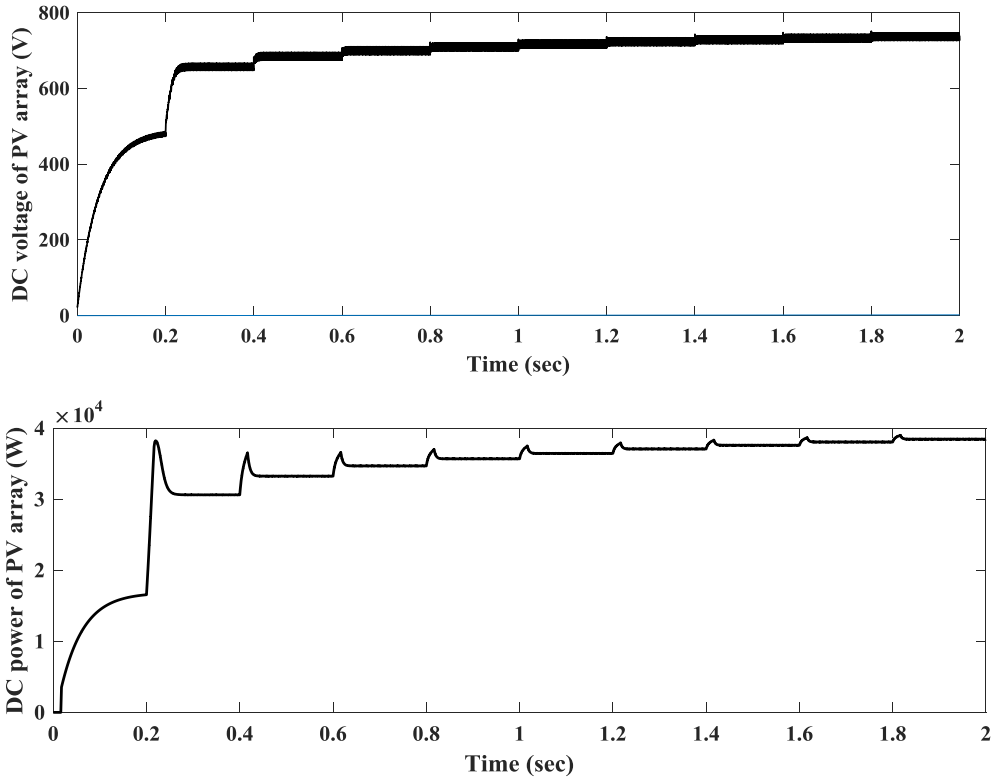

Fig. 3.12 ─ DC output voltage and power of PV array

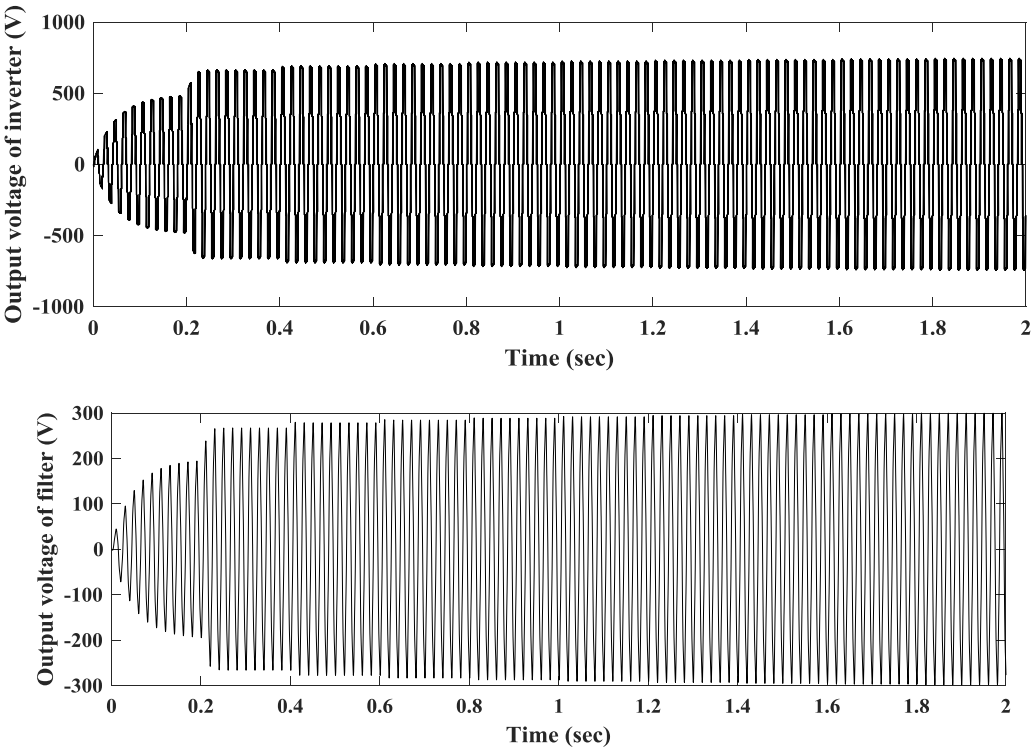

Fig. 3.13 ─ Output voltages of inverter, filter and grid

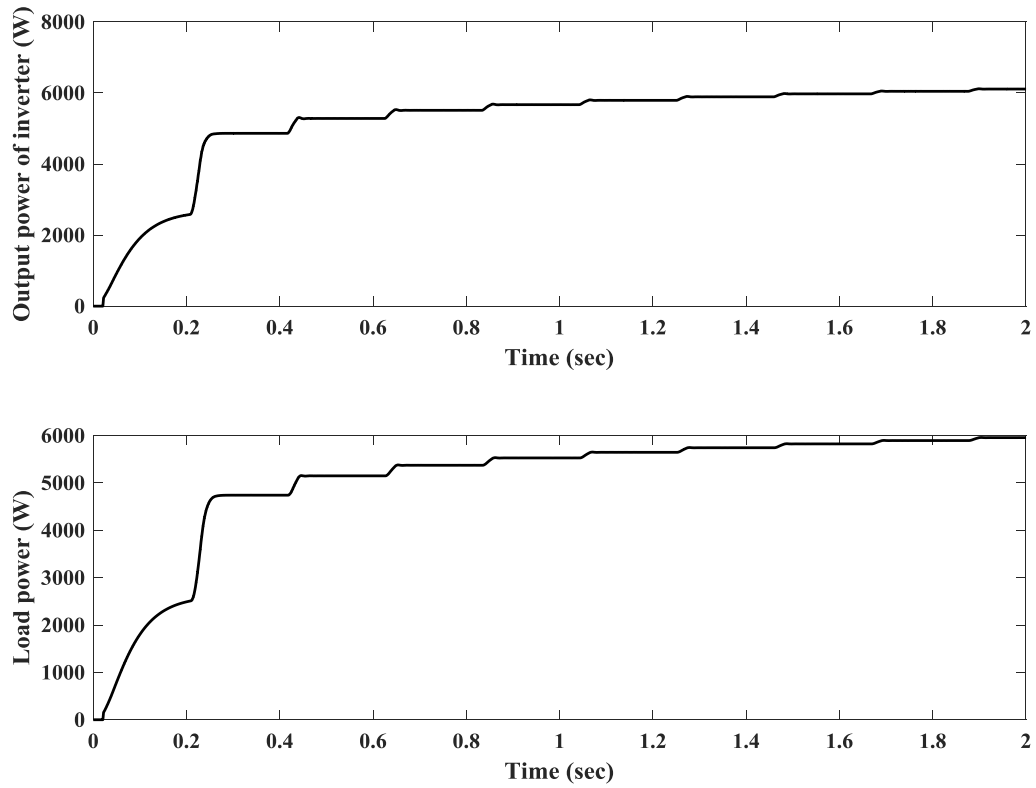

Fig. 3.14 ─ Output power of inverter and load

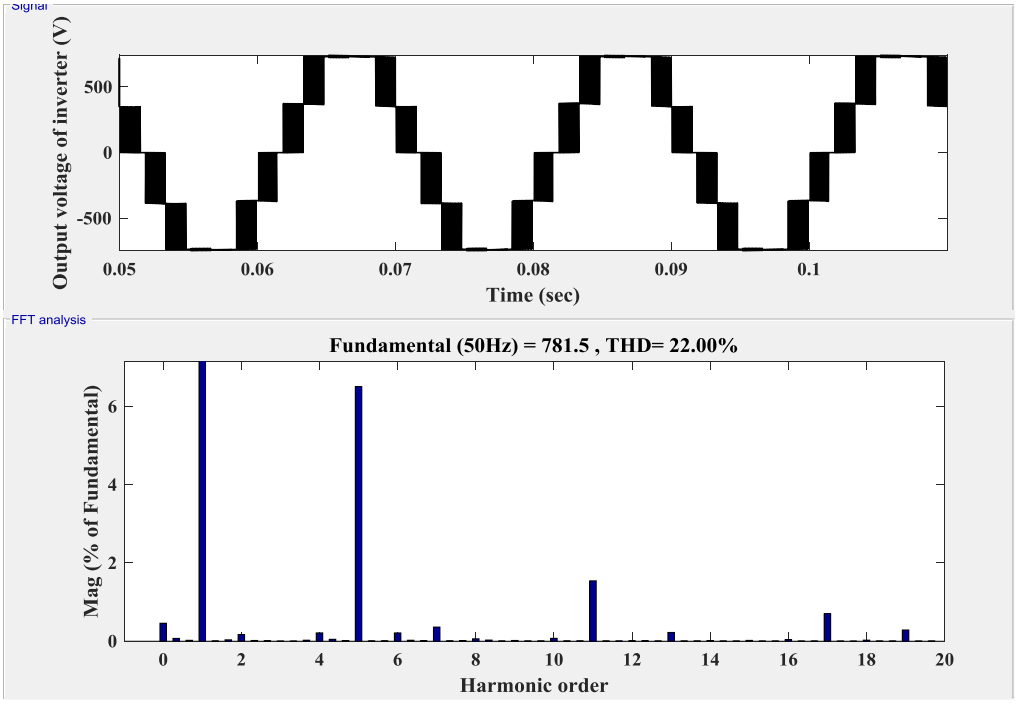

Fig. 3.15a ─ The output voltage of inverter and harmonics

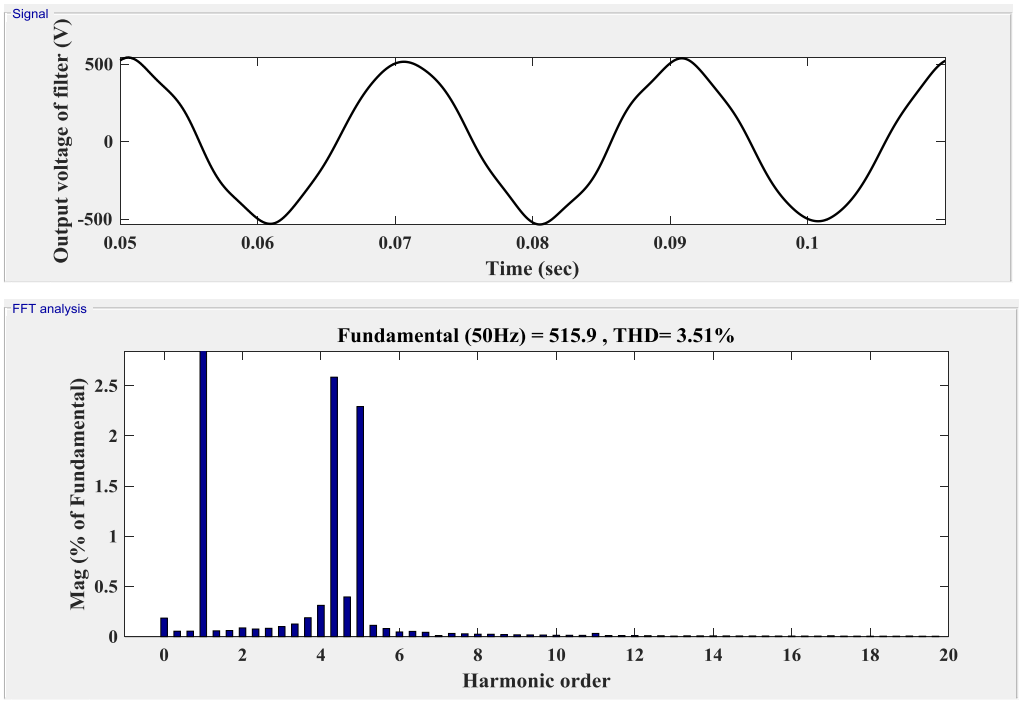

Fig. 3.15b ─ The output voltage of filter and harmonics

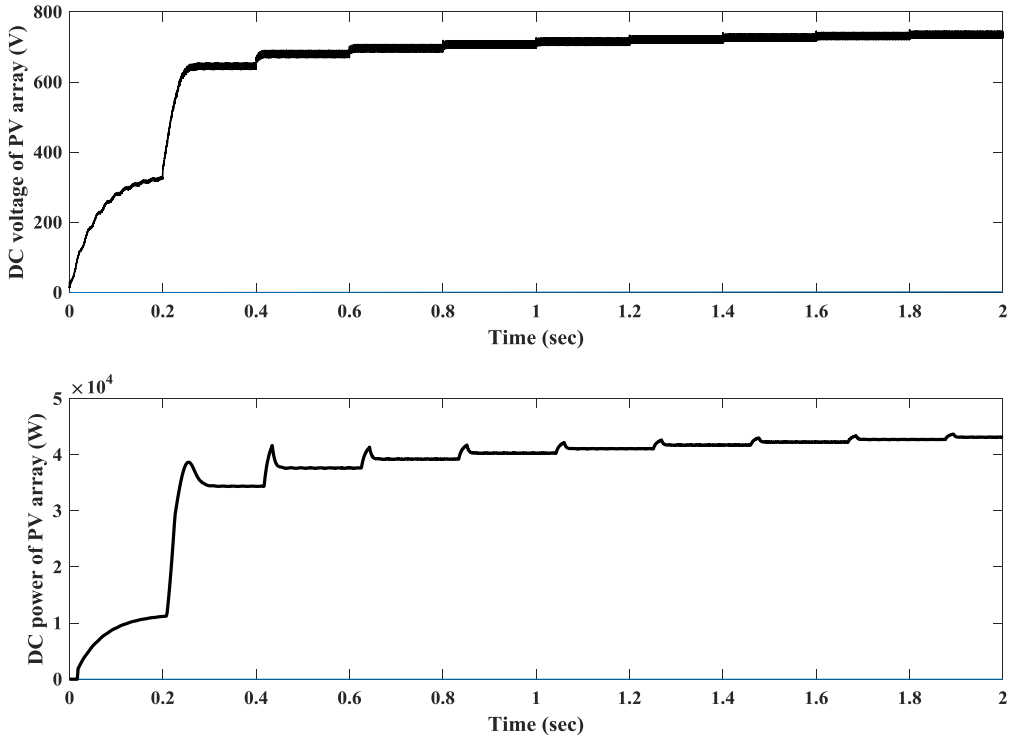

Fig. 3.16 ─ DC output voltage and power of PV array

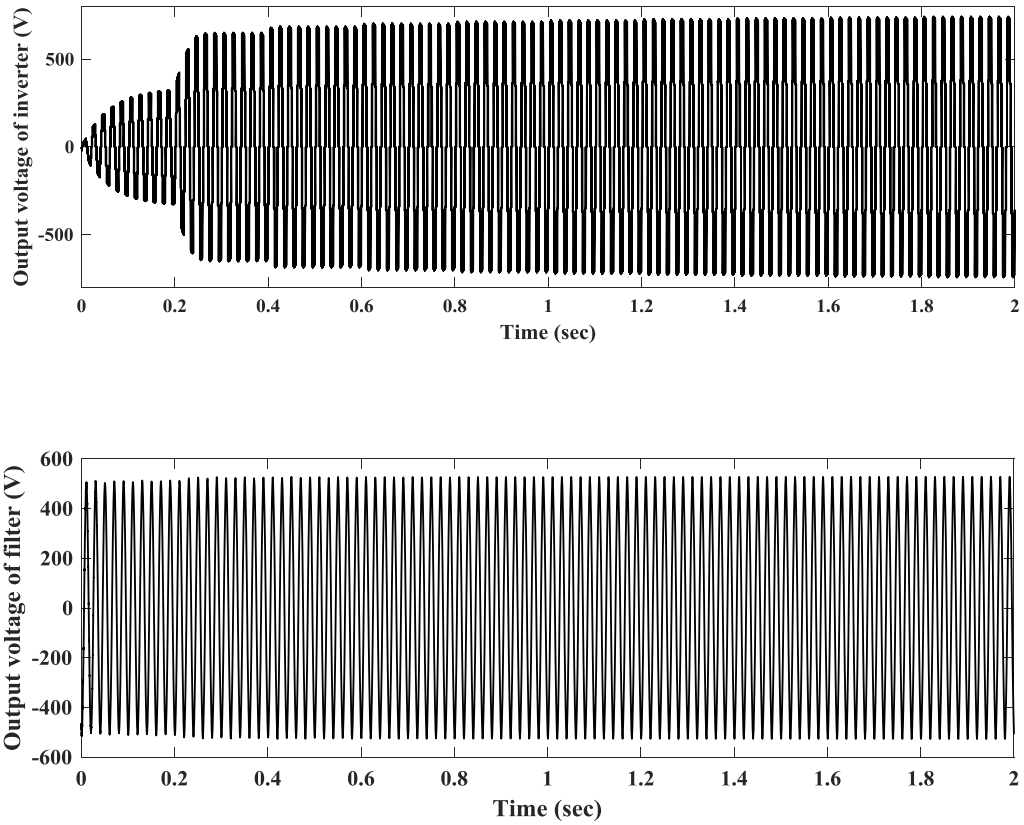

Fig. 3.17 ─ Output voltages of inverter, filter and grid

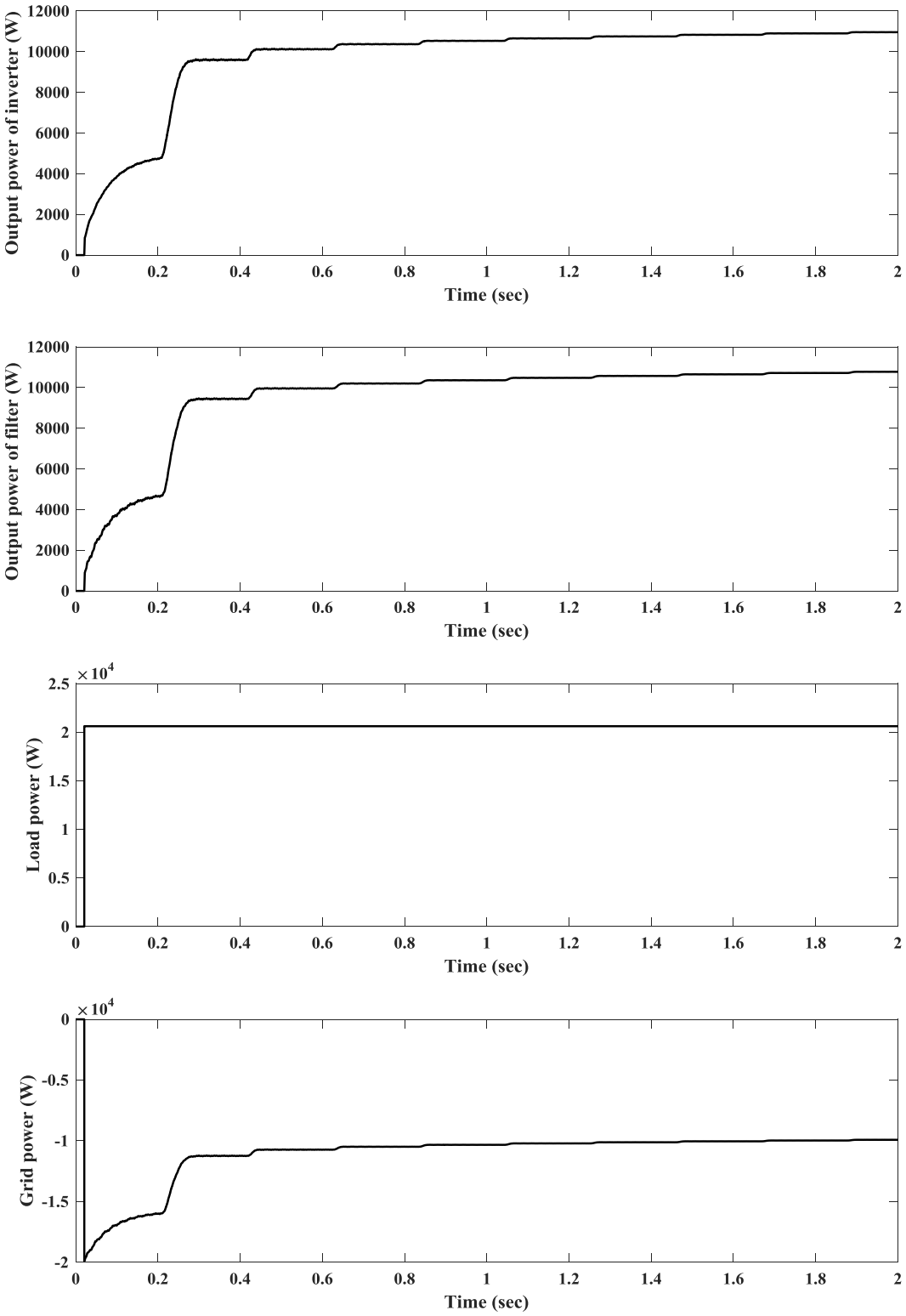

Fig. 3.18 ─ Output power of inverter, filter, load and grid

Equivalent circuit PV generator during fault

During the fault PV generator considers as source in series different reactance depending on the case of current peak currents (in the interval (0–0.02) sec, ultra-transient currents and voltage (in the interval (0.02–0.1) sec and steady state short-circuit currents. Table 3.2 shows sub-transient, transient and steady state reactance values of 250 kW PV generator with values of current. Fig. 3.19 shows the terminal voltage. Fig. 3.20 shows the output current with DC component during fault. From table 3.2, DC component can be plotted by the equation: (1735-1250)*e $^{(-t/0.02)}$ +1250. DC component is different from Synchronous generator because the control limit current during fault.

Table 3.2 ─ Sub-transient, transient and steady-state reactance values of 250 kW PV generator with values of current

E(V)	I(A)	I’(A)	I’’(A)	x(ohm)	x'(ohm)	x’’(ohm)
205	852	1250	1735	0.24	0.164	0.12

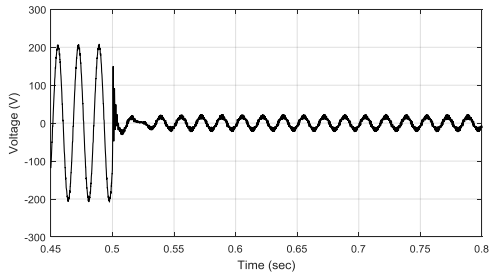

Fig. 3.19 ─ Terminal voltage of PV generator

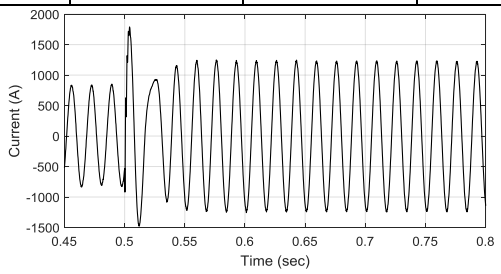

Fig. 3.20 ─ Output current with dc component during fault

Chapter 4. Transient analysis of AC and DC microgrid with effective of SFCL

A microgrid is a subsystem with low power rating from few kW to several MW which has individual control system to save the energy to specific area. The microgrid can be working in two modes grid-connected and isolated. The current DG sources can be connected to electric power system through interfacing convertersthe protection scheme for AC or DC microgrids is a challenge these days. The protection scheme of microgrid is focused to shield the microgrid parts like sources, batteries, converters and feeders using protection devices and recover aspects during the fault for grid-connected and isolated modes. The various kinds of protection schemes have been applied in both AC and DC microgrids where each one has advantages and disadvantages.

4.1 Microgrid System Configuration

The system can be divided into AC bus and DC bus. The common connection point is the point of connection DG sources and battery system to the distribution network. AC microgrid is small subsystem containing DG sources and load circuits. The power from DC-based DG units must be transformed to AC electric network. To treat the problems in a distributed network produced from connection the interfacing converter of DG sources, the LVDC distributed network is used which presents a novel conception. DC MG configurations contains the low voltage DC links based on bipolar configurations where the loads can be coupled across the positive polarity and the ground or between the two polarities. The LVDC distribution network can improve the efficiency of delivering power to the distribution network [116]. The AC microgrid which consists of PV and battery connected to AC bus through DC/DC and DC/AC converters, as well as PMSG wind turbine connected to AC/DC and DC/AC converters, is shown in Fig. 4.1. The AC load is connected to AC bus. The AC microgrid is connected to grid through transformer. The DC microgrid which

consists to PV and battery connected to DC bus through DC/DC converter as well as PMSG wind turbine connected to AC/DC converter. The DC load is connected to DC bus. A bidirectional DC/AC converter integrates the DC microgrid with the utility grid as shown in Fig. 4.2. Under Frequency Load Shedding has been studied for improving the transient stability of the islanded microgrid by executing in multiple stages depending upon the system requirement described in [17]. The microgrid stability performance is examined with different load types, including RLC and IM loads is analyzed in [117]. Ref. [118] presented the control technique to DC microgrid which depends on DC-link voltage regulation using small-signal analysis with designing two loops control. The voltage-based droop control and fuzzy controller for power to droop control based on voltage presented in [119]. The performance of DC microgrid has been investigated with influence distributed controller and constant power loads to cover certain area of droop gain [120].

4.2 System Description

AC and DC microgrids, as shown in Figs. 4.1 and 4.2, are consisted of three renewable energy sources; the wind turbine of 1.5 MVA, 575 V and 100 kW PV array. The batterybank is connected DC or AC bus of DC and AC microgrids respectively. The rate of DC/AC inverter is different from AC and DC microgrid which depends on the rate of the source (wind, PV) in AC microgrid. The short circuit power of the grid is 25kV, 2500 MVA. 1 MW load is connected to microgrid as shown in Figs. 4.1 and 4.2.

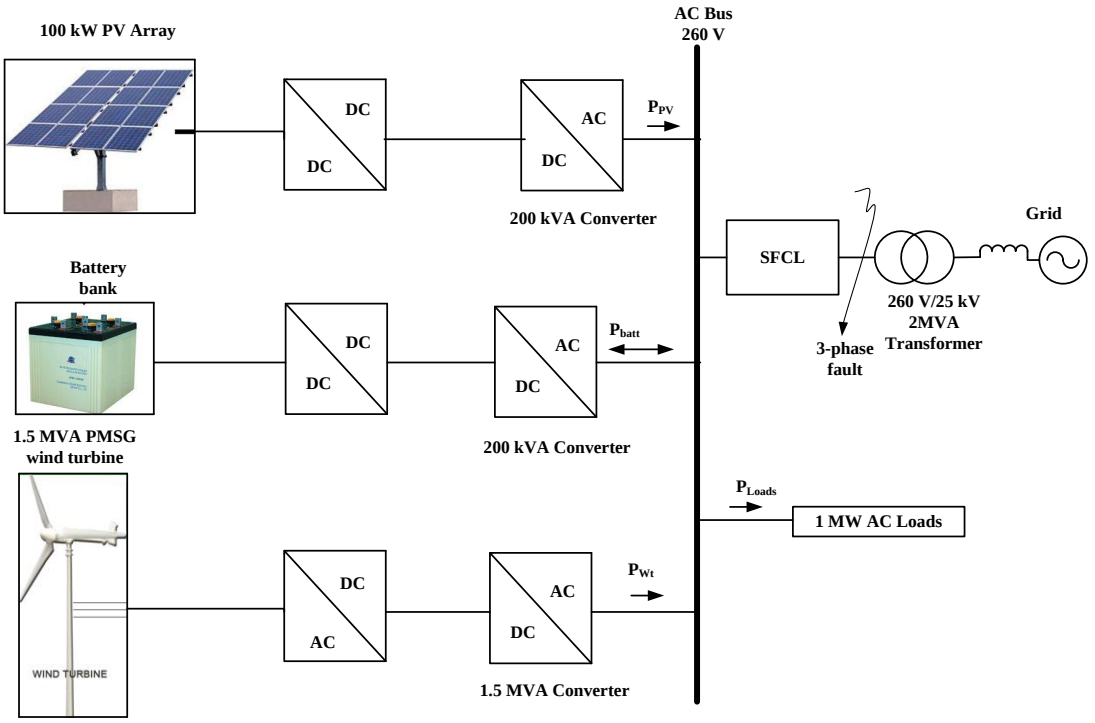

Fig. 4.1 ─ Layout of AC microgrid

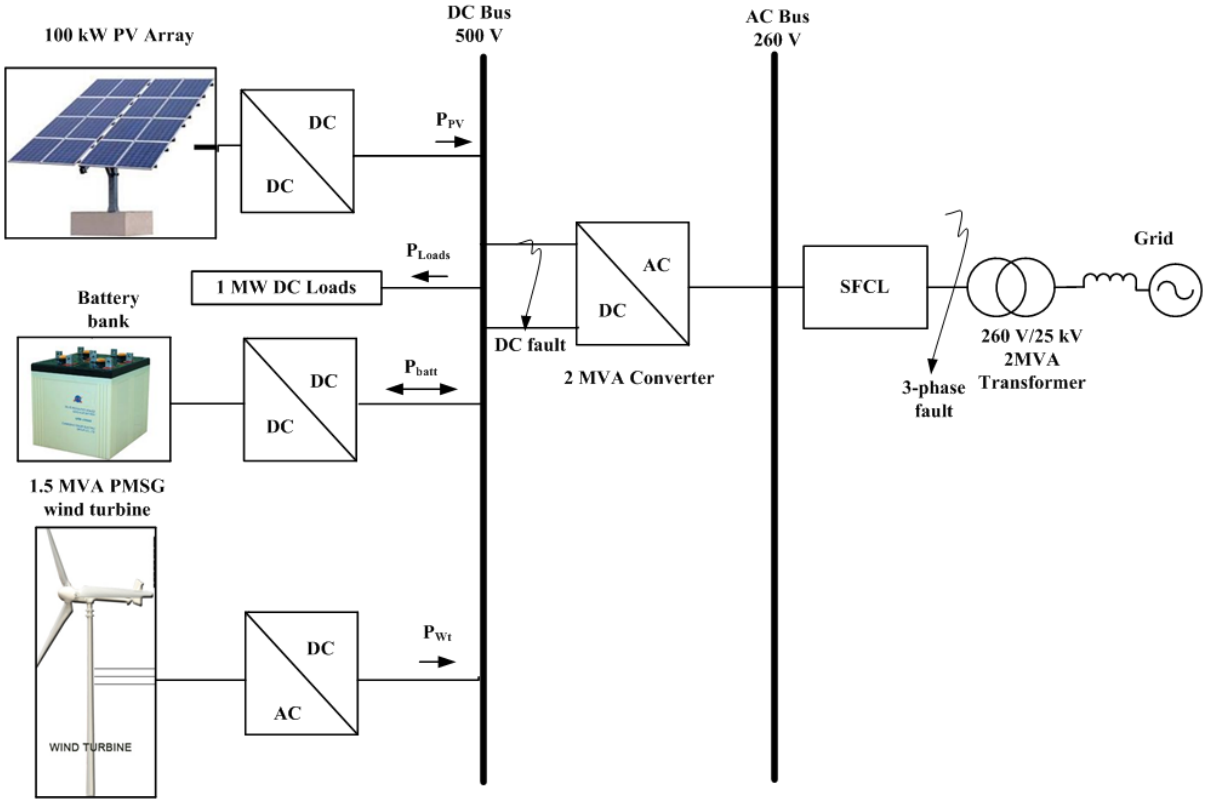

Fig. 4.2 ─ Layout of DC microgrid

4.3 Simulation Studies

In the simulation studies, the transient analysis of AC and DC microgrids was investigated. A three-phase-to-ground fault is applied to the connection point between the microgrid and the grid at t =3 sec for the duration of 0.2 sec as shown in Figs. 4.1 and 4.2. The wind speed and irradiation values are 12 m/sec and 1000 W/m^2 respectively. Simulated circuits are given in appendix A.2 and A.3.

A. Three-phase- to- ground fault of AC Microgrid.

A three-phase-to-ground fault is applied to the connection point between the microgrid and the grid at t =3 sec for the duration of 0.2 sec, in Fig. 4.1. Fig. 4.3 shows the temporal variation of the grid current and AC microgrid current. Figure 4.4 shows the temporal variation of the active and reactive power of AC microgrid. As shown in Figs. 4.3 and 4.4, without SFCL, the grid current oscillated to 90000 A during small time then it recovered pre-fault value as well as the AC microgrid current has oscillated around 10000 A. The active and reactive power of AC microgrid has oscillated to 4 MW and 23 MVAr respectively. However, with the SFCL, the grid current oscillated to 30000 A during small time then it recovered pre-fault value as well as the AC microgrid current has oscillated to very small value about 1500 A. The active and reactive power of AC microgrid are almost constants with reactive power oscillating to about 1MVAr. The currents and power of AC microgrid recovered the pre-fault values within a small time of less than 0.1 sec.

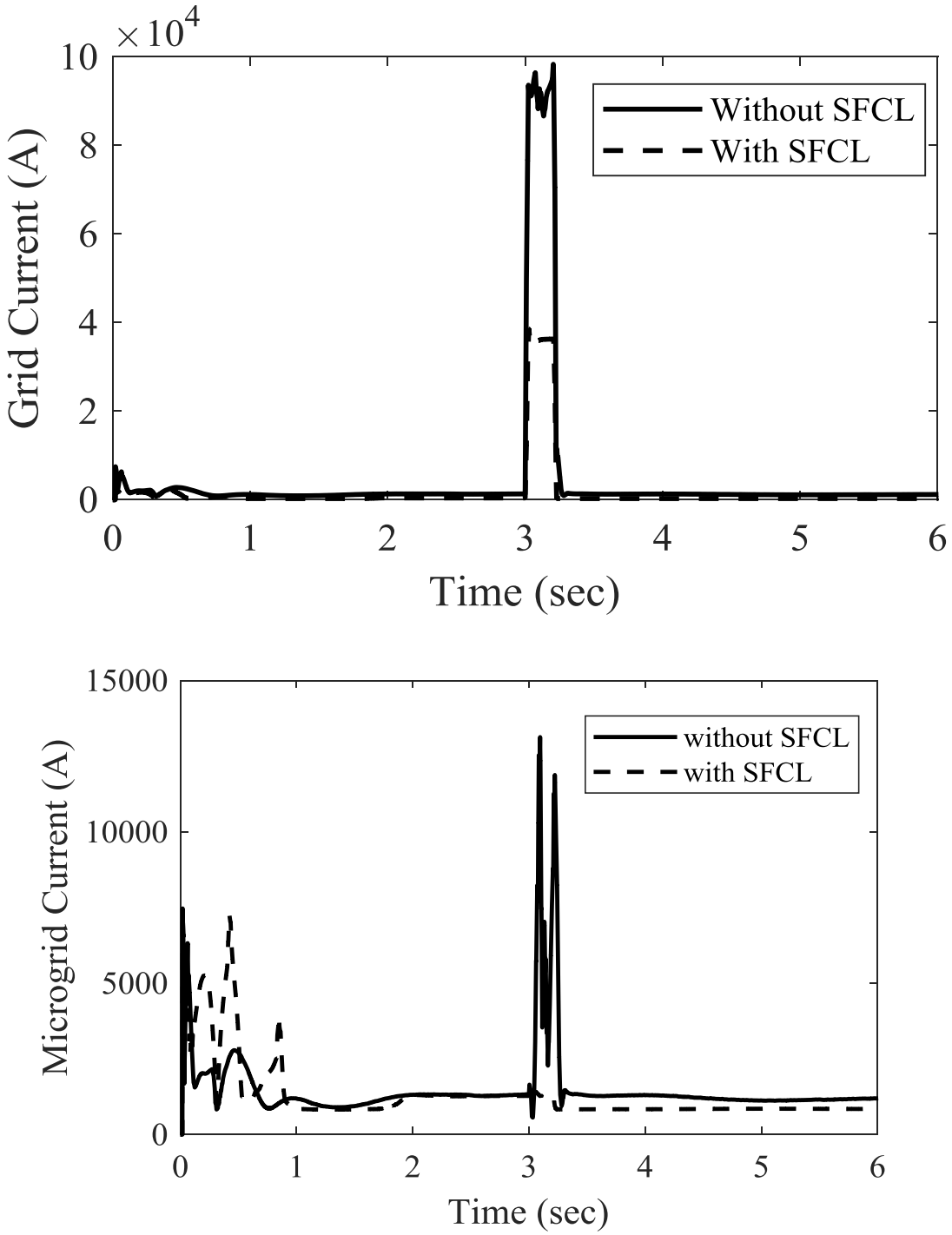

Fig. 4.3 ─ Temporal variation of the grid current and AC microgrid current

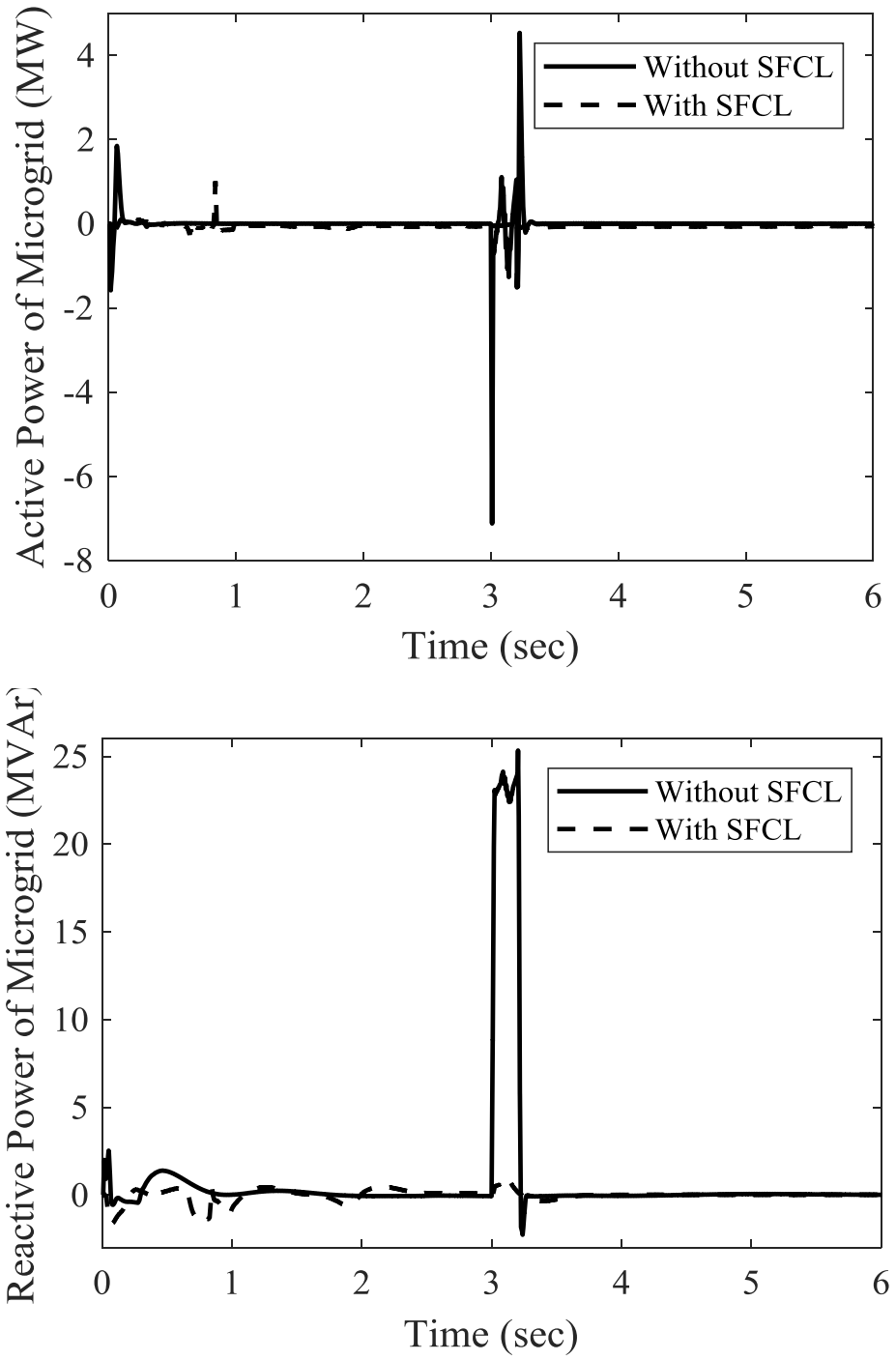

Fig. 4.4 ─ Temporal variation of the active and reactive power of AC microgrid

B. Three-phase- to- ground fault of DC Microgrid.

A three-phase-to-ground fault is applied to the connection point between the DC microgrid and the grid at t =3 sec for the duration of 0.2 sec, in Fig. 4.2.

Figure 4.5 shows the temporal variation of the grid current and DC microgrid current. Figure 4.6 shows the temporal variation of the active and reactive power of DC microgrid As shown in Figs. 4.5 and 4.6, without SFCL, the grid current oscillated to 5200 A during small time then it recovered pre-fault value in 3 sec as well as the DC microgrid current has oscillated around 4200 A. The active and reactive power of DC microgrid has oscillated to 0.85 MW and 1.7 MVAr respectively. However, with the SFCL, the grid current oscillated to 5200 A during small time then it recovered pre-fault value as well as the DC microgrid current has oscillated to a very small value about 1500 A. The active and reactive power of DC microgrid has oscillated to 0.3 MW and 0.6 MVAr respectively. The currents and power of AC microgrid recovered the pre-fault values within a small time less than 3 sec.

Table. 4.1 shows a comparison between the values of currents and the active and reactive power of AC and DC microgrids during the fault and pre-fault values.

From the above results, the oscillating currents are very high in AC microgrid comparison to oscillating currents of DC microgrid during the fault without and with SFCL. The SFCL minimized the oscillating currents and the active and reactive power of AC and DC microgrid to range 20-30%. The SFCL is used to protect the AC and DC microgrid from the high current by minimizing current value within the limited value. The time required to recover pre-fault values of AC microgrid (0.1 sec) is less than those times of DC microgrid (3 sec).

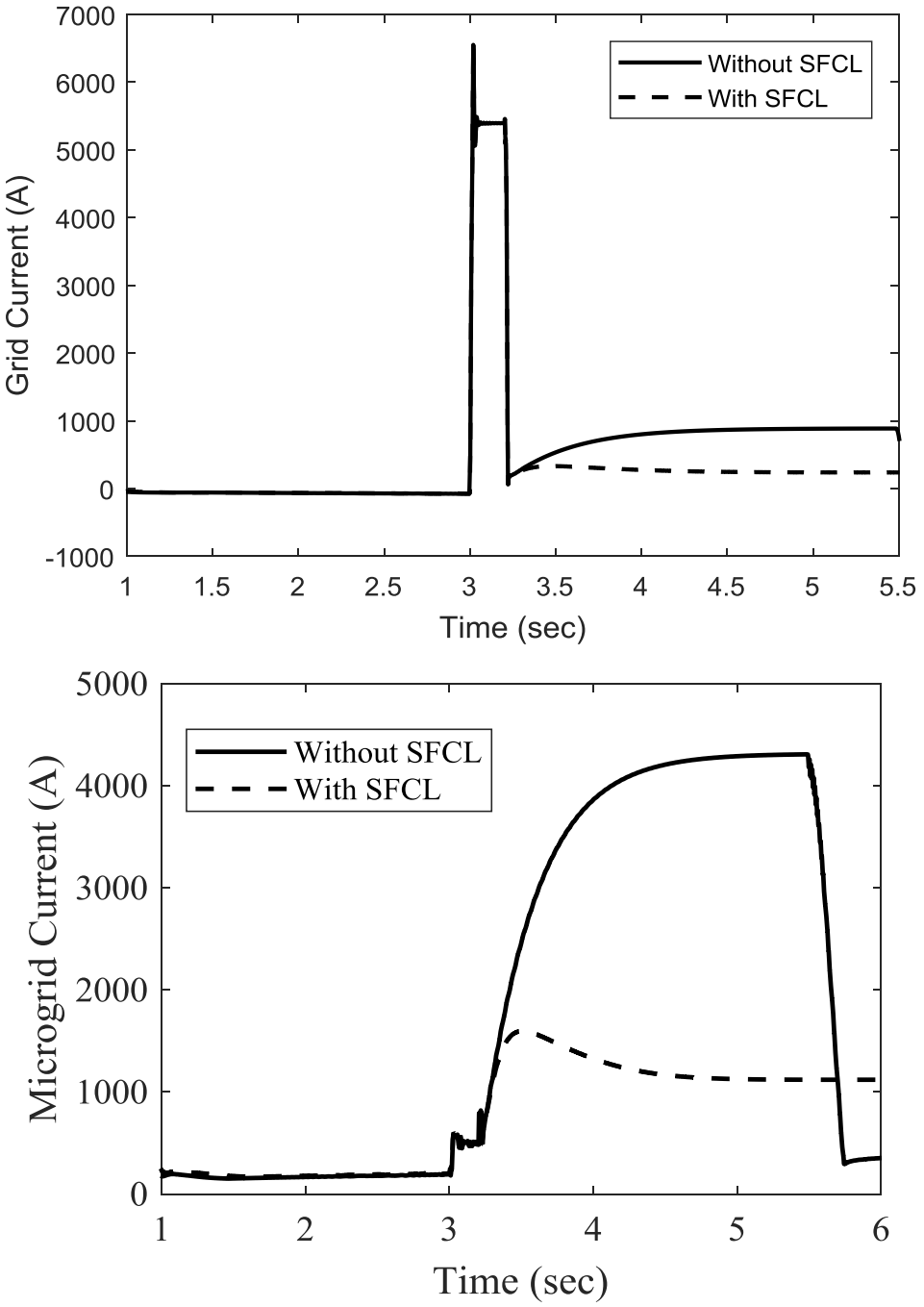

Fig. 4.5 ─ Temporal variation of the grid current and DC microgrid current

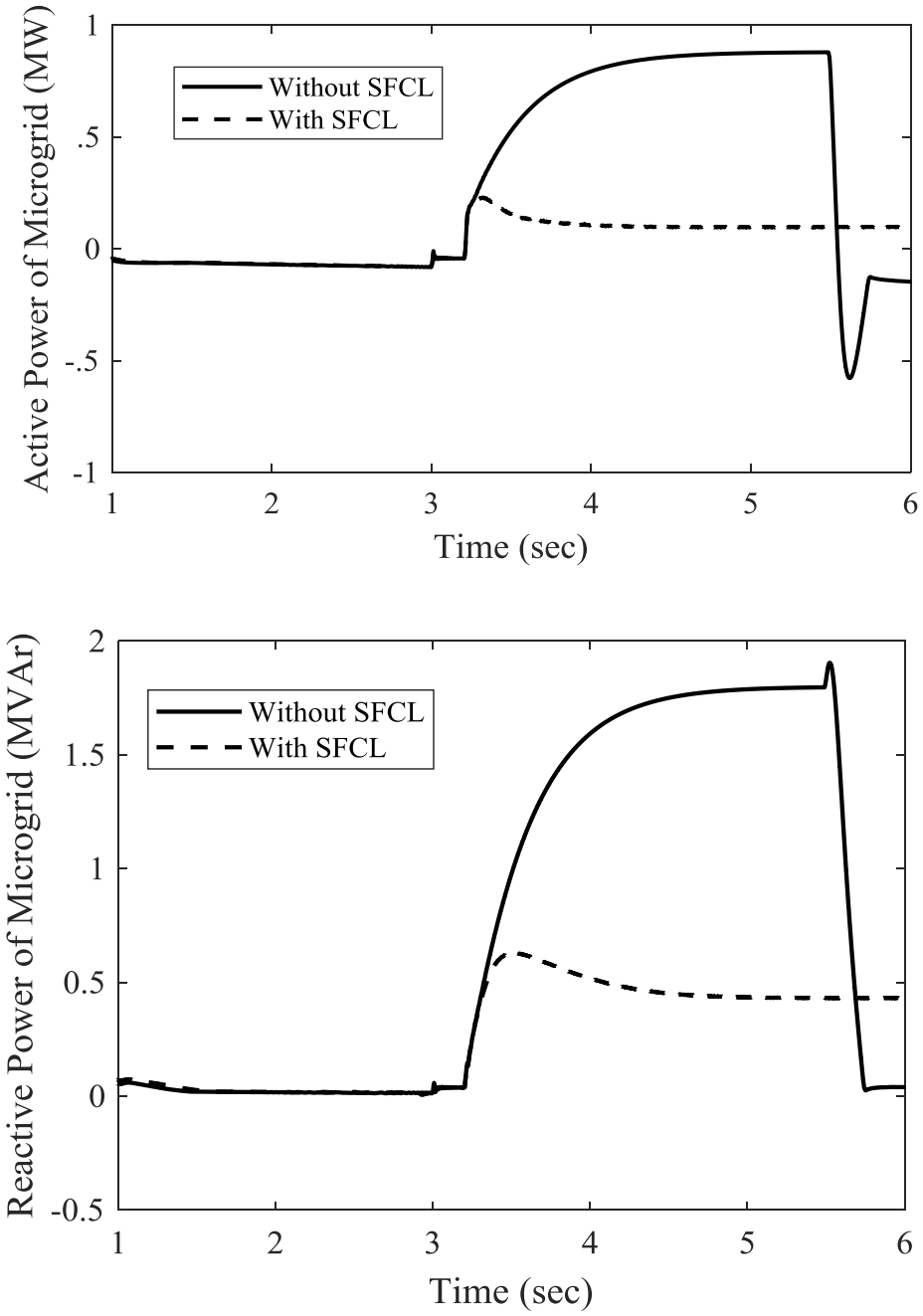

Fig. 4.6 ─ Temporal variation of the active and reactive power of DC microgrid

Table. 4.1. ─ Comparison between values of currents and the active and reactive power of AC and DC microgrids during the fault and pre-fault values

		Grid Current (A)		Microgrid Current (A)		Active Power of Microgrid (MW)		Reactive Power of Microgrid (MVAr)	
		Pre-Fault Value	Value During Fault	Pre-Fault Value	Value During Fault	Pre-Fault Value	Value During Fault	Pre-Fault Value	Value During Fault
AC Microgrid	Without SFCL	1000	90000	1000	10000	0.3	4	0.5	23
	With SFCL	1000	30000	1000	1500	0.3	0.3	0.5	1
DC Microgrid	Without SFCL	100	5200	100	4200	0.1	0.85	0.1	1.7
	With SFCL	100	5200	100	1500	0.1	0.3	0.1	0.6

DC fault. The DC fault is applied to DC microgrid at t =3 sec for the duration of 0.2 sec. Fig. 4.7 shows (a) DC current of PV, (b) DC current of battery, (c) DC current of wind turbine, (d) Total DC current and (e) AC current of microgrid. As shown in Fig. 4.7, during the fault, the DC current increased to feed the fault, but the converter limit current to its limit. The AC current of microgrid decreased because the dc voltage of inverter decreased.

The short circuit current calculation of AC and DC microgrid is calculated to detect and coordinate protection system where the short circuit current depends on the configuration of system. SFCL is use to limit fault current in AC and DC microgrid. In DC system, Fault currents have much higher rates of rise when compared to AC

systems due to commonly employed DC capacitors in the output of power converters which normally discharge through cables with low impedance values.

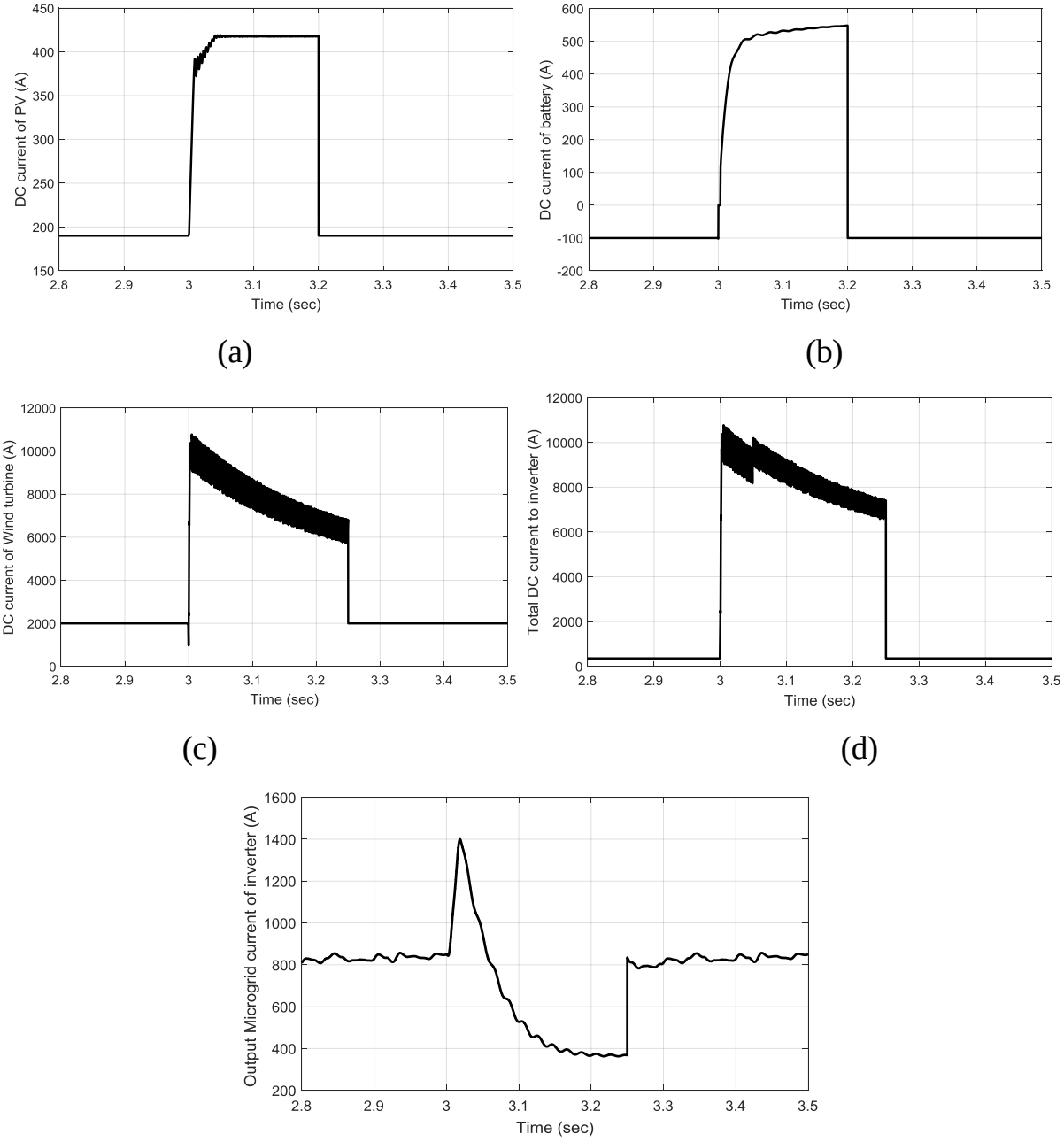

Fig. 4.7 ─ (a) DC current of PV, (b) DC current of battery, (c) DC current of wind turbine, (d) Total DC current and (e) AC current of microgrid.

Chapter 5. Short Current Calculation and Static Security Risk for Grid-connected and Isolated Microgrid

5.1 Research Method

5.1.1 Power flow calculation

A. Power flow of Grid-connected microgrid

The origin and formulation of the Newton-Raphson method were dated the back to late 1960s. It is a numerical method that approaches a set of non-linear instantaneous calculations to a set of linear instantaneous calculations using Taylor's series expansion and the terms are restricted to the first estimate.

It is the most iterative technique utilized for the power flow since its intermingling qualities are generally increasingly incredible contrasted with other elective procedures and the unwavering quality of the Newton-Raphson approach is nearly acceptable since it can unravel cases that lead to uniqueness with other well-known procedures. Being not normal for generator based DG, the output characteristic for inverter-based DG is principally overwhelmed by its control unit. In power flow calculation, the equal models of DGs under various control are extraordinary. In constant power control, the DG ought to equivalent to PQ bus while in constant voltage control, the DG ought to equivalent to the PV bus if the reactive power output from DG is within a limit. But if the reactive power output from DG exceeds its limit, the DG ought to equivalent to PQ bus. Consequently, the equivalent model of inverter-based DG is mostly equivalent to PQ bus or PV bus. For the calculation method, the back/forward sweep method and the Newton-Raphson method are generally used similar to conventional power flow method.

B. Power flow of isolated microgrid

The power flow analysis of isolated microgrid is different from grid-connected microgrid where there is no slack bus. DG units are for the most part worked in droop mode amid the isolated mode of operation of the microgrid. The droop

technique largely gives a superior alternative to authority over the load to be shared by the various generation units because, in droop strategy, power-sharing is relative to the rating of the distinctive DG units. In the droop method of operation, the settings of the droop coefficient of the DG units ought to be picked with the end goal that the loads have partaken in the extent to their ratings. The active and reactive power shared by the DG units is constrained by P–f droop and Q–V droop attributes, separately. In the grid-connected mode, DGs by and large work in the (P–Q) or (P–V) mode. Generally, the non-linear equations of the power flow problem are unraveled utilizing the Newton Raphson (NR) calculations. Many researches were solved the power flow of isolated microgrid using modified newton Raphson [94] and a Newton-Trust region method [95]. A Newton-Trust region method is used to solve the power flow in this thesis.

The three-phase injected active and reactive power from a DG unit operating with droop control can be expressed in the power flow formulation as follows:

$$P_{DG} = \frac{1}{m_p}(\omega^* - \omega)$$

$$Q_{DG} = \frac{1}{n_p}(V_{DG}^* - V_{DG}) \quad (5.1)$$

Where P_{DG} and Q_{DG} are active and reactive power of DG, ω^* and ω are the nominal and operating frequency of the system, V_{DG}^* and V_{DG} are the nominal and operating voltage of DG, m_p and n_p are the active power static droop gain and the reactive power static droop gain

Regularly the DG sources are designed with a current limiter to constrain the generation of the DG source to its rated active and reactive limits P_{max} and Q_{max}. To take the DG current limits into thought in the power flow definition, the determined DG active and reactive power generations are contrasted with their predefined limits. If the calculated power exceeds its limits, the DG changes from droop-mode to PQ mode and the predetermined power is reserved at the limit value

5.1.2 Fault current calculation

The fault current calculation of distribution networks containing DG sources and storage energy system has been explained in sec. 1.11. Short circuit calculation of grid-connected and isolated microgrid calculate using two methods, virtual impedance method, and proposed method. The proposed method is an improved method of calculation short circuit current where it is used the effect of droop control inverter-based DG. This model is explained in [121].

The output current of an inverter is effectively limited by its control system. The current limit is depending on the current rating of the semiconductors which is proportional to the expense of the inverter. This rating is normally not more than twice the inverter's rating in order to limit. The response of an inverter to a sudden collapse of terminal voltage is in this manner represented by the control and current limiting strategy. This behavior is regularly non-linear and can therefore not be directly represented in the traditional fault analysis techniques. By analyzing the fault response of a popular type of grid connected inverter control strategy, a load-flow based technique is used for analyzing distribution networks containing inverter interfaced generation. The technique effectively recognizes which inverters go into current limit mode and it accurately predicts the fault currents and voltages in the network. For inverters connected to a large grid this should not pose any problems. Alternatively, root mean square current limiting on a per phase basis can be implemented in the natural reference frame. The output current of inverter is shown in Fig. 5.1. During normal operation, the inverter can be represented as a positive sequence P&Q source behind a coupling reactance. During voltage sags when the current threshold is exceeded, the grid connected inverter can be represented as a constant positive sequence current source in parallel with the filter capacitor. Figure 5.2 shows the output current of PV system during fault in different values of irradiation.

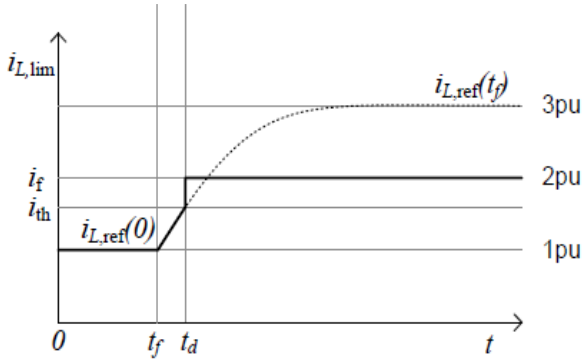

Fig. 5.1 ─ Single inverter fault response

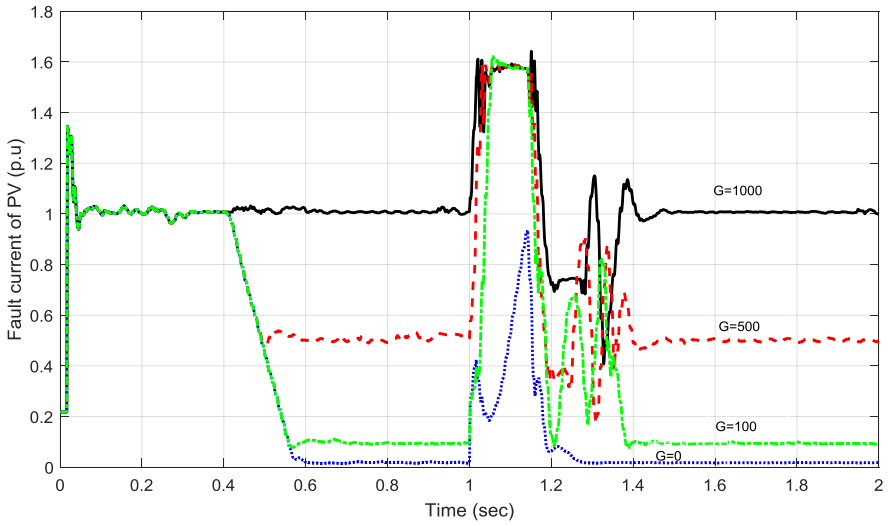

Fig. 5.2 ─ Output current of PV system during fault in different values of irradiation

A. Virtual impedance method

For a fault at any bus, the value of the fault currents from any DG source is very high and the inverter control limits its current to 2 p.u of the inverter rating only. Each inverter is represented by variable virtual impedance, which limits fault current to 2 p.u. By changing the fault location, the virtual impedance changes to maintain the fault current constant at 2 p.u. To cope with this problem, the following Algorithm [107]:

1. Each inverter is represented by a very small virtual impedance.
2. R/ X ratio of the inverter virtual impedance is assumed to equal to the R/X ratio of the transmission line, to which the inverter connected.
3. When a 3 -phase fault occurs at any bus, the fault current fed from each inverter is calculated.

4. Check the value of each inverter fault current. If it exceeds 2 p.u of the inverter rating, increase. Fig. 5.3 shows the equivalent circuit of DG during fault.

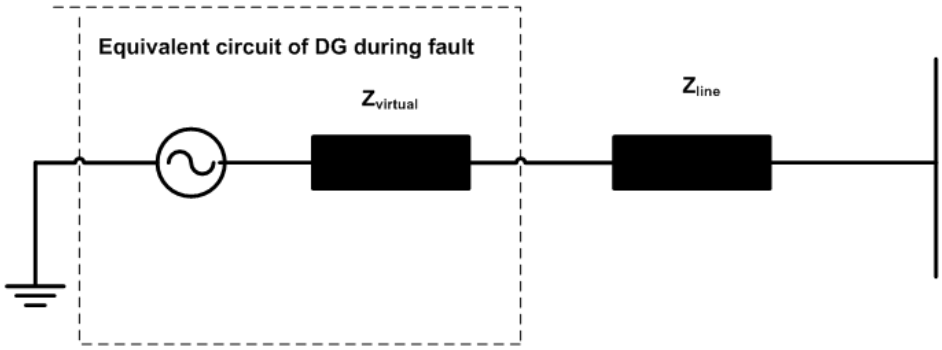

Fig. 5.3 ─ The equivalent circuit of DG during fault

B. The proposed method

1- Calculate voltage and output power of buses of IEEE 33 bus with 5 DGs as shown in Fig. 5.4 using solution of the Power flow.

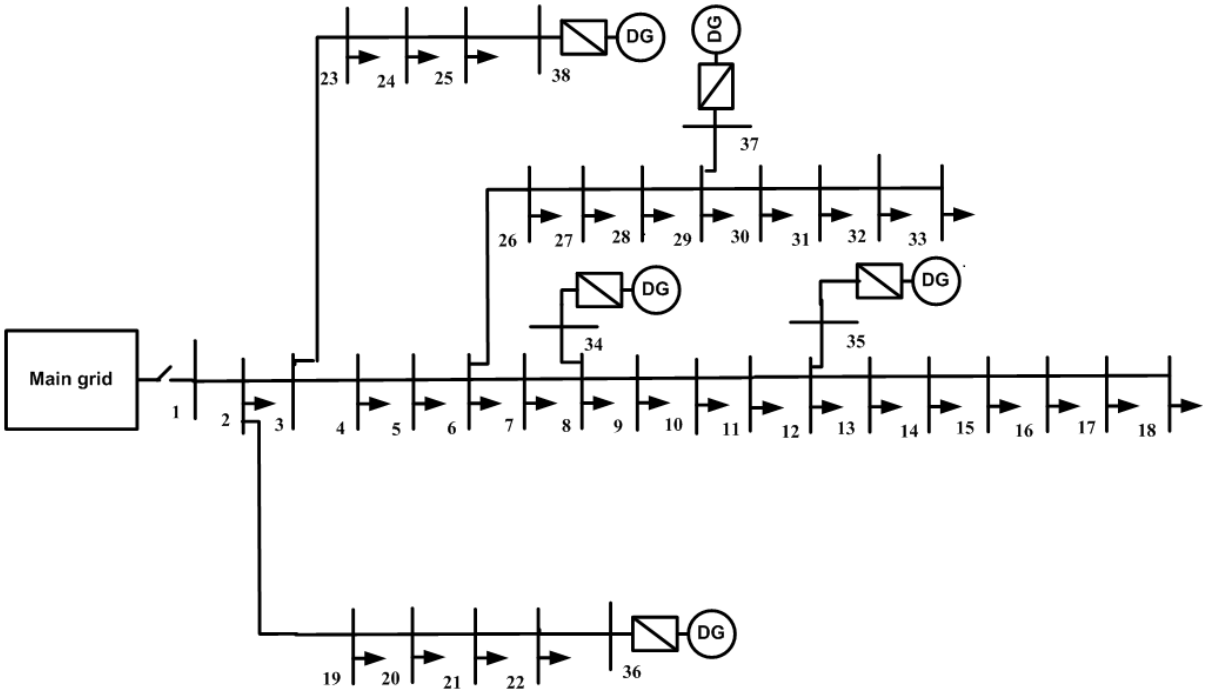

Fig. 5.4 ─ IEEE 33 bus with 5 DGs Isolated Microgrid

2- Using calculated data in step 1, calculate fault currents of feeders and voltages of buses during fault according to the algorithm as shown in Fig. 5.5.

3- From the flow chart:

a) Assume the bus voltage is equal to the measured voltage from step 1 (V=Vm) and initial values of fault currents, calculate the impedance matrix of system Z_{bus}. Then, determine the faulted bus number n_f and fault impedance Z_f. With all other voltage sources set to zero, the voltage at the faulted bus is $-V_f$, and the current entering the faulted bus is $-I_f$, Therefore, the nodal equation becomes

$$\begin{bmatrix} Y_{11} & \cdots & Y_{n1} \\ \vdots & \ddots & \vdots \\ Y_{1n} & \cdots & Y_{nn} \end{bmatrix} \begin{bmatrix} \Delta V_1 \\ -V_f \\ \Delta V_n \end{bmatrix} = \begin{bmatrix} 0 \\ -I_f \\ 0 \end{bmatrix} \tag{5.2}$$

where ΔV_1, ……., ΔV_n are the changes in the voltages at those busses due to the fault current $-I_f$, V_f is the prefault value of the voltage at the faulted bus.

Using the bus impedance

$$\begin{bmatrix} \Delta V_1 \\ -V_f \\ \Delta V_n \end{bmatrix} = \begin{bmatrix} Z_{11} & \cdots & Z_{n1} \\ \vdots & \ddots & \vdots \\ Z_{1n} & \cdots & Z_{nn} \end{bmatrix} \begin{bmatrix} 0 \\ -I_f \\ 0 \end{bmatrix} \tag{5.3}$$

where $Z_{bus} = Y_{bus}^{-1}$

Calculation of new bus impedance by adding the new grounding admittance of grounding impedance (z_f)

$$Y_{iif} = Y_{iinf} + \frac{1}{z_f} \tag{5.4}$$

Where Y_{iif} and Y_{iinf} are the self-admittance of faulted bus *i* of postfault and prefault admittances

Calculate fault voltages buses

$$\text{At faulted bus:} \quad V_f = I_f Z_{ff} \tag{5.5}$$

$$\text{Other buses:} \quad V_{fk} = V_{fk0}\left(1 - \frac{Z_{kn}}{Z_{nn}}\right) \tag{5.6}$$

Calculate feeder fault current connected between n and k buses

$$I_{fnk} = \frac{V_{fn} - V_{fk}}{Z_{nk}} \tag{5.7}$$

The short circuit current contribution of DG is controlled to analyze the equivalent model of inverter-based DG. There are three cases to calculate this short circuit current contribution of DG dependently on the bus voltage of DG.

(1) If $V_{DG} \geq 0.9\ p.u$, DG still maintains original constant power control.

$$I_d = \frac{P_{DG}}{V_{DG}} \quad , I_q = \frac{Q_{DG}}{V_{DG}} \tag{5.8}$$

Where V_{DG} is the bus voltage of DG is, $P_{DG}\ and\ Q_{DG}$ are the active power and reactive power outputs of DG respectively.

(2) If $0.4\ p.u < V_{DG} < 0.9\ p.u$, DG starts to feed more reactive power current

$$I_d = \frac{P_{DG}}{V_{DG}} \ , \quad I_q = k(1 - V_{DG})I_n \tag{5.9}$$

whereI_n is the p.u current of inverter-based DG, k is the voltage adjustment coefficient of reactive power current output of DG, adjusted value 2.

$$\text{If} \quad I_d^2 + I_q^2 > (I_{DGmax})^2 \Rightarrow |I_{DG}| = I_{DGmax}\ , \theta = \tan^{-1}\frac{I_q}{I_{DGmax}} \tag{5.10}$$

(3) If $V_{DG} \leq 0.4\ p.u$, DG feed only reactive power current.

$$I_d = 0 \quad , I_q = I_{max} \tag{5.11}$$

The short circuit current contribution:

$$I_{DG} = I_d + jI_q \tag{5.12}$$

The fault current I_{fr}at bus *r* :

$$I_{fr} = \sum_k^N I_{frk} \tag{5.13}$$

whereI_{frk} is the feeder fault current connected between *r* and *k* buses and *N* is the number of feeders connected to bus *r*.

b) Calculate the error of voltage and current to satisfy accuracy (10^{-4})

4- Repeat steps from step 1 to step 4 for another DGS location.

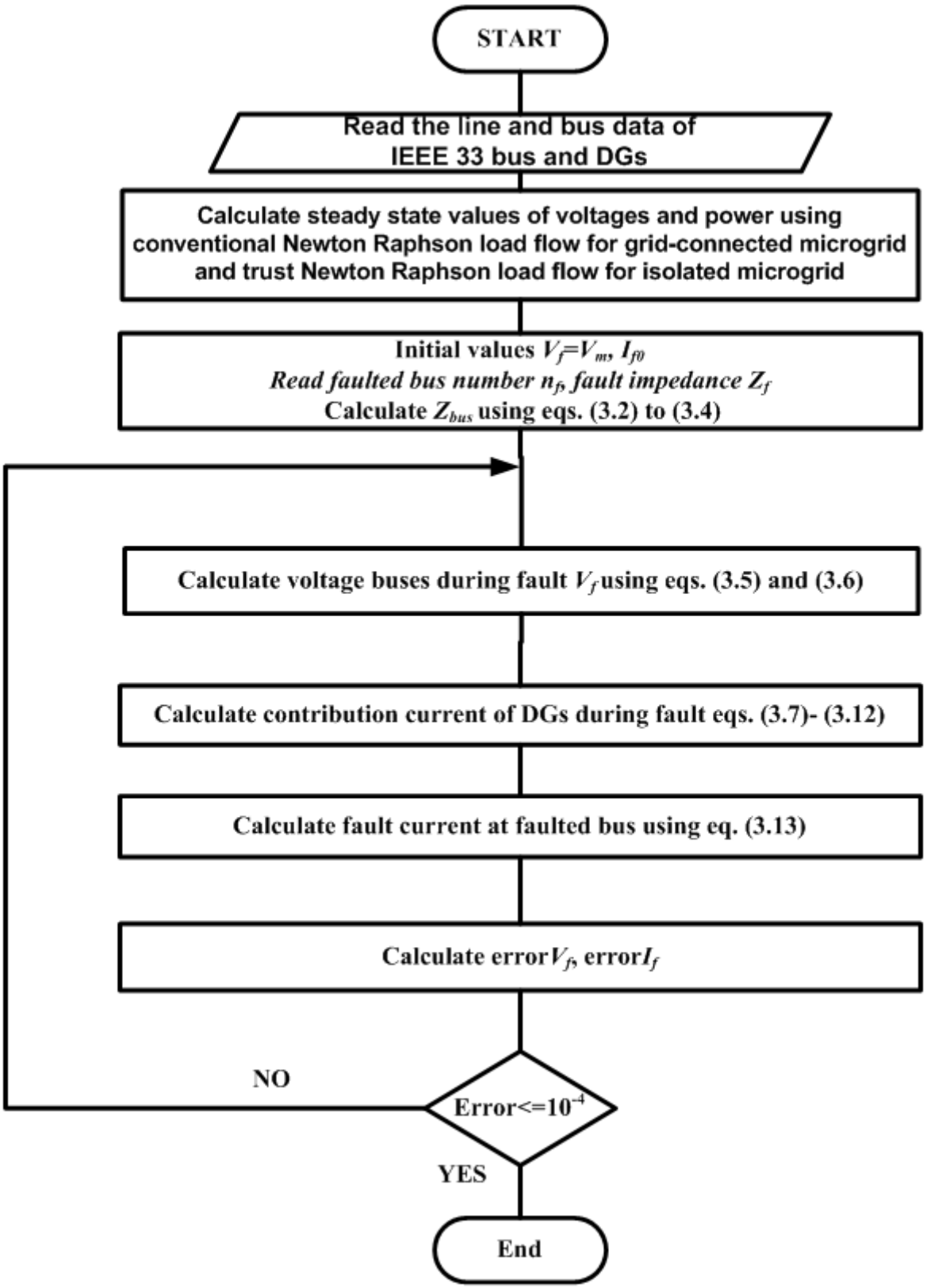

Fig. 5.5 ─ Flow chart of the proposed method

5.1.3 Operation Scenario of the distribution system during the fault

The short circuit current due to three-phase to ground fault applied to the distribution system is very high. For that, the protection device of the system will disconnect the faulted bus. For the faulted bus, the distribution system will divide into small subsystems, grid-connected and isolated. For example; when the fault occurs at bus #3. The protection device will disconnect faulted bus #3. The distribution system will divide into three subsystems as shown in Fig. 5.6.

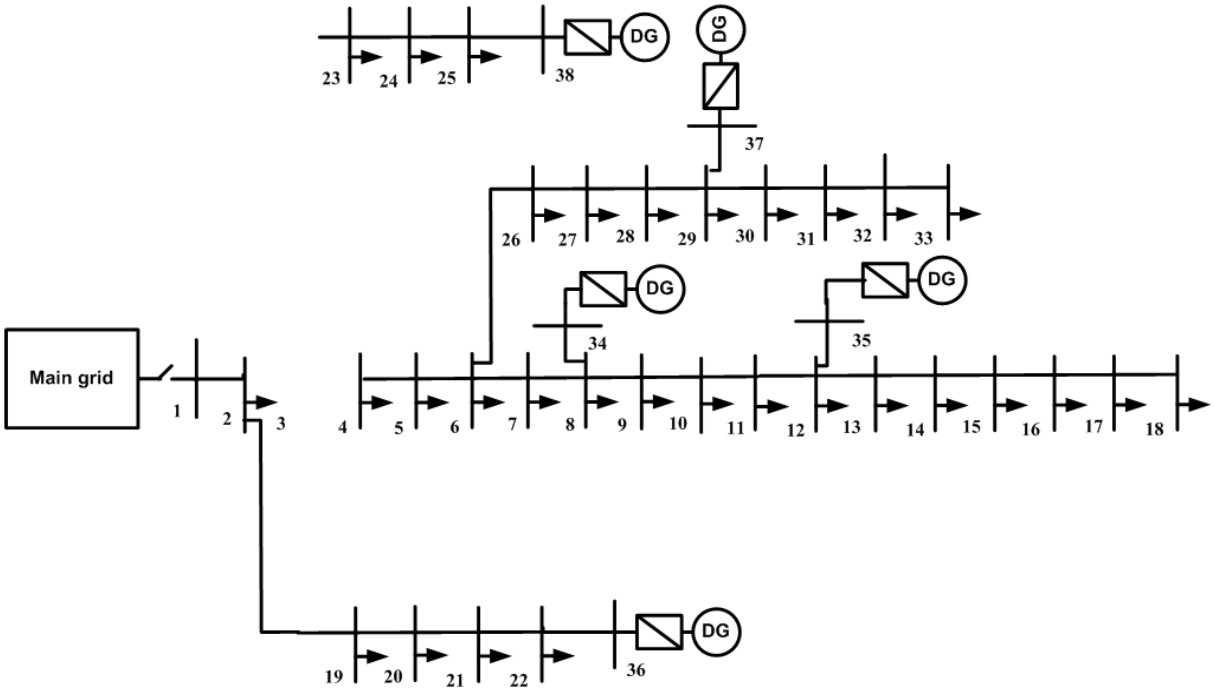

Fig. 5.6 ─ Three subsystems due to the removed faulted bus #3

5.1.4 Static Security risk

The static security risk index (R) in this thesis includes loss load risk index (L/r_j) , nodal voltage limit violation risk index $R(V/r_j)$ and frequency limit violation risk index $R(f/r_j)$.

The static security risk $R(r_j)$ of the system can be obtained by

$$R(r_j) = \propto_L R(L/r_j) + \propto_V R(V/r_j) + \propto_f R(f/r_j) = \propto_L P_r(r_j) S_{sev}(L/r_j) + \propto_V P_r(r_j) S_{sev}(V/r_j) + \propto_f P_r(r_j) S_{sev}(f/r_j) \quad (5.14)$$

where, $S_{sev}(L/r_j)$, $S_{sev}(V/r_j)$ and $S_{sev}(f/r_j)$are the severity of loss load, node voltage limit violation and frequency limit violation under outage r_j respectively, $\propto_L$, $\propto_V$ and $\propto_f$ are their corresponding weight values, respectively, and $P_r(r_j)$ is the probability of the occurrence of the jth component failed.

The severity of the fault can be obtained by [122]

$$S_{sev}(C/r_j) = S_{sev}(x_c) = e^{x_c} - 1 \tag{5.15}$$

The loss value of loss load x_L is obtained by

$$x_L = \frac{\sum_{h=1}^{N_{FL}} P_{FLh}}{\sum_{y=1}^{N_{ZL}} P_{ZLy}} \tag{5.16}$$

where N_{FL}, N_{ZL}, $P_{FLh}$and P_{ZLy} are the total number of loss load, the total number of load, the loss active power of the hth, and the active power of the yth of load point, respectively.

The nodal voltage limit violation loss value x_V is obtained by

$$x_V = \begin{cases} V_{min} - V_i & 0 \le V_i \le V_{min} \\ 0 & V_{min} \le V_i \le V_{max} \\ V_i - V_{max} & V_i > V_{max} \end{cases} \tag{5.17}$$

where$V_i$is the voltage amplitude of node *i*, V_{max} and V_{min} are the set voltage upper and lower limits, respectively.

The frequency limit violation loss value x_f is obtained by

$$x_f = \begin{cases} f_{min} - f & 0 \le f \le f_{min} \\ 0 & f_{min} \le f \le f_{max} \\ f - f_{max} & f > f_{max} \end{cases} \tag{5.18}$$

where$f$ is the frequency of the system,f_{max} and f_{min} are the upper and lower limits of the set steady-state frequency, respectively

5.1.5 Load Shedding Strategy

Compare the total output of the DG of system or islanded DGs subsystem with the total active power of the load to determine the load shedding, if $P_{DGZ} \ge P_{LZ}(1+\sigma)$ and $P_{DGZ} \le P_{DGZmax}$ there is no load shedding. However, two methods used to calculate the load-shedding value P_{Lsh}

a. Compare the output of DGs with the total active power of the load. In this case, the load flow program does not have any results where the values of voltages, currents, and power of buses are not convergent.

$$P_{DGZ} < P_{LZ}(1+\sigma) \tag{5.19}$$

$$P_{Laftersh} = \frac{P_{DGZ}}{(1+\sigma)} \tag{5.20}$$

$$P_{Lsh} = P_{Lz} - P_{Laftersh} \tag{5.21}$$

where P_{DGZ},P_{LZ} and $P_{Laftersh}$are the total active output of the DG device, the total active power of the load in the system, or subsystem of islanded DGs and the total active power of the load after shedding respectively and σ is the net loss coefficient.

b. Compare the output of DGs with a maximum output of DGs. In this case, the load flow program has results but the values of voltages are small and the output of power of DG is greater than its limit.

$$P_{DGZ} > P_{DGZmax} \tag{5.22}$$

$$P_{Lsh} = P_{DGZ} - P_{DGZmax} \tag{5.23}$$

where P_{DGZ}, P_{DGZmax} and $P_{Lsh}$are the total active output of the DGs, the total maximum active output of the DGs and the total active power of the load shedding respectively andσ is the net loss coefficient

5.2 System under study

In this thesis, the short circuit current calculation is tested on the IEEE 33-bus distribution system, whose rated voltage is 10 kV as shown in Fig. 5.4. The same inverter-based DGs are connected to buses 8, 12, 22, 25 and 29. Table. 5.1 shows the buses and lines data of the IEEE 33-bus. Table 5.2 shows DGS locations, nominal settings, and ratings.

Table. 5.1. ─ The buses and lines data of the IEEE 33-bus

From	To	R (p.u)	X(p.u)	Line rate (MW)	Load at receiving bus	
1	2	0.0574	0.0293	5.0000	Pl(kW)	Ql(kW)
2	3	0.3070	0.1564	5.0000	100	60
3	4	0.2279	0.1161	5.0000	90	40
4	5	0.2373	0.1209	5.0000	120	80
5	6	0.5100	0.4402	5.0000	60	30
6	7	0.1166	0.3853	5.0000	60	20
7	8	0.4430	0.1464	5.0000	200	100
8	9	0.6413	0.4608	5.0000	200	100
9	10	0.6501	0.4608	5.0000	60	20
10	11	0.1224	0.0405	2.5300	60	20
11	12	0.2331	0.0771	2.5300	45	30
12	13	0.9141	0.7192	2.5300	60	35
13	14	0.3372	0.4439	2.5300	60	35
14	15	0.3680	0.3275	2.5300	120	80
15	16	0.4647	0.3394	2.5300	60	10
16	17	0.8026	1.0716	2.5300	60	20
17	18	0.4558	0.3574	2.5300	60	20
2	19	0.1021	0.0974	2.5300	90	40
19	20	0.9366	0.8440	2.5300	90	40
20	21	0.2550	0.2979	2.5300	90	40
21	22	0.4414	0.5836	2.5300	90	40
3	23	0.2809	0.1920	2.5300	90	40
23	24	0.5592	0.4415	2.5300	90	50
24	25	0.5579	0.4366	2.5300	420	200
6	26	0.1264	0.0644	2.5300	420	200
26	27	0.1770	0.0901	2.5300	60	25
27	28	0.6594	0.5814	2.5300	60	25
28	29	0.5007	0.4362	2.5300	60	20
29	30	0.3160	0.1610	2.5300	120	70
30	31	0.6067	0.5996	2.5300	200	100
31	32	0.1933	0.2253	2.5300	150	70
32	33	0.2123	0.3301	2.5300	210	100
					60	40

Table. 5.2. ─ DGS locations, nominal settings, and ratings

DG No.	Location	ω (p.u)	V (p.u)	S_{max} (p.u)	Q_{max} (p.u)
1	34	1	1.01	3	1.8
2	35	1	1.01	1.5	0.9
3	36	1	1.01	0.5	0.3
4	37	1	1.01	1.0	0.6
5	38	1	1.01	0.5	0.3

5.3 Results and Analysis

A three-phase fault is applied to the IEEE 38-bus distribution system, shown in Fig. 5.4. The short circuit current is calculated using virtual impedance and proposed a method for a grid-connected and isolated microgrid in four cases of the locations of DGs in IEEE 33-bus distribution in Table. 5.3, the base power and base voltage are 1 MVA and 12.6 kV.

Table. 5.3. ─ Four cases of the location of DGs in IEEE 33-bus distribution

DG bus No.	Connected to bus No.			
	Case 1	Case 2	Case 3	Case 4
34	8	1	1	3
35	9	18	8	12
36	12	22	9	21
37	18	25	14	24
38	24	33	18	29

Functional dependence of the peak current on the capacity of the converter. During the fault, DG can be considered as source in series different reactance depending on the case of current peak current, ultra-transient current and steady state short-circuit current. These values depend on the capacity of converter. Table 4 shows sub-transient, transient and steady-state reactance values of wind

turbine PMSG with different capacity of converter. Fig. 25 shows the functional characteristic of peak current with capacity of converter of wind turbine during fault. Table 5 shows sub-transient, transient and steady-state reactance values of PV generator with different capacity of converter. Fig. 26 shows the functional characteristic of peak current with capacity of converter of wind turbine during fault.

Table 5.4 ─ Sub-transient, transient and steady-state reactance values of wind turbine PMSG with different capacity of converter

Capacity of converter (MW)	E(V)	I(A)	I’(A)	I’’(A)	x (ohm)	x’ (ohm)	x''(ohm)
1.5	500	1470	3552	4671	0.34	0.14	0.11
1	500	945	1247	1980	0.53	0.4	0.25
0.8	500	850	1208	1939	0.59	0.41	0.26
0.425	500	462	1133	1541	1.1	0.44	0.32
0.1	500	184	1100	1270	2.7	0.45	0.39

Table 5.5 ─ Sub-transient, transient and steady-state reactance values PV generator with different capacity of converter

Capacity of converter (kW)	E(V)	I(A)	I’(A)	I’’(A)	x(ohm)	x'(ohm)	x’’(ohm)
250	205	852	1250	1735	0.24	0.164	0.12
200	205	708	1243	1621	0.29	0.165	0.126
150	205	510	1240	1503	0.4	0.165	0.136
100	205	348	1234	1421	0.59	0.166	0.144
50	205	190	1211	1336	1.1	0.17	0.153

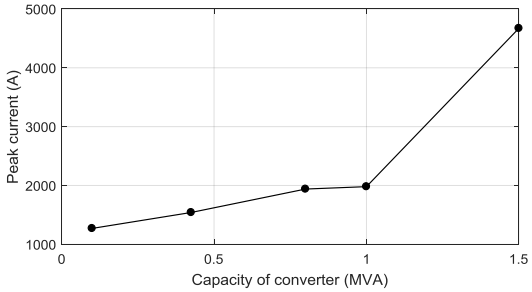

Fig. 5.7 ─ Peak current with capacity of converter of wind turbine PMSG during fault

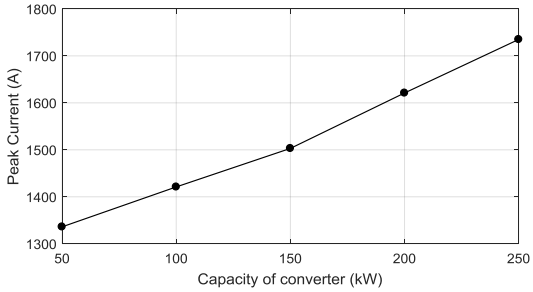

Fig. 5.8 ─ Peak current with capacity of converter of PV generator during fault

5.3.1 Grid-connected Microgrid

A three-phase-to-ground fault is applied to the IEEE 38-bus distribution system, Fig. 5.4, at bus No. 8. The fault current value at bus No. 8 is calculated using virtual impedance and proposed methods. Table. 5.6 shows the value of short circuit current at bus No. 8 for four cases. Table. 5.7 shows the voltages profile values of DG buses during the fault in two methods. Table. 5.8 shows the output short circuit current values of DG buses during the fault in two methods. The numbers A, B, C, D, and E are the values of the connected bus with DGs as in Table. 5.3.

Table. 5.6. ─ The value of short circuit current at bus No. 8 for four cases in two methods

Fault current	Case 1	Case 2	Case 3	Case 4
virtual impedance method (p.u)	72.90	47.71	69.99	52.94
proposed method (p.u)	42.80	32.56	40.80	42.45

Table. 5.7. ─ The voltages profile values of DG buses during the fault in two methods

DG bus	Case1		case 2		Case 3		Case 4	
	Virtual impedance	Proposed method	Virtual impedance	Proposed method	Virtual impedance	Proposed method	Virtual impedance	Proposed method
34	0.2378	0.2378	0.9032	0.9032	0.8751	0.875	0.8120	0.820
35	0.3989	0.3989	0.6029	0.6029	0.2386	0.236	0.4102	0.402
36	0.5377	0.5375	0.9268	0.926	0.3877	0.387	0.9265	0.925
37	0.6831	0.683	0.7982	0.7981	0.5940	0.590	0.7964	0.794
38	0.7549	0.759	0.5946	0.5946	0.7392	0.732	0.5084	0.508

Table. 5.8. ─ The output short circuit current values of DG buses during the fault in two methods

DG bus	Case1		case 2		Case 3		Case 4	
	Virtual impedance	Proposed method	Virtual impedance	Proposed method	Virtual impedance	Proposed method	Virtual impedance	Proposed method
34	13.5	2.0	3.1	0.02	3.8	0.37	3.98	0.56
35	10.93	1.80	7.07	1.19	13.55	2.0	10.92	1.77
36	8.93	1.39	2.50	0.11	11.17	1.84	2.64	0.11
37	6.16	0.95	3.97	0.61	7.64	1.22	4.09	0.61
38	5.08	0.74	7.06	1.22	5.52	0.78	8.51	1.47

From the results presented in Table. 5.8, due to the droop control model inverter-based DG, the short circuit current contribution of the proposed system within the limit of its limit value of inverter (2 p.u). In contrast, the virtual impedance cannot limit this current value of DG within its limit when the fault occurs near the DG bus. For that, the fault current value calculated using the proposed method is less than its value calculating by the virtual impedance method by more than 30%, as shown in Table. 5.6. While the short circuit current contribution of DG depends on the location of the fault near or not from DG, the increasing percentage of fault current after installing DG at certain locations is different. From Table. 5.6, the highest value of fault current is 72.90 p.u by the virtual impedance method and 42.80 p.u by the proposed method in case 1 compared to other cases where all DGs connected to the same feeder (Bus #6-Bus #18) near the fault. The contribution short circuit currents of DGs are the highest values in case 1, 13.5 p.u, 10.93 p.u, 8.93 p.u, 6.16 p.u and 5.08 p.u by virtual impedance method and 2.0 p.u, 1.80 p.u, 1.39 p.u, 0.95 p.u and 0.74 by the proposed method. In contrast, in case 2 the lowest value of fault current is 47.71 p.u by virtual impedance method and 32.56 p.u by a proposed method where all DGs connected to buses far from fault. The contribution short circuit currents of DGs are also the lowest

values in case 2, 3.14 p.u, 7.07 p.u, 2.50 p.u, 3.97 p.u and 7.06 p.u by virtual impedance method and 0.02 p.u, 1.19 p.u, 0.11 p.u, 0.61 p.u and 1.22 p.u by the proposed method.

A Three-phase to ground fault is applied to all buses. To calculate the value of fault current in all buses using virtual impedance and proposed methods. Fig. 5.9 shows the value of fault current in all buses using virtual impedance and proposed methods. Figs. 5.10 to 5.14 show the contribution currents of 5 DGs using virtual impedance and proposed methods.

As shown in Fig. 5.9, the fault current value which is calculated using the proposed method is lower than its value by the virtual impedance method. The fault current values are higher at buses near the main grid for two methods, their values are 119 p.u at bus #1, 110 p.u at bus #2, 109.5 p.u at bus #19 and 73.2 p.u at bus #23 for proposed method compared to 153 p.u at bus #1, 151 p.u at bus #2, 131.7 p.u at bus #3 and 131.5 p.u at bus #19 for the virtual impedance method. From Figs. 5.10 to 5.14, the short circuit current contribution values of DGs connected to buses #8, 12, 22, 25 and 29 are within their limit value of inverter-based DG (2 p.u) for proposed method during the fault. For the virtual impedance method, the short circuit current contribution values of DGs are very high when the fault occurs at the bus which they are connected. These values are 13.5 p.u for DG 1 at faulted bus #8, 13.3 p.u for DG 2 at faulted bus #12, 14.1 p.u for DG 3 at faulted bus #22, 16.2 p.u for DG 4 at faulted bus #25 and 15.7 p.u for DG 5 at faulted bus #29.

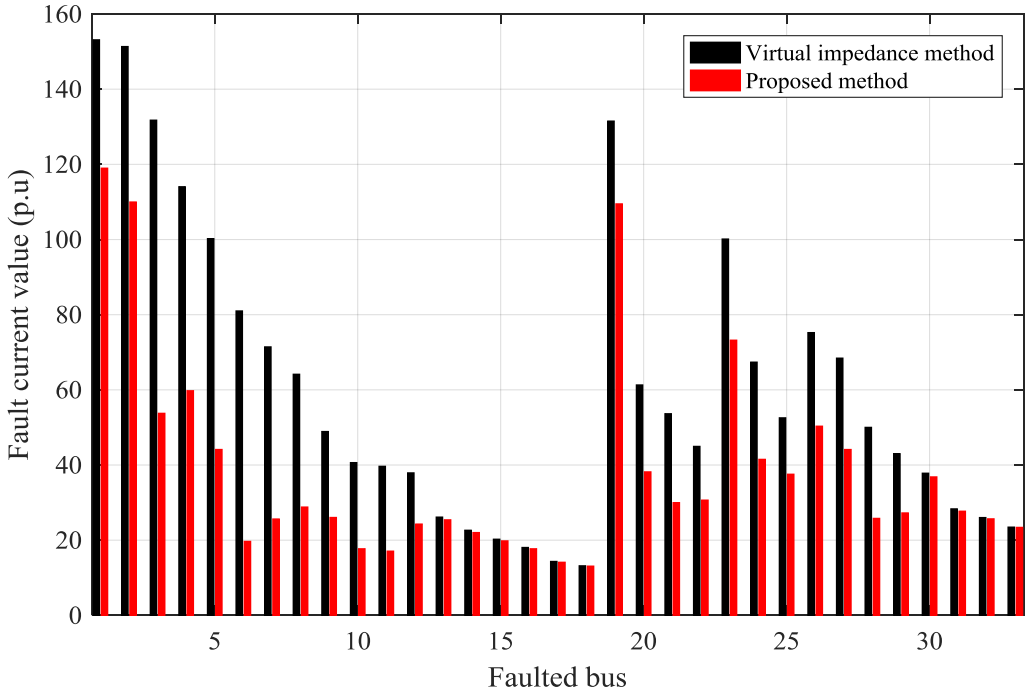

Fig. 5.9 ─ The value of fault current in all buses using virtual impedance and proposed methods

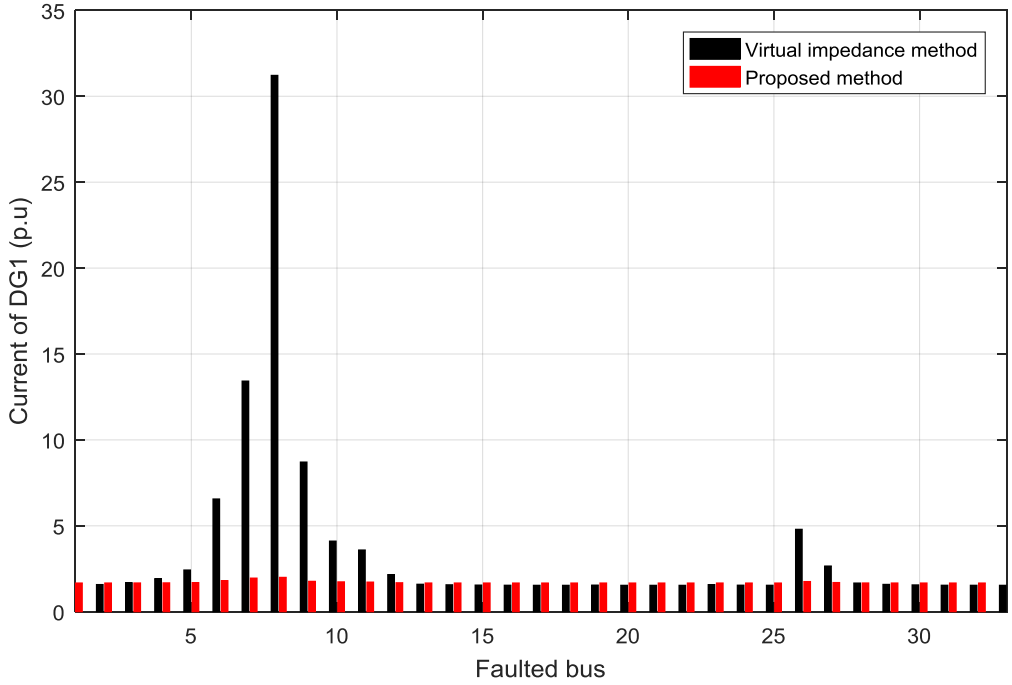

Fig. 5.10 ─ The contribution current of DG 1 using virtual impedance and proposed methods

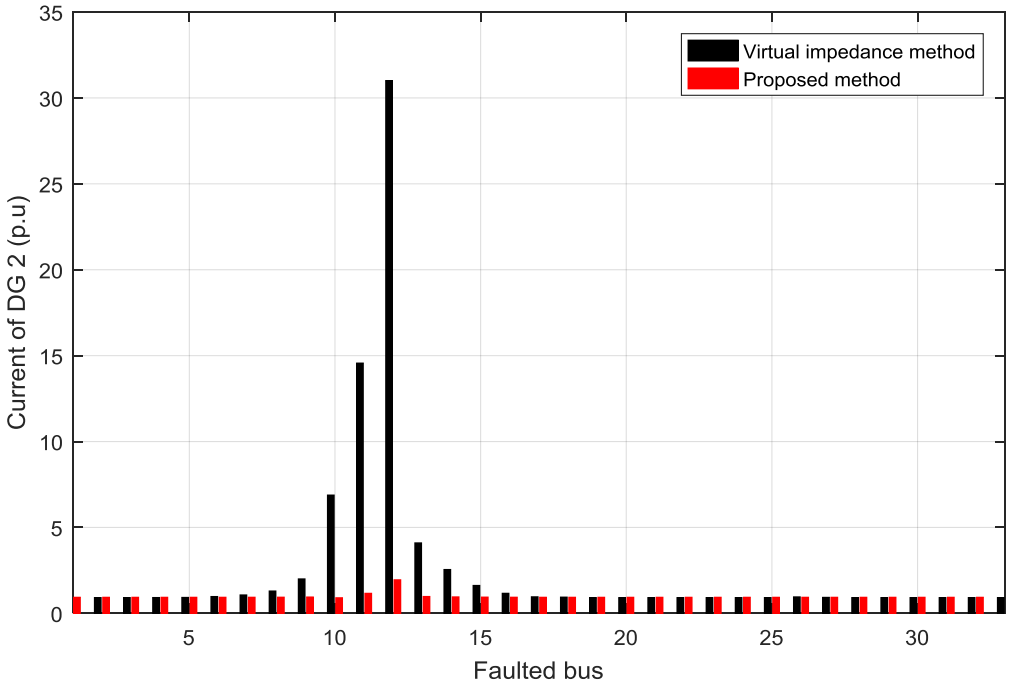

Fig. 5.11 ─ The contribution current of DG 2 using virtual impedance and proposed methods

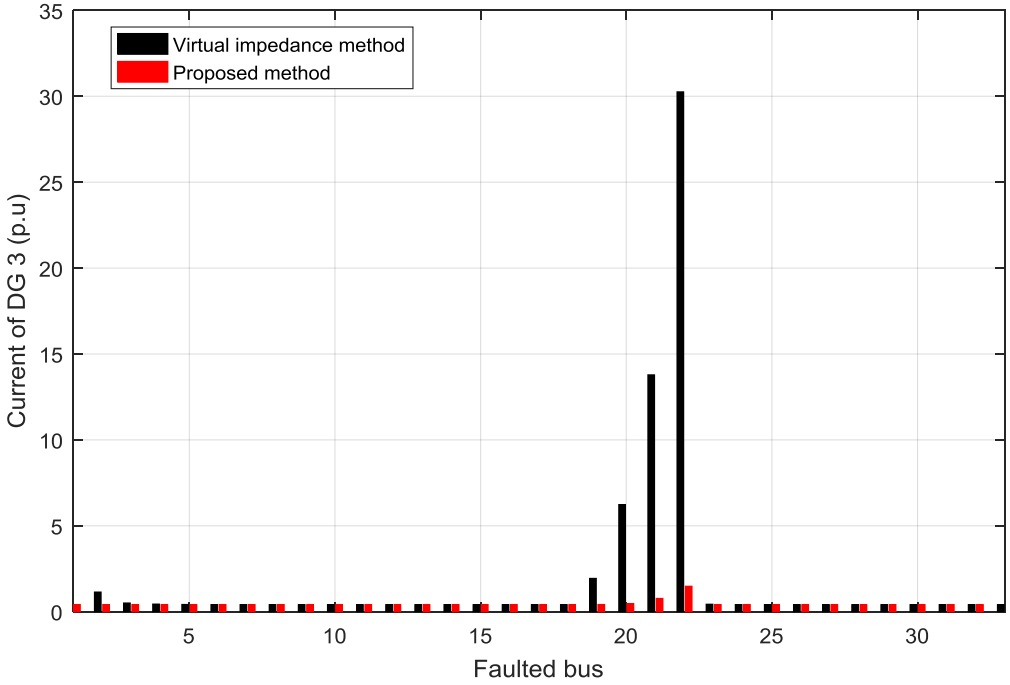

Fig. 5.12 ─ The contribution current of DG 3 using virtual impedance and proposed methods

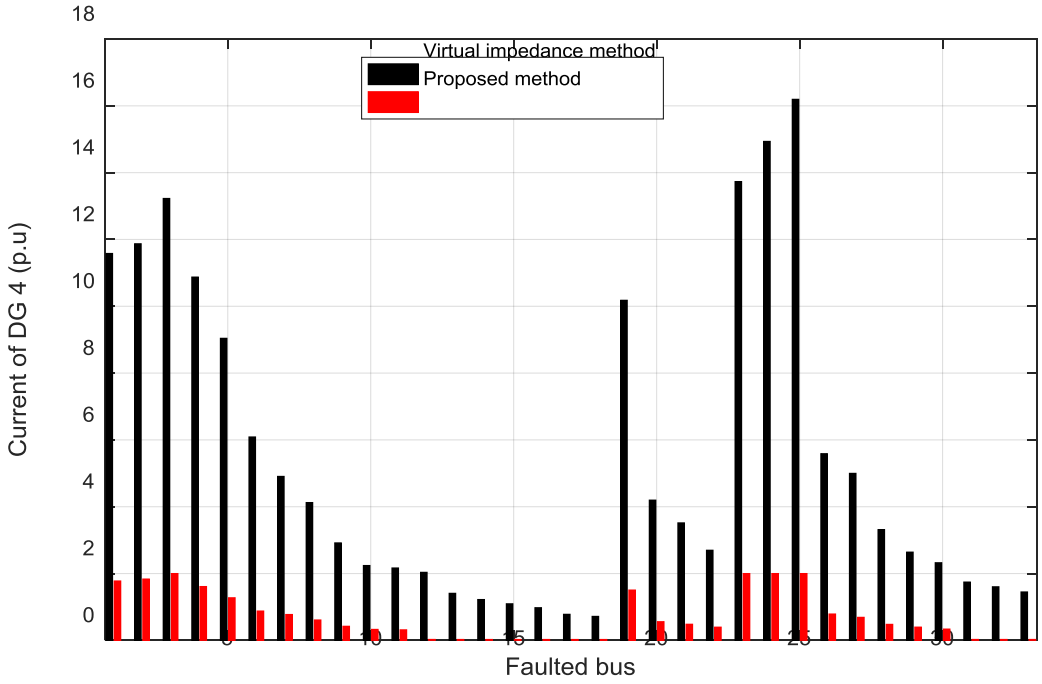

Fig. 5.13 ─ The contribution current of DG 4 using virtual impedance and proposed methods

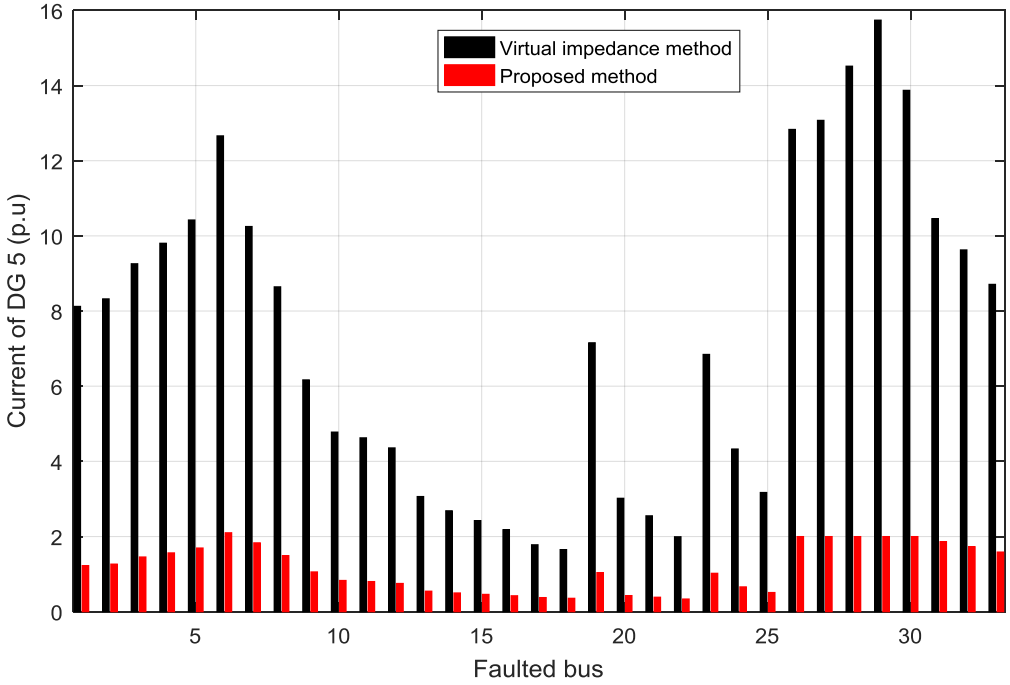

Fig. 5.14 ─ The contribution current of DG 5 using virtual impedance and proposed methods

Static Security Risk Assessment Results

Due to the short circuit current value, the protection device will disconnect the faulted bus, the distribution system divided into subsystems. The power flow program is used to calculate the voltage and active power of all buses. The static security risk (R) and load shedding can be calculated using equations from (5.14) to (5.18). Which the values of the constants are $\propto_L = \propto_V = \propto_f = 0.005$, $P_r(r_j) = 1/33$, $V_{max} = 1.05$, $V_{min} = 0.95$, $f_{max} = 1.05$ and $f_{min} = 0.95$. The net loss coefficient can be calculated using the steady-state load flow of the IEEE distribution system $\sigma = \frac{P_{netlosses}}{P_{gnet}}$, $P_{netlosses}$ are the net losses of the system, P_{gnet} is the total generation of the system. Table. 5.9 shows the static security risk and load shedding values during the fault at buses #2, 3, 4, 6, 7, 8,12 and 13.

Table. 5.9. ─ The static security risk and load shedding values

Faulted bus No.	R, %	Load shedding (kW)
2	0.0485	100
3	0.1237	530
4	0.0255	120
6	0.049	60
7	0.026	200
8	0.05	200
12	0.1955	510
13	0.1477	450

Due to the fault at bus #3 the isolated subsystem which has buses # 23, 24, 25 and 38, the total active power of the load is greater than the active power generation of DG at bus #38. The values of voltages equal to zero and this subsystem need to shedding load. The value of the shedding load calculated by reducing the load by the percentage of load after shedding to total load. The static security risk is

high value as a result of fault occur near the main grid at buses 2, 12 and 13. When the fault occurs at buses 12, 13 to 18, the all load shedding is failure load. Due to the fault, the protection devices will remove the faulted bus which explained in sec. 5.1.3. The operation scenario divides the distribution system to grid-connected and isolated subsystems. Each subsystem works as a small distribution system. The newton-raphson and trust newton raphson load flows are used to calculate the steady-state operation of subsystems, as well as the load shedding, which can calculate using strategy in sec 5.1.5. Fig. 5.15 shows bus voltages at faulted bus #3 before and after load shedding. Others faulted buses #2, 4, 6, 7, 8, 12 and 13 do not need to load shedding. The bus voltages of faulted buses #2, 4, 6, 7, 8, 12 and 13 are shown in Figs. 5.16 and 5.17.

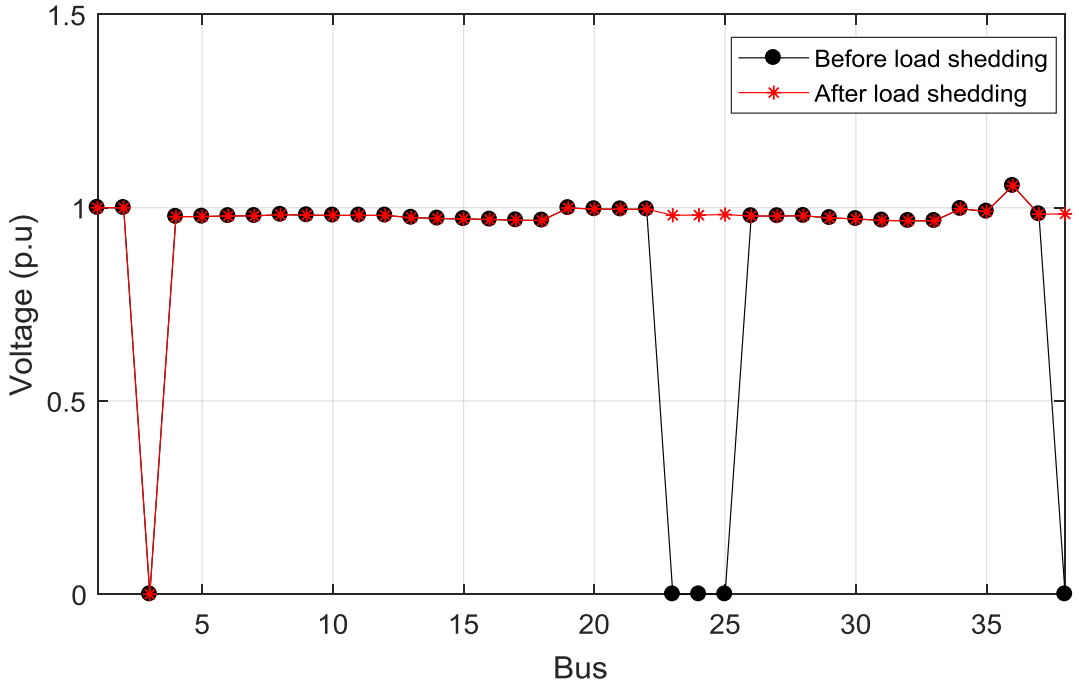

Fig. 5.15 ─ Bus voltages at faulted bus #3 before and after load shedding

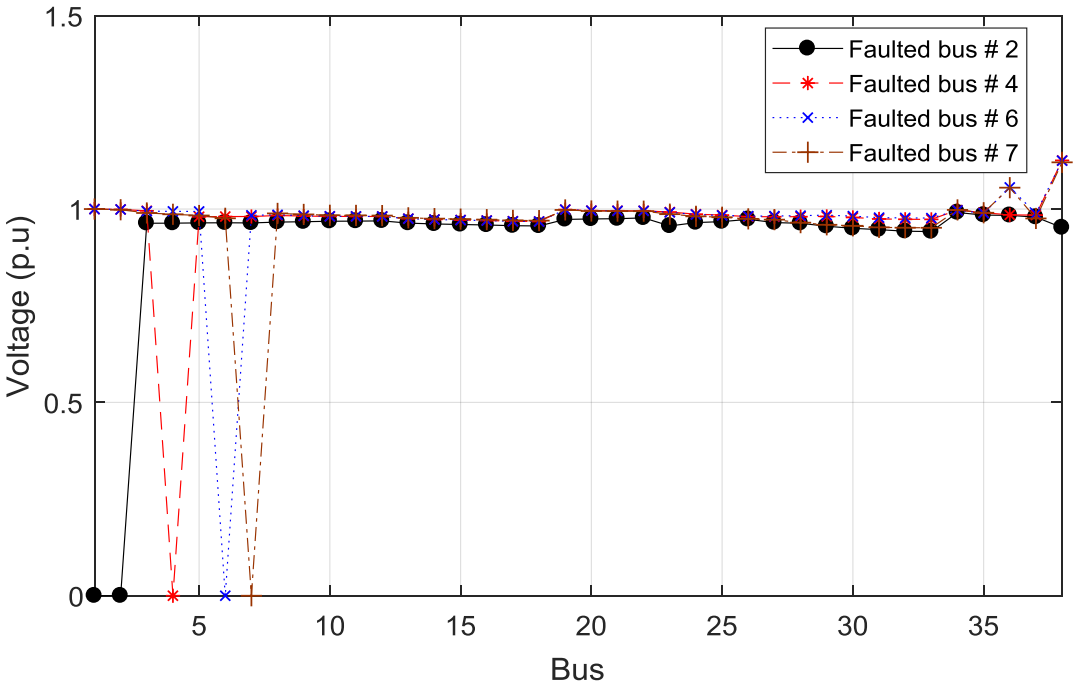

Fig. 5.16 ─ Bus voltages at faulted bus #2, 4, 6 and 7

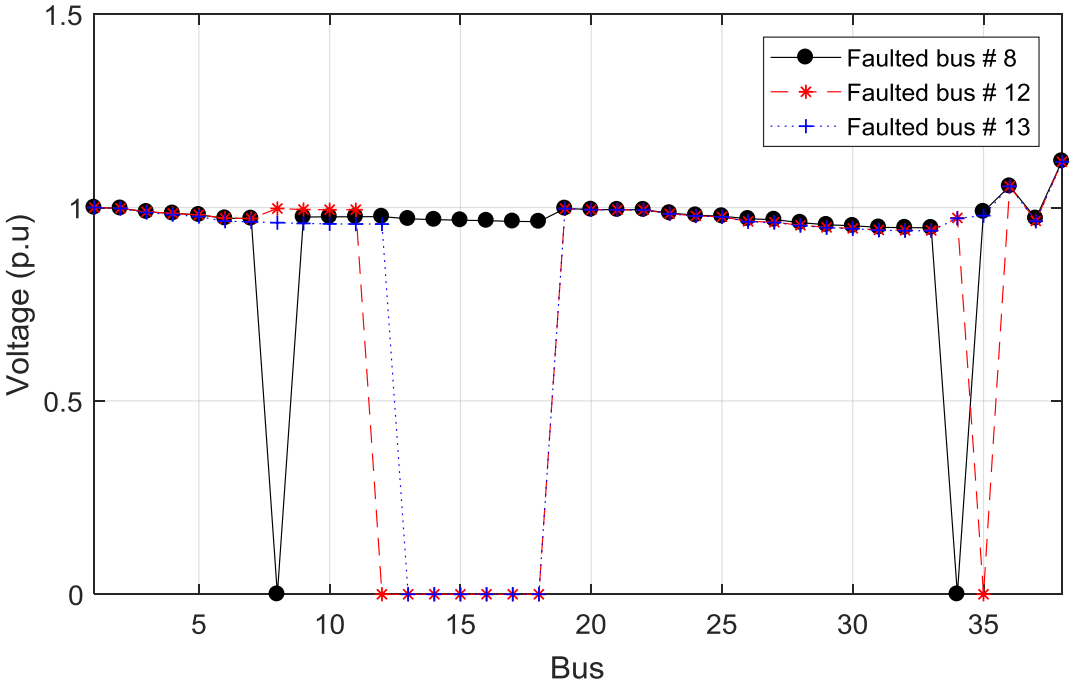

Fig. 5.17 ─ Bus voltages at faulted bus #8, 12 and 13

As shown in Fig. 5.15, the voltages profile is improved after load shedding where the total output of the generator can feed the total load after shedding and total

losses of the subsystem. Figs. 5.16 and 5.17 given, the voltages profiles are better for faulted buses which do not need load shedding. The generation units of subsystems have the ability to feed their total load before shedding and total losses.

5.3.2 Isolated Microgrid

A three-phase-to-ground fault is applied to the system at bus No. 8. The fault current value in bus No. 8 is calculated using virtual impedance and proposed methods. The one-line diagram for both test systems is shown in Fig. 5.4. Table. 5.10 shows the value of short circuit current at bus No. 8 for four cases. Table. 5.11 shows the voltages profile values of DG buses during the fault in two methods. Table. 5.12 shows the output short circuit current values of DG buses during the fault in two methods. The numbers A, B, C, D, and E are the values of the connected bus with DGs as in Table. 5.3.

Table. 5.10. ─ The value of short circuit current at bus No. 8 for four cases in two methods

Fault current	Case 1	Case 2	Case 3	Case 4
virtual impedance method (p.u)	45.90	42.59	46.38	43.11
proposed method (p.u)	22.96	22.68	23.24	22.96

Table. 5.11. ─ The voltages profile values of DG buses during the fault in two methods

DG bus	Case1		case 2		Case 3		Case 4	
	Virtual impedance	Proposed method	Virtual impedance	Proposed method	Virtual impedance	Proposed method	Virtual impedance	Proposed method
34	0.5474	0.544	0.9947	0.994	0.9864	0.9864	0.9956	0.996
35	0.8390	0.830	0.9892	0.989	0.5452	0.542	0.9768	0.976
36	0.9733	0.973	0.9797	0.977	0.8346	0.834	0.9812	0.982
37	0.9989	0.998	0.9813	0.981	0.9935	0.995	0.9833	0.983
38	0.9100	0.910	0.9443	0.943	0.9929	0.991	0.9540	0.950

Table. 5.12. ─ The output short circuit current values of DG buses during the fault in two methods

DG bus	Case1		case 2		Case 3		Case 4	
	Virtual impedance	Proposed method	Virtual impedance	Proposed method	Virtual impedance	Proposed method	Virtual impedance	Proposed method
34	31.08	2.0	1.30	1.56	1.68	1.76	1.28	1.54
35	10.78	1.05	0.77	0.84	30.96	1.96	1.31	0.94
36	0.71	0.35	0.33	0.33	10.33	0.58	0.32	0.32
37	0.77	1.05	1.29	1.28	1.02	1.06	1.24	1.23
38	0.47	0.44	0.42	0.42	0.23	0.27	0.60	0.41

From the results presented in Table. 5.12, due to the droop control model inverter-based DG, the short circuit current contribution of the proposed system within the limit of its limit value of inverter (2 p.u). In contrast, the virtual impedance cannot limit this current value of DG within its limit when the fault occurs near the DG bus. For that, the fault current value calculated using the proposed method is less than its value calculating by the virtual impedance method by approximately 50%, as shown in Table. 5.10. In contrast the results of grid-connected microgrid, in isolated microgrid, the fault current value does not depend on location of DG the location near or far from fault, the fault current values are in range (42.5 – 46) p.u by virtual impedance method and in range (22.6 – 23.2) p.u by proposed

method in four cases. From Table. 5.10, the highest value of fault current is 46.38 p.u by the virtual impedance method and 23.24 p.u by the proposed method in case 3 compared to other cases. The contribution short circuit currents values of DGs are 1.68 p.u, 30.96 p.u, 10.33 p.u, 1.02 p.u and 0.23 p.u by virtual impedance method and 1.76 p.u, 1.96 p.u, 0.58 p.u, 1.06 p.u and 0.27 by the proposed method. In case 2 the lowest value of fault current is 42.59 p.u by the virtual impedance method and 22.68 p.u by the proposed method. The contribution short circuit currents values of DGs are in case 2, 1.30 p.u, 0.77 p.u, 0.33 p.u,1.29 p.u and 0.42 p.u by virtual impedance method and 1.56 p.u, 0.84 p.u, 0.33 p.u, 1.28 p.u and 0.42 p.u by the proposed method.

A Three-phase to ground fault is applied to all buses. To calculate the value of fault current in all buses using virtual impedance and proposed methods. Fig. 5.18 shows the value of fault current in all buses using virtual impedance and proposed methods. Figs. 5.19 to 5.23 show the contribution currents of 5 DGs using virtual impedance and proposed methods.

As shown in Fig. 5.18, the fault current value which is calculated using the proposed method is lower than its value by the virtual impedance method. In contrast the grid-connected microgrid, the fault current values is higher at buses near the DGs connection for two methods, their values are 62.7 p.u at bus #3, 62.3 p.u at bus #6, 54.3 p.u at bus #19 and 50.4 p.u at bus #26 for the proposed method compared to 202.4 p.u at bus #2, 112.5 p.u at bus #11, 122.25 p.u at bus #19 and 117.75 p.u at bus 26 for the virtual impedance method. From Figs. 5.19 to 5.23, the short circuit current contribution values of DGs connected to buses 8, 12, 22, 25 and 29 are within their limit value of inverter-based DG (2 p.u) for proposed method during the fault. For the virtual impedance method, the short circuit current contribution values of DGs are very high when the fault occurs at the bus which they are connected. These values are 31.1 p.u for DG 1 at faulted bus #8, 31.1 p.u for DG 2 at faulted bus #12, 30.6 p.u for DG 3 at faulted bus #22, 18.3 p.u for DG 4 at faulted bus #25 and 49.5 p.u for DG 5 at faulted bus #29,

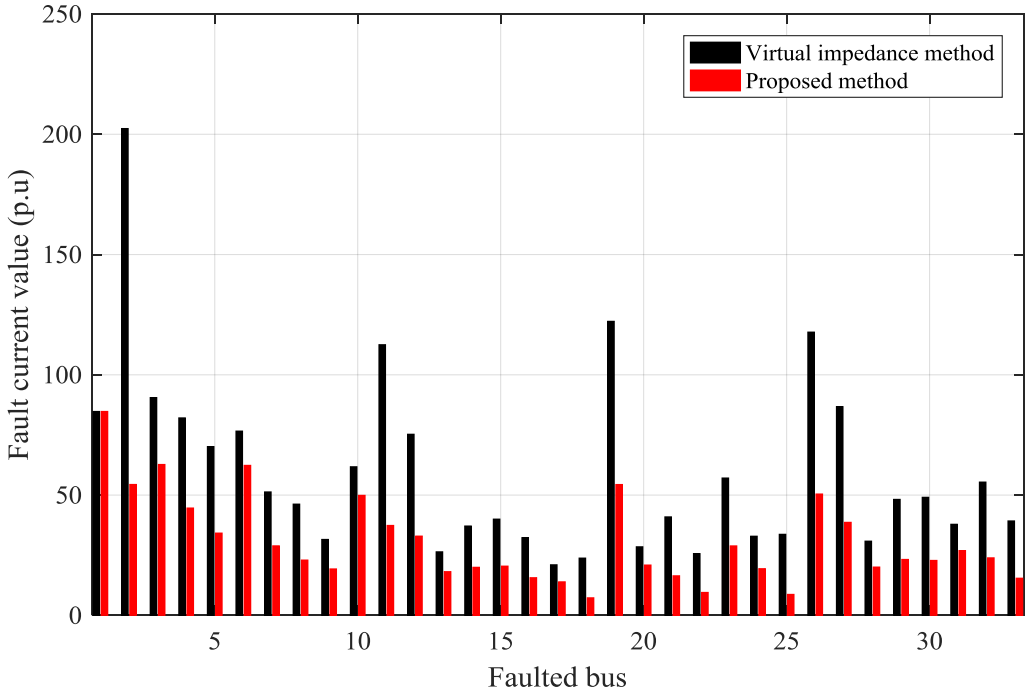

Fig. 5.18 ─ The value of fault current in all buses using virtual impedance and proposed methods

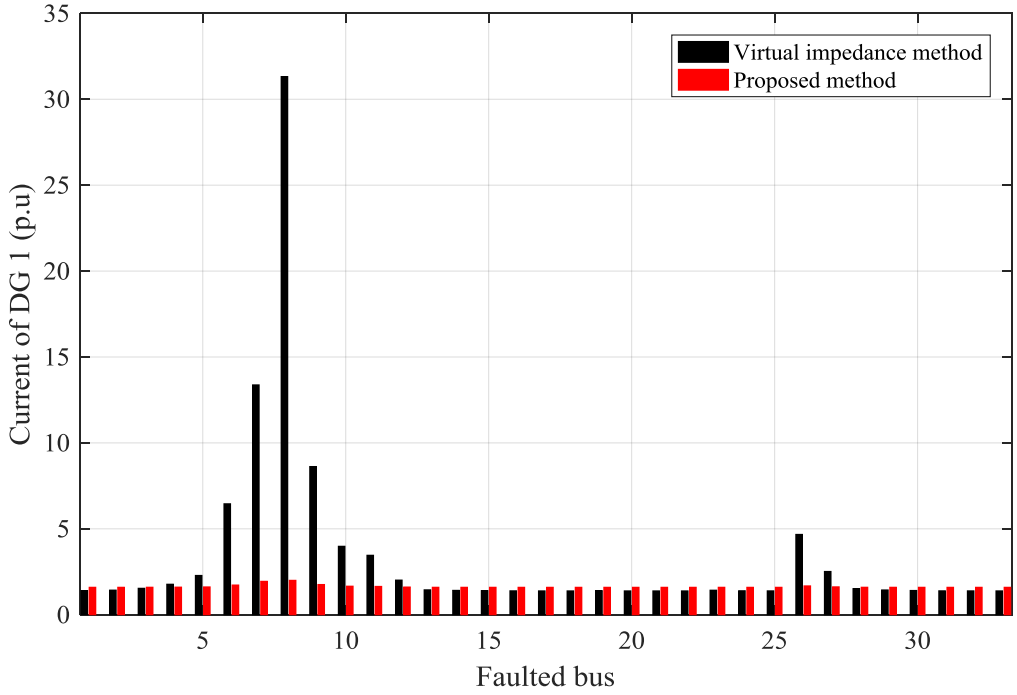

Fig. 5.19 ─ The contribution current of DG 1 using virtual impedance and proposed methods

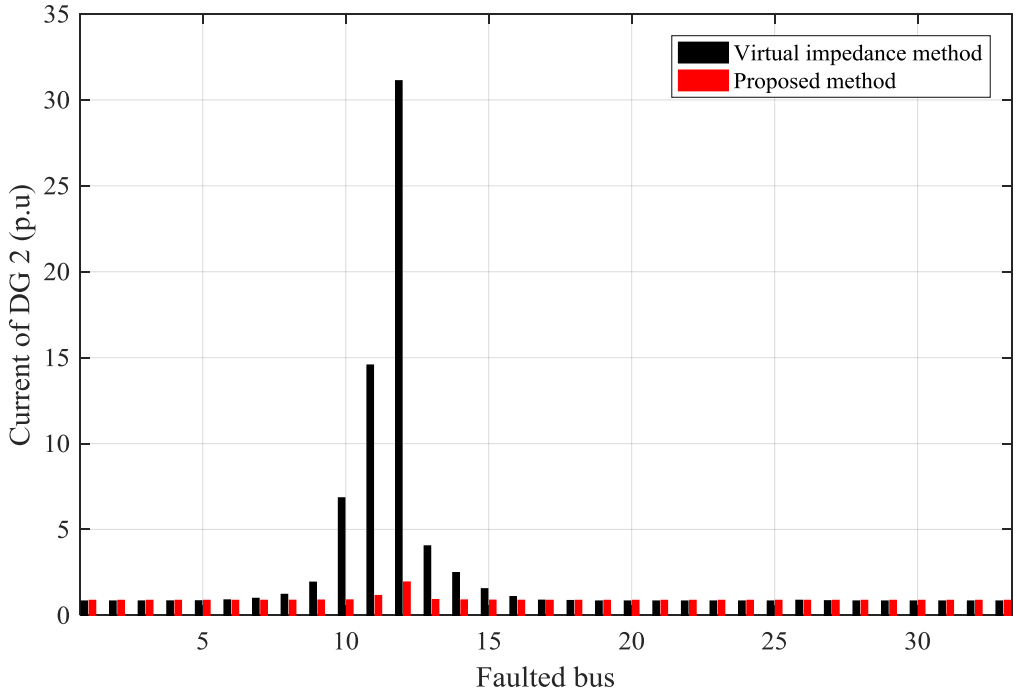

Fig. 5.20 ─ The contribution current of DG 2 using virtual impedance and proposed methods

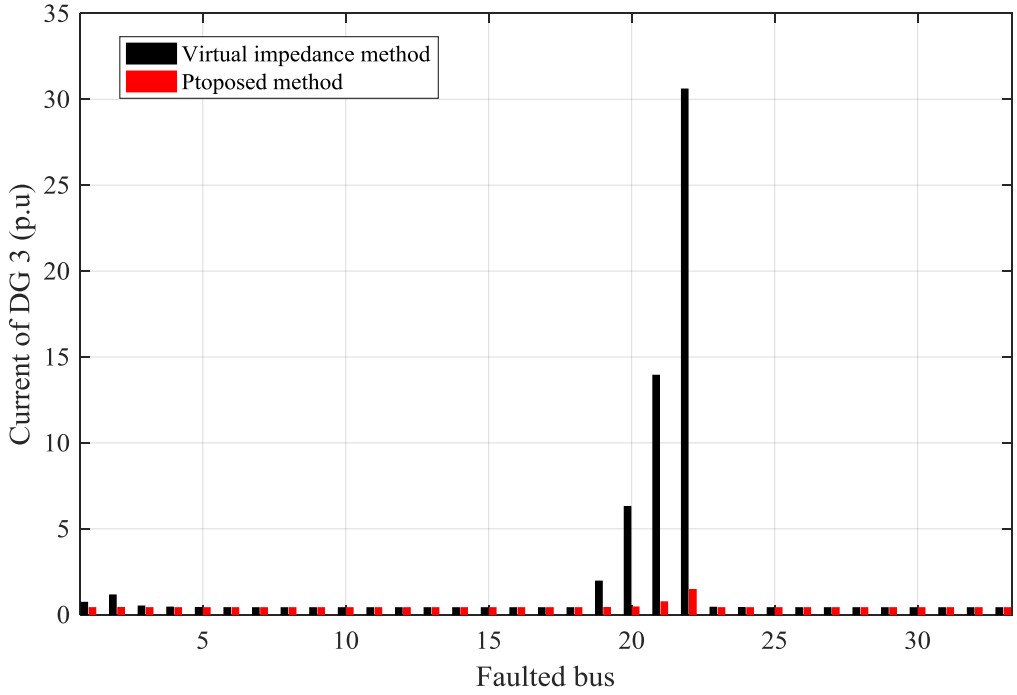

Fig. 5.21 ─ The contribution current of DG 3 using virtual impedance and proposed methods

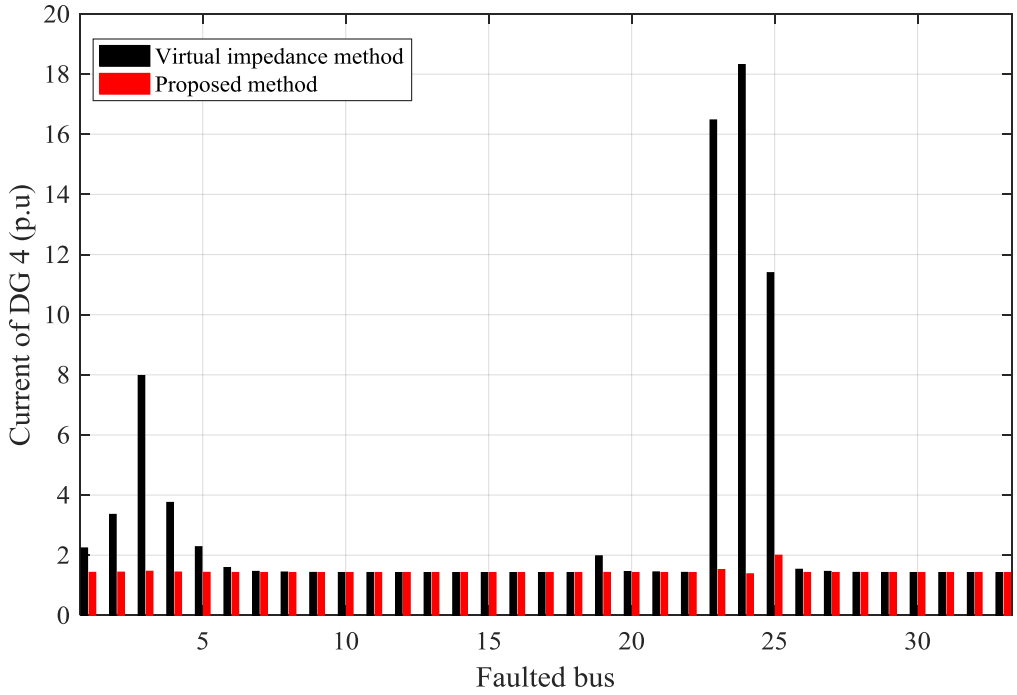

Fig. 5.22 ─ The contribution current of DG 4 using virtual impedance and proposed methods

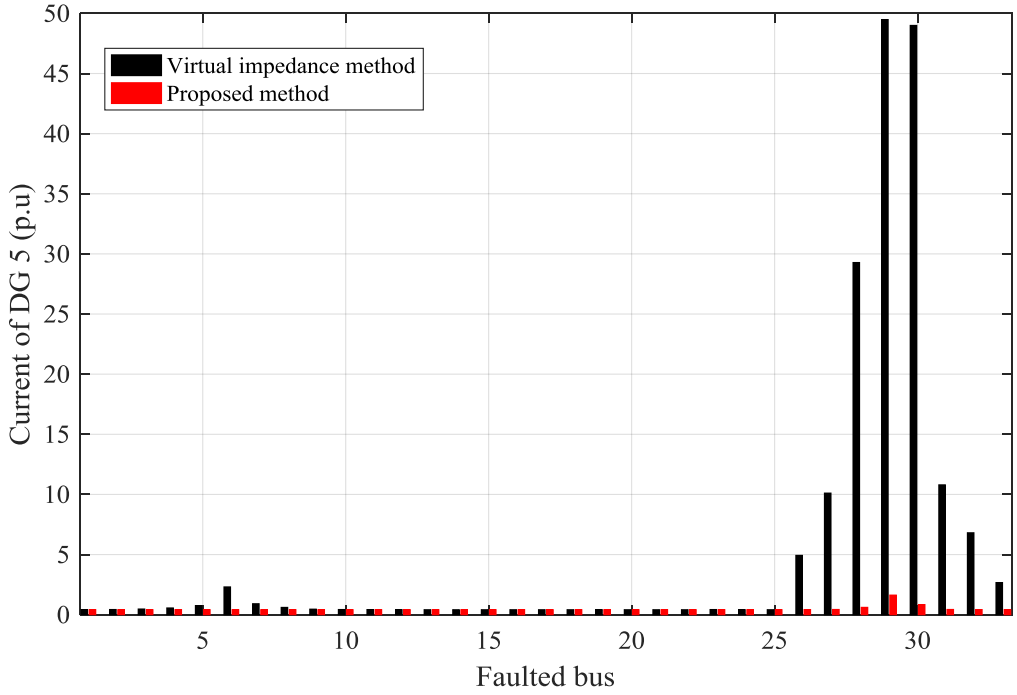

Fig. 5.23 ─ The contribution current of DG 5 using virtual impedance and proposed methods

Static Security Risk Assessment Results

Due to the short circuit current value, the protection device will disconnect the faulted bus, the distribution system divided into subsystems. The power flow program is used to calculate the voltage and active power of all buses. The static security risk (R) and load shedding can be calculated using equations from (5.14) to (5.18). Which the values of the constants are $\propto_L = \propto_V = \propto_f = 0.005$, $P_r(r_j) = 1/33$, $V_{max} = 1.05$, $V_{min} = 0.95$, $f_{max} = 1.05$ and $f_{min} = 0.95$. The net loss coefficient can be calculated using the steady state load flow of the IEEE distribution system $\sigma = \frac{P_{netlosses}}{P_{gnet}}$, $P_{netlosses}$ are the net losses of the system, P_{gnet} is the total generation of the system. Table. 5.13 shows the static security risk and load shedding values during the fault at buses #2, 3, 4, 6, 7, 8,12 and 13.

Table. 5.13. — The static security risk and load shedding values

Faulted bus No.	R before load shedding, %	R after load shedding, %	Load shedding (kW)
2	0.0485	0.0485	100
3	0.1249	0.0244	530
4	0.3205	0.0245	430
6	0.3693	0.0243	740
7	0.0266	0.0252	993.1
8	0.0519	0.0494	1190
12	0.1944	0.1944	510
13	0.1461	0.1461	450

Due to the fault at bus #2, 12 and 13 do not need to load shedding. The bus voltages of faulted buses #2, 12 and 13 are shown in Fig. 5.24. The other faulted buses # 3, 4, 6, 7 and 8, the total active power of the load is greater than active power generation of DG in some isolated subsystems. The load shedding strategy used to minimize the load. Before load shedding, the static security risk is high value as a result of the fault. While a total load of subsystems is higher than their

generation units. The load failure and load shedding need to remove to improve the value of static security risk. After load shedding the static security risk decreased its value to about 0.025 %. Due to fault at bus #8, the voltages profiles minimized to values less than 0.95 p.u and the generation unit output power exceeded its limit power. For that, the load shedding of faulted bus #8 is higher to improve the voltage profile but the static security risk is very small before and after load shedding. When the fault occurs at buses 12, 13 to 18, the all load shedding is failure load.

Due to the fault, the protection devices will remove the faulted bus, which explained in sec. 5.1.3. The operation scenario divides the distribution system to isolated subsystems. Each subsystem works as a small distribution system. The trust newton raphson load flow is used to calculate the steady-state operation of subsystems, as well as the load shedding, can calculate using strategy in sec 3.2.1.5. Figure 5.25 shows bus voltages at faulted bus #3 before and after load shedding. Figure 5.26 shows bus voltages at faulted bus #4 before and after load shedding. Figure 5.27 shows bus voltages at faulted bus #6 before and after load shedding. Figure 5.28 shows bus voltages at faulted bus #7 before and after load shedding. Figure 5.29 shows bus voltages at faulted bus #8 before and after load shedding.

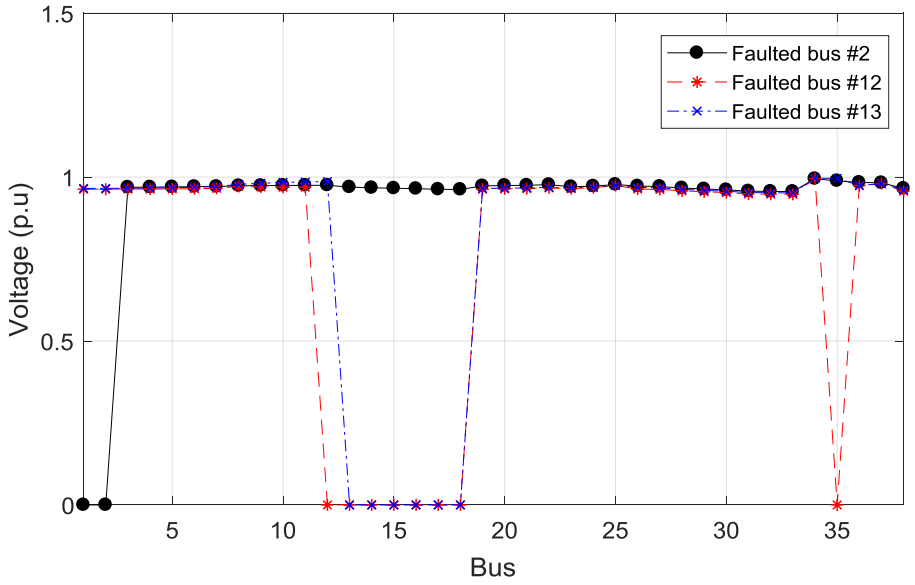

Fig. 5.24 ─ Bus voltages at faulted bus #2, 12 and 13

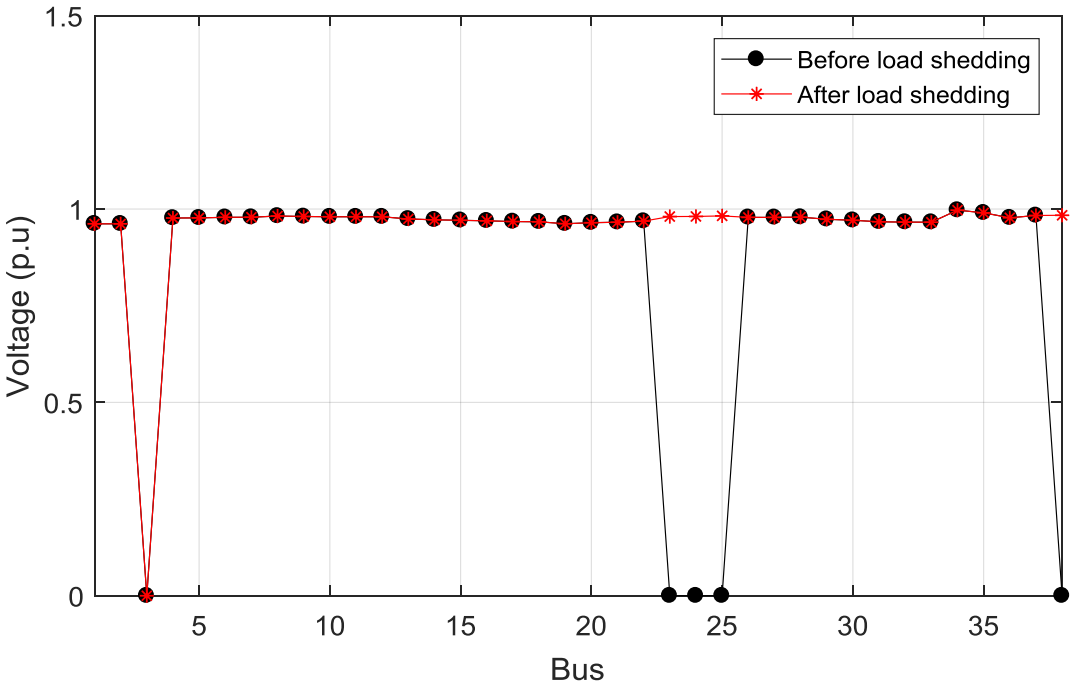

Fig. 5.25 ─ Bus voltages at faulted bus #3 before and after load shedding

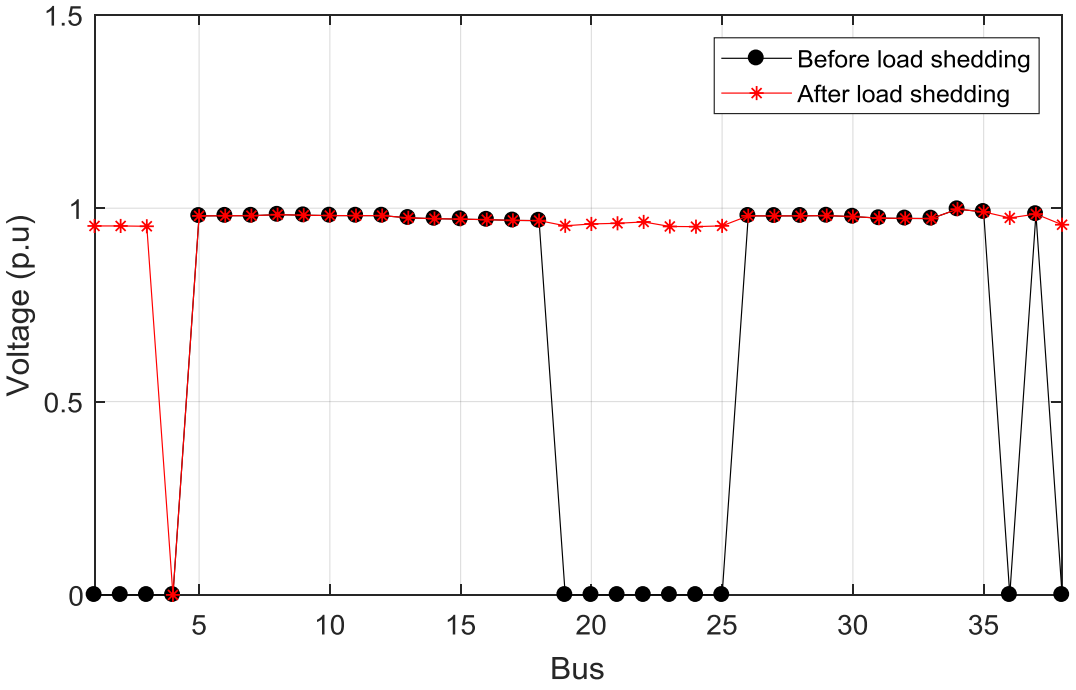

Fig. 5.26 ─ Bus voltages at faulted bus #4 before and after load shedding

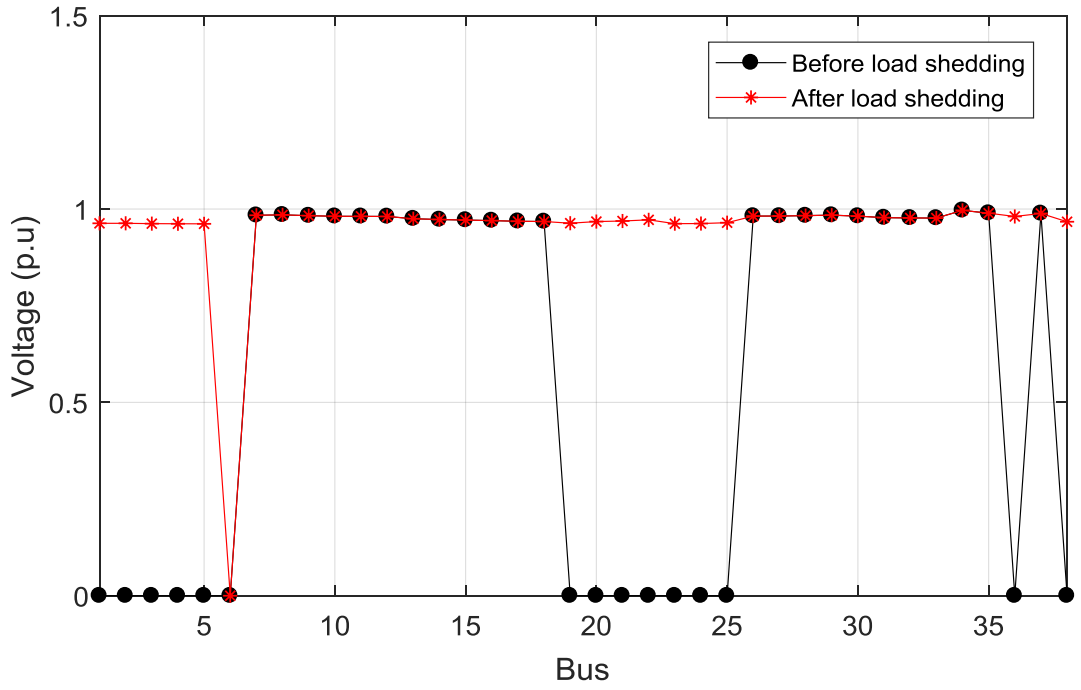

Fig. 5.27 ─ Bus voltages at faulted bus #6 before and after load shedding

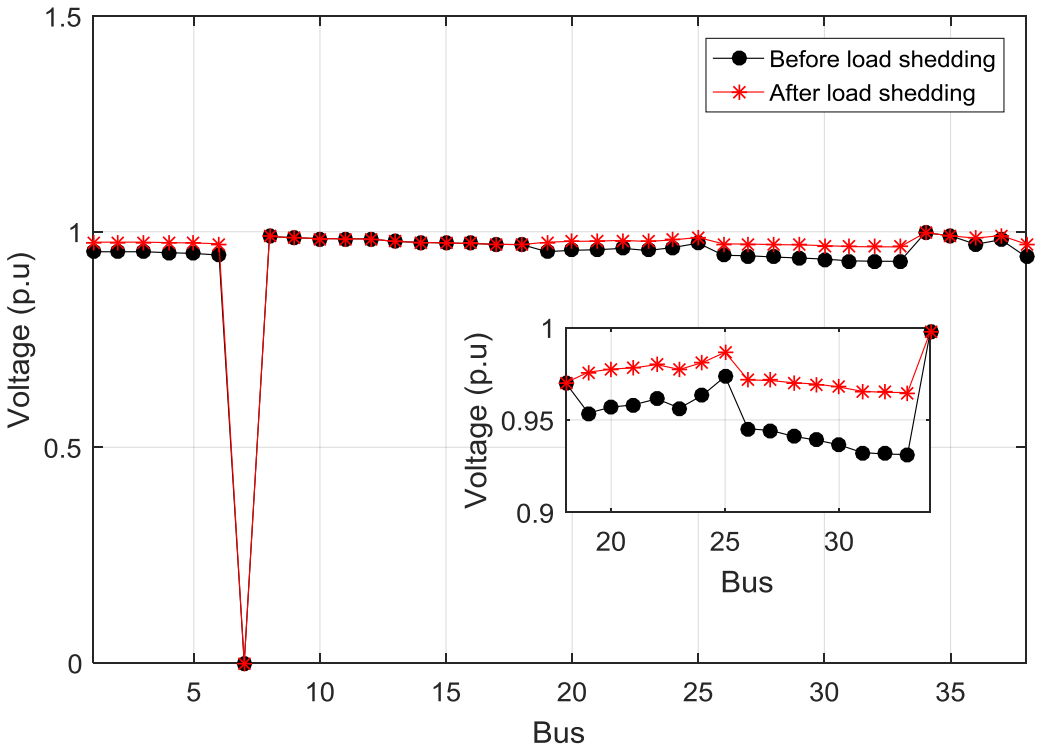

Fig. 5.28 ─ Bus voltages at faulted bus #7 before and after load shedding

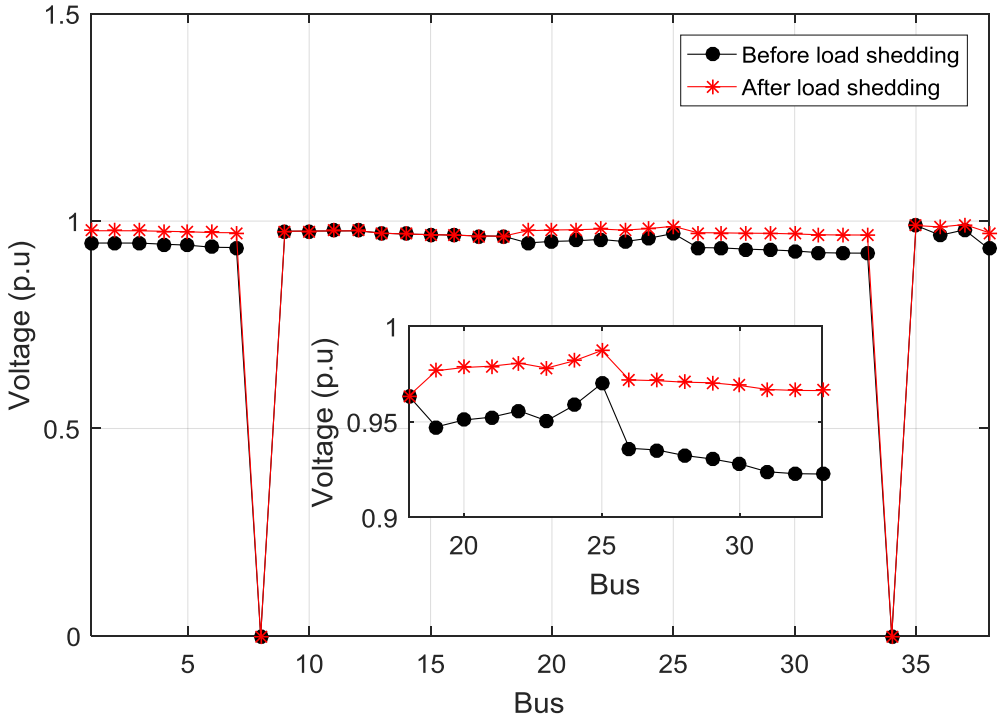

Fig. 5.29 ─ Bus voltages at faulted bus #8 before and after load shedding

As shown in Fig. 5.24, the voltages profiles are better for faulted buses 2, 12 and 13, which does not need load shedding. The generation units of subsystems have the ability to feed their total load before shedding and total losses. Figs. 5.25 to 5.29 given, the voltages profile is improved after load shedding where the total output of the generator can feed the total load after shedding and total losses of the subsystem. Due to the fault at bus #3, the isolated subsystem that has buses # 23, 24, 25 and 38, the total active power of the load is greater than the active power generation of DG at bus #38. The values of voltages equal to zero and this subsystem need to shedding load. The value of the shedding load calculated by reducing the load by the percentage of load after shedding to total load. As well as the fault at buses #4 and #6, the isolated subsystem which has buses #1, 2, 3, 19, 20, 21, 22, 23, 24, 25, 36, 38 and buses #1, 2, 3, 4, 5, 19, 20, 21, 22, 23, 24, 25, 36, 38 respectively. Due to fault at bus #7 and #8, the voltages profiles are less than 0.95 p.u and the generation unit output power is exceeded its limit power. For that, the load shedding of faulted bus #7 and #8 is higher to improve the voltage profile.

Conclusions and Suggestions for Future Research Work

Conclusions of the present work are reported along with the suggested future related research work.

Conclusions

1. The main directions of development of the electric power industry of Egypt are considered. The most promising development of renewable energy generation system was recognized using wind and solar energy by the construction of relatively high power wind and solar power plants and distributed generation to provide electricity to consumers in remote areas.
2. The analysis of the distributed generation control system, most common full converter wind turbine PMSG in Egypt on normal and emergency modes (including short circuit modes) for the operation of distribution network. It has been shown that the greatest influence on the value of short circuit currents was exerted by: converter control systems in which PI-controllers with cascade control loops, where external control loops are used to regulate DC voltage and reactive power, and internal control loops are used to regulate current; speed regulator for exceeding the permissible rotor speed of the wind turbine generator; LVRT system is the function to maintain the wind turbine generator mode with a short term voltage reduction in the external circuit. The necessity of differential accounting of the regulation system has been investigated which regulate the rotational speed of a wind turbine; wind turbine current; provision of the STATCOM mode.
3. The principles and modeling structures have been developed in the MATLAB / SIMULINK software system of normal and emergency operation modes of the inverter-based DG for grid-connected and isolated microgrids. The simulation allowed to identify the main patterns of

behavior of the inverter-based DG during emergency mode; to evaluate the generalized parameters of inverter-based DG for calculating short circuit currents in AC and DC networks; to get the necessary P-V and I-V characteristics of the DG for the analysis of the electric modes. A number of service programs have been developed for the simulation. The simulation was tested for PV system at a power plant in Aswan (Kom ombo).

4. The main functional characteristic of PV system has been investigated, the necessary account was analyzed for both normal and emergency (including short circuit) modes, maximum power point tracking, built on the set of current-voltage characteristics of PV system. In order to simulate the control of PV system during design and training, the use of the Arduino Nano 3x microcontroller has been proposed. To coordinate the microcontroller with the simulation, a hardware-software system was developed.
5. Based on the simulation results of normal and emergency modes of inverter-based DG, it could be concluded that the use of LCL filters is necessary configured to mitigate for 5 and 11 harmonic components.
6. The specifics of calculation of short circuit currents in hybrid microgrid have been analyzed. The significant influence on the value of short circuit currents was made by taking into account the specific properties of the interlinking converter.
7. The most significant factor in the calculation of short circuit currents is the limitation by the control system of the converter output current. To take this factor into account, it was proposed to present inverter-based DG of a three cases volt-ampere characteristic. On the basis of the three cases model, a mathematical method for calculating short circuit currents has been developed. The method was tested on the IEEE-33 bus circuit. Based

on test calculations, it was concluded that there is a significant error in a virtual impedance method for calculating short circuit currents.

8. On the basis of existing methods for calculating the reliability indicators of distribution systems, a methodology has been developed for calculating, according to the "N-1" criterion, the operational reliability indicators of microgrid taking into account to control the actions for voltage and frequency deviations. As the main indicator of reliability, a static security risk was adopted. In this purpose, a program has been developed and test calculations have been performed. The calculations showed that the "N-k" criteria is needed to take into account of a higher order, k> 1. The conclusion is drawn on the need for further research in the field of operational reliability.

Suggestions for Future Work

1. Eliminate fluctuation and intermittency of power supply by wind or solar power in distribution network.
2. Design digital control of smart grid using microcontroller. Analysis and characterization of smart grid system under transient conditions and suggestion the protection schemes.
3. Design and operate radial distribution networks within a market environment with high penetration of RES and energy storage systems using network reinforcement programs and smart gird technologies.
4. Developing of efficient and effective Self-healing and Voltage/Reactive-power (Volt/Var) control algorithms to improve the reliability and performance of distribution networks. The developed algorithms should work autonomously in minimum possible time and handle real distribution networks.

List of symbols and Abbreviations

Symbol	Description
E	Voltage Magnitude
f	Frequency
P_m	Mechanical Power from the Wind
P	Air Density
A_r	Area Swept
v_{wind}	Equivalent Wind Speed of the Turbine.
R_{rotor}	Radius of Rotor.
C_p	Rotor Power Coefficient
λ	Tip Speed Ratio
ω_t	Rotor Angular Speed at the Wind Turbine
L_s	Equivalent Reactance
R	Equivalent Resistance
e	Excitation Electromotive Force
ω_r	Angular Speed of the Rotor
Ψ_f	Rotor Flux
Ψ	Excitation Component
T_{em}	Torque Component
v_{NO}	Voltage of Three Phase Midpoint
i_L	Load Current
V	Voltage
i	Current
d,q	Direct, Quadrature Axis Components
s	Stator Quantities.
N_s	No. of Series-Connected Modules per

String	
N_p	No. of Parallel Strings
K_f	Temperature Co-efficient
G	Solar Irradiation Level
X_T	Relative Reactance of the Transformer
K_T	Impedance Correction Factors for Transformers
V_s	Grid R.M.S. Phase Voltage
f_s	Inverter Switching Frequency
i_{ripple}	Percentage of the Inverter Current
I_{inv}	Inverter Current
L_g	Grid Side Inductance
L_i	Inverter Side Inductance
C_f	Capacitance of LCL Filter
P_n	Inverter Rated Power
ω_n	Operating Frequency
M_f	Frequency Modulation Ratio
m_a	Amplitude Modulation Ratio
P_{DG}	Active Power of DG
Q_{DG}	Reactive Power of DG
m_p	Active Power Static Droop Gain
n_p	Reactive Power Static Droop Gain
Z_{bus}	Impedance Matrix of System
N_f	Faulted Bus Number
Z_f	Fault Impedance
V_f	Faulted Bus
I_f	Current Entering the Faulted Bus

k	Voltage Coefficient of Reactive Power Current Output of DG
R	Security Risk Index
S_{sev}	Severity of the Fault
P_r	Probability of the Occurrence
$\propto$	Weight Value
P_{Lsh}	Load-Shedding Value
P_{DGZ}	Total Active Output of the DG Device
P_{LZ}	Total Active Power of the Load in the System, or Subsystem
$P_{Laftersh}$	Total Active Power of the Load after Shedding
σ	Net Loss Coefficient

Abbreviation	**Description**
DG	Distributed Generator
PV	Photovoltaic
PMSG	Permanent Magnet Synchronous Generator
LVRT	Low Voltage ride-through
STATCOM	Static Synchronous Compensator
NPC	Neutral Point Clamped Converter
MPPT	Maximum Power Point Tracking
SPWM	Sinusoidal Pulse Width Modulation
THD	Total Harmonic Distortion
MG	Microgrid
DER	Distributed Energy Resources
SFCL	Superconducting Fault Current Limiter
PCC	Point of Common Coupling

CPL	Constant Power Load
HFAC	High frequency AC
EPG	Electrical Power Grid
RETs	Renewable Energy Technologies
DESS	Distributed Energy Storage System
VSC	Voltage Source Converter
ZSI	*Z*-source inverter
PR	Proportional-resonant
PI	Proportional–integral
APS	Average Power Sharing
DFIG	Doubly Fed Induction Generator
SMC	Sliding Mode Controller
GSC	Grid Side Converter
BDBBC	Bidirectional Buck-Boost Converter
FRT	Fault-Ride Through
DD	Direct-Driven
OCC	Once Cycle Control
BFV	Best Fixed Voltage
RCC	Ripple Correlation Control
PSO	Particle Swarm Optimization
FPGA	Field-Programmable Gate Array
TRL	Transfer Reinforcement Learning
PSC	Partial Shading Conditions
MFA	Modified Firefly Algorithm
FA	Firefly Algorithm
FP	Flower Pollination
LAB	Lead Acid Battery

SOC	State of Charge
FCI	Flying Capacitor Inverter
TNPC	T-Type Neutral Point Clamped Inverters
NPP	Neutral Point Piloted Converters
IC	Internal Combustion
CHP	Combined Heat and Power
PEM-FC	Polymer Membrane-Type Fuel Cell
CSI	Current-Source-Interface
MI	Multiple-Input
BESS	Battery Energy Storage System
MCC	Microgrid Central Controller
MO	Market Operator
NR	Newton Raphson
SCADA	Supervisory Control and Data Acquisition System
ODC	Operational Data Center
DO	Demand-Offer
LV	Low Voltage
MV	Medium Voltage

References

[1] Xiaohang Jin, Wei Qiao, Yayu Peng, Fangzhou Cheng and Liyan Qu (2016),” Quantitative Evaluation of Wind Turbine Faults Under Variable Operational Conditions”, IEEE Transactions on Industry Applications, Vol. 52, No. 3, pp. 2061 – 2069, 2016.

[2] J. Yang, J.E., Fletcher and J. O’Reilly (2011), “Permanent Magnet Synchronous Generator Based Wind Power Generation System Fault Protection Schemes”, Renewable Power Generation (RPG 2011), IET Conference, pp. 1 – 5, 2011.

[3] Mohammadreza Fakhari, Moghaddam Arani, Yasser Abdel-Rady and I. Mohamed (2016),” Assessment and Enhancement of a Full-Scale PMSG-Based Wind Power Generator Performance Under Faults, IEEE Transactions on Energy Conversion, Vol. 31, No. 2, pp. 728 – 739, 2016.

[4] Libao Shi, Shuming Sun, Liangzhong Yao, Yixin Ni and Masoud Bazargan (2014),” Effects of Wind Generation Intermittency and Volatility on Power System Transient Stability”, IET Renewable Power Generation, Vol. 8, No. 5, pp. 509 – 521, 2014.

[5] M. M. A. Mahfouz, A. M. Amin and E. B. Youssef (2011),” Improvement The Integration of Zafarana Wind Farm Connected To Egyptian Unified Power Grid”, Universities' Power Engineering Conference (UPEC), Proceedings of 2011 46th International, Pages: 1 – 6, 2011.

[6] Muoka, Md. Enamul Haque, ,Ameen Gargoom, and Michael Negnevitsky, 2015, "DSP-Based Hands-On Laboratory Experiments for Photovoltaic Power Systems", IEEE Transactions On Education, Vol. 58, No. 1, pp. 39-47.

[7] A. Zabihinejad and P. Viarouge, 2014, “Design of Direct Power Controller for a High Power Neutral Point Clamped Converter using Real time Simulator” World Academy of Science, Engineering and Technology, Energy and Power Engineering, Vol. 1, No.1, pp. 187.

[8] Rodriguez, J., Bernet, S., Steimer and P.K., Lizama, I.E., 2010,'A Survey on Neutral-Point-Clamped Inverters', IEEE Trans. on Ind. Elec., Vol.57, No.7, pp. 2219–2230.

[9] Abbes M, Behadi J, Ben Abdelghani Bennai A., 2014, "Design and Control of a direct drive wind turbine equipped with multilevel converters". Renewable energy, Vol. 35, No. 5, pp. 936-945.

[10] A. Nabae, I. Takahashi and H. Akagi, 1981, "A new neutral point clamped PWM inverter", IEEE Trans. Ind. Appl., Vol. 17, No.5, pp. 518–523.

[11] P. W. Hammond, 1997," A new approach to enhance power quality for medium voltage AC drives", IEEE Trans. Ind. Appl., Vol. 33, No. 1, pp. 202-208.

[12] F. Khoucha, S. MounaLagoun, K. Marouani, A. Kheloui and M. Benbouzid, 2010, "Hybrid Cascaded H-Bridge Multilevel-Inverter Induction Motor-Drive Direct Torque Control for Automotive Applications". IEEE Transactions on Industrial Electronics, Institute of Electrical and Electronics Engineers, Vol. 57, No. 3, pp. 892-899.

[13] T. A. Meynard, H. Foch, P. Thomas, J. Couralt, R. Jakob, and m. Naherstaedt, 2002, "Multicel converters: Basic concepts and industry application", IEEE Trans. Ind. Electron., Vol. 49, No. 5, pp. 955-964.

[14] F. Z. Peng, 2003, "Z-source inverter", IEEE Trans Ind. Appl., Vol. 39, No. 2, pp. 504 510.

[15] Y. Li, J. Anderson, F. Z. Peng, and D.Liu, 2009, "Quasi-Z-source inverter for photovoltaic power generation systems". 24th Ann. IEEE Appl. Power Elect. Conf, Washington, DC, pp. 918 924.

[16] C. Protogeropoulos, B. J. Brinkworth, R. H. Marshall and B. M. Cross, 1991, "Evaluation of Two Theoretical Models in Simulating the Performance Of Amorphous – Silicon Solar Cells," 10th European Photovoltaic Solar Energy Conference, Lisbon, Portugal.

[17] Richa Singh and Mukesh Kirar," Transient Stability Analysis and Improvement in Microgrid", 2016 International Conference on Electrical Power and Energy Systems (ICEPES), Maulana Azad National Institute of Technology, Bhopal, India. Dec 14-16, 2016, pp. 239 – 245.

[18] Kathleen Cavanagh , Julia A. Belk, and Konstantin Turitsyn," Transient Stability Guarantees for Ad Hoc DC Microgrids" , IEEE Control Systems Letters, Vol. 2, No. 1, January 2018, pp. 139 – 144.

[19] Eklas Hossaina, Ron Perezb, Adel Nasirib and Ramazan Bayindir, "Stability improvement of microgrids in the presence of constant power loads", Electrical Power and Energy Systems, Vol. 96, 2018 pp. 442–456.

[20] Huaxi Zheng, Roger A. Dougal and Mohd. Hasan Ali," Transient Stability Analysis of High Frequency AC Microgrids", SoutheastCon, 2017, pp.1-8.

[21] HAN Minxiao, SU Xiaoling,LIN shaobo, ZHAO Zhengkui," Transient Analysis and Control for Microgrid Stability Controller", 2013 IEEE Grenoble Conference, 2013, pp.1-6.

[22] Jiahui Zhua, Xiaodong Zhenga, Ming Qiua, Zhipeng Zhangb, Jianwei Lib and Weijia Yuanb," Application Simulation of a Resistive Type Superconducting Fault Current Limiter (SFCL) in a Transmission and Wind Power System", Energy Procedia, Vol. 75, 2015, pp. 716 – 721.

[23] G. Didier, C.H. Bonnard, T. Lubin and J. Lévêque," Comparison between inductive and resistive SFCL in terms of current limitation and power system transient stability", Electric Power Systems Research, Vol. 125, 2015, pp.150–158.

[24] S.Bhasker, Anisha.K, P.Ganesh Venkata Siva Teja," A Coordinated Voltage Control using OLTC, Voltage Regulator and DG for a Distribution Feeder", International Journal of Advanced Research in Electrical, Electronics and Instrumentation Engineering, Vol. 5, Issue 5, May 2016, pp. 3927-3932.

[25] Andres Ovalle, Gustavo Ramos, Seddik Bacha, Ahmad Hably, and Axel Rumeau, "Decentralized control of Voltage Source Converters in Microgrids

based on the Application of Instantaneous Power Theory", IEEE Transactions on Industrial Electronics, Institute of Electrical and Electronics Engineers, 2014, 62 (2), pp.1152-1162.

[26] Johanna Barr and Ritwik Majumder, "Integration of Distributed Generation in the Volt/VAR Management System for Active Distribution Networks", IEEE Transactions on Smart Grid, Vol. 6, No. 2, March 2015, pp. 576-586.

[27] Özgun Girgin and Mustafa Hadi Sarul," A hybrid control strategy for Z-source inverter DG systems", Automatika, 2019, Vol. 60, No. 4, pp. 500–509.

[28] Jinwei He and Yun Wei Li," Hybrid Voltage and Current Control Approach for DG-Grid Interfacing Converters with LCL filters Smart grid", IEEE Transactions on Industrial Electronics, 2013, Vol. 60, Iss. 5, pp. 1797-1809.

[29] Thipnatee Sansawatt, Luis F. Ochoa and Gareth P. Harrison, "Smart Decentralized Control of DG for Voltage and Thermal Constraint Management", IEEE Transactions on Power Systems, 2012, Vol. 27, Iss.3, 1637-1645.

[30] Noel Richard Merritt, Chandan Chakraborty and Prabodh Bajpai, "New Voltage Control Strategies for VSC-Based DG Units in an Unbalanced Microgrid", IEEE Transactions on Sustainable Energy, Vol. 8, No. 3, July 2017, pp. 1127-1139.

[31] Zhiqiang Guo, Deshang Sha and Xiaozhong Liao," Voltage magnitude and frequency control of three-phase voltage source inverter for seamless transfer", IET Power Electron., 2014, Vol. 7, Iss. 1, pp. 200–208.

[32] Huanhai Xin, Rui Zhao, Leiqi Zhang, Zhen Wang, Kit Po Wong and Wei Wei, "A Decentralized Hierarchical Control Structure and Self-Optimizing Control Strategy for F-P Type DGs in Islanded Microgrids", IEEE Transactions on Smart Grid, Vol. 7, No. 1, January 2016, pp. 3-5.

[33] Chia-Nan Wang, Wen-Chang Lin, and Xuan-Khoa Le, " Modelling of a PMSG Wind Turbine with Autonomous Control", Hindawi Publishing Corporation Mathematical Problems in Engineering, Volume 2014, Article ID 856173, pp. 1- 9, http://dx.doi.org/10.1155/2014/856173

[34] Chun Wei, Zhe Zhang, Wei Qiao and Liyan Qu (2016),” An Adaptive Network-Based Reinforcement Learning Method For MPPT Control Of PMSG Wind Energy Conversion Systems”, IEEE Transactions on Power Electronics, Vol. 31, Issue 11, pp. 7837 – 7848, 2016.

[35] Daeheon Jeong, Chunghun Kim, YonghaoGui and Chung Choo Chung,” Sliding Mode Control for LVRT of a PMSG Wind Turbine Using Stored Energy in Rotor Inertia”, 2016 IEEE Power and Energy Society General Meeting (PESGM), pp. 1-5, 2016.

[36] Tongzhou Ji, Xiongfeng He, Xianyun Li, Kun Liu and Mei Zhang (2014),” Performance Analysis and Research on LVRT of PMSG Wind Power Systems With SDBR”, Control Conference (CCC) 2014, 33rd Chinese, pp. 6953 – 6958, 2014.

[37] Miteshkumar Popat, Bin Wu and Navid R. Zargari (2013),”Fault Ride-Through Capability of Cascaded Current-Source Converter-Based Offshore Wind Farm”, IEEE Transactions on Sustainable Energy, Vol. 4, No. 2, pp. 314 – 323, 2013.

[38] Yu Zou and Jiangbiao He (2016), “Comprehensive Modeling, Simulation And Experimental Validation of Permanent Magnet Synchronous Generator Wind Power System”, 2016 IEEE/IAS 52nd Industrial and Commercial Power Systems Technical Conference (I&CPS), pp. 1 – 9, 2016.

[39] Guangchen Liu, Fangfang Shi, Chao Zhang and Shengtie Wang (2015),”An Integrated Control Strategy of PMSG-Based Wind Turbine Generation System to Improve Its Fault Ride-Through Capability by Using an Energy Storage Device”, International Conference on Renewable Power Generation (RPG 2015), pp. 1 – 6, 2015.

[40] Sheng-wen Liu and Guang-qing Bao, ” A Novel LVRT of Permanent Magnet Direct-Driven Wind Turbine”, 2011 Asia-Pacific Power and Energy Engineering Conference, pp. 1-4, 2011.

[41] Keqing Qu, Hao Zhou, Yuehong Xing, Zuojin Ding and Ningyi He,” A LVRT Method for Wind Power PMSG System with Z-source Inverter”, 2011 IEEE Power Engineering and Automation Conference, pp. 146-149, 2011.

[42] Mian Wang, Ye Tian, Xia Feng, and Guozhu Chen, Member, IEEE,” A Hybrid LVRT Control Scheme for PMSG Wind Power System”, 2012 IEEE 7th International Power Electronics and Motion Control Conference - ECCE Asia, pp. 1173 – 1177, June 2-5, 2012, Harbin, China

[43] Hui Zeng, Yu Zhu and Jinsong Liu,” Verification of DFIG and PMSG wind turbines' L VRT characteristics through field testing”, 2012 IEEE International Conference on Power System Technology (POWERCON), pp. 1-6, 2012.

[44] Venkata Yaramasu, Bin Wu, Salvador Alepuz, and Samir Kouro, ” Predictive Control for Low-Voltage Ride-Through Enhancement of Three-Level-Boost and NPC-Converter-Based PMSG Wind Turbine”, IEEE Transactions On Industrial Electronics, Vol. 61, No. 12, pp. 6832-6843, December 2014.

[45] Mazen Abdel-Salam, Adel Ahmed, Mahmoud Amery, Mohamed Swify, Ahmed El-kousy and Khairy Sayed, 2011, " Design and Implementation of Stand-alone Residential PV System ", 2011 IEEE Jordan Conference on Applied Electrical Engineering and Computing Technologies (AEECT), pp. 1-5.

[46] Ravi Nath Tripathi, Alka Singh and Tsuyoshi Hanamoto, 2015,” Design and control of LCL filter interfaced grid connected solar photovoltaic (SPV) system using power balance theory”, Electrical Power and Energy Systems, Vol. 69, pp. 264–272.

[47] S. Sheik Mohammed, D. Devaraj and T. P. Imthias Ahamed, 2016, " Maximum power point tracking system for stand alone solar PV power system using Adaptive Neuro-Fuzzy Inference System", 2016 Biennial International Conference on Power and Energy Systems: Towards Sustainable Energy (PESTSE), pp. 1-4.

[48] B.H. Khan, Non- conventional energy technologies, McGrawHill Publications, 2005.

[49] Mohan Kolhe, "Techno-Economic Optimum Sizing of a Stand-Alone Solar Photovoltaic System", IEEE Transactions on Energy Conversion, Vol. 24, No. 2, June 2009 511-519.

[50] G. W. Hart, H. M. Branz, and C. H. Cox, "Experimental tests of openloop maximum-power-point tracking techniques," Solar Cells, vol. 13, pp. 185–195, 1984.

[51] T. Esram, P. L. Chapman, "Comparison of Photovoltaic Array Maximum Power Point Tracking Techniques," IEEE, 2006.

[52] E. N. Costogue and S. Lindena, "Comparison of candidate solar array maximum power utilization approaches," in Intersociety Energy Conversion Eng. Conf., 1976, pp. 1449–1456.

[53] W. J. A. Teulings, J. C. Marpinard, A. Capel, and D. O'Sullivan, "A new maximum power point tracking system," in Proc. 24th Annu. IEEE Power Electron. Spec. Conf., 1993, pp. 833–838.

[54] A. Al-Amoudi and L. Zhang, "Optimal control of a grid-connected PV system for maximum power point tracking and unity power factor," in Proc. Seventh Int. Conf. Power Electron. Variable Speed Drives, 1998, pp. 80–85.

[55] K. Irisawa, T. Saito, I. Takano, and Y. Sawada, "Maximum power point tracking control of photovoltaic generation system under non-uniform insolation by means of monitoring cells," in Conf. Record Twenty-Eight IEEE Photovoltaic Spec. Conf., 2000, pp. 1707–1710.

[56] M. A. S. Masoum, H. Dehbonei, and E. F. Fuchs, “Theoretical and experimental analyses of photovoltaic systems with voltage and current-based maximum power-point tracking,” IEEE Trans. Energy Convers., vol. 17, no. 4, pp. 514–522, Dec. 2002.

[57] N. Mutoh, T. Matuo, K. Okada, and M. Sakai, “Prediction-data-based maximum-power-point-tracking method for photovoltaic power generation systems,” in Proc. 33rd Annu. IEEE Power Electron. Spec. Conf., 2002, pp. 1489– 1494

[58] A. S. Kislovski and R. Redl, “Maximum-power-tracking using positive feedback,” in Proc. 25th Annu. IEEE Power Electron. Spec. Conf., 1994, pp. 1065–1068.

[59] J. Arias, F. F. Linera, J. Martin-Ramos, A. M. Pernia, and J. Cambronero, “A modular PV regulator based on microcontroller with maximum power point tracking,” in Proc. IEEE Ind. Appl. Conf., 2004, pp. 1178–1184.

[60] C.-T. Pan, J.-Y. Chen, C.-P. Chu, and Y.-S. Huang, “A fast maximum power point tracker for photovoltaic power systems,” in Proc. 25th Annu. Conf. IEEE Ind. Electron. Soc., 1999, pp. 390–393.

[61] H. Sugimoto and H. Dong, “A new scheme for maximum photovoltaic power tracking control,” in Proc. Power Convers. Conf., 1997, pp. 691–696.

[62] S. J. Chiang, K. T. Chang, and C. Y. Yen, “Residential photovoltaic energy storage system,” IEEE Trans. Ind. Electron., vol. 45, no. 3, pp. 385–394, Jun. 1998.

[63] T. Kitano, M. Matsui, and D.-h. Xu, “Power sensor-less MPPT control scheme utilizing power balance at DC linksystem design to ensure stability and response,” in Proc. 27th Annu. Conf. IEEE Ind. Electron. Soc., 2001, pp. 1309–1314.

[64] B. M.Wilamowski and X. Li, “Fuzzy system basedmaximum power point tracking for PV system,” in Proc. 28th Annu. Conf. IEEE Ind. Electron. Soc., 2002, pp. 3280–3284.

[65] N. Patcharaprakiti and S. Premrudeepreechacharn, “Maximum power point tracking using adaptive fuzzy logic control for grid-connected photovoltaic system,” in IEEE Power Eng. Soc. Winter Meet., 2002, pp. 372–377.

[66] T. Hiyama, S. Kouzuma, and T. Imakubo, “Identification of optimal operating point of PV modules using neural network for real-time maximum power tracking control,” IEEE Trans. Energy Convers., vol. 10, no. 2, pp. 360–367, Jun. 1995.

[67] Moussaab Bounabi, Karim Kaced, Mohamed Salah Ait-Cheikh, Cherif Larbes, Zine elabadine Dahmane, and Naeem Ramzan,” Modelling and performance analysis of different multilevel inverter topologies using PSO-MPPT technique for grid connected photovoltaic systems”, J. Renewable Sustainable Energy 10, 043507 (2018), pp. 1-20.

[68] Lhoussain El Bahir and Touria Hassboun,” Accurate Maximum Power Point Tracking Algorithm Based on a Photovoltaic Device Model”, International Journal of Photoenergy, Vol. 2017, Article ID 5693941, pp.1-10.

[69] Duy C. Huynh ; Thu A.T. Nguyen ; Matthew W. Dunnigan and Markus A. Mueller,” maximum Power Point Tracking of Solar Photovoltaic Panels using Advanced Perturbation and Observation Algorithm”, 2013 IEEE 8th Conference on Industrial Electronics and Applications (ICIEA), 2013, pp. 864-869.

[70] Min Ding, Dong Lv, Chen Yang, Shi Li, Qi Fang, Bo Yang and Xiaoshun Zhang,” Global Maximum Power Point Tracking of PV Systems under Partial Shading Condition: A Transfer Reinforcement Learning Approach”, Appl. Sci. 2019, Vol. 9, 2769; pp. 1-12. doi:10.3390/app9132769

[71] Javad Farzaneh, Reza Keypour and Mojtaba Ahmadieh Khanesar,” A New Maximum Power Point Tracking Based on Modified Firefly Algorithm for PV System Under Partial Shading Conditions”, Technol Econ Smart Grids Sustain Energy, Vol. 3, iss. 9,2018, pp. 1-13. https://doi.org/10.1007/s40866-018-0048-7

[72] Mingxuan Mao, Qichang Duan, Li Zhang, Hao Chen, Bei Hu1 and Pan Duan,” Maximum Power Point Tracking for Cascaded PV-Converter Modules

Using Two-Stage Particle Swarm Optimization", Scientific Reports, Vol. 7, Article number: 9381 2017, pp. 1-10.

[73] Liqun Shang, Weiwei Zhu, Pengwei Li and Hangchen Guo," Maximum power point tracking of PV system under partial shading conditions through flower pollination algorithm", Protection and Control of Modern Power Systems, Vol.3, Article number 38, (2018), pp. 1-7.

[74] L. Barote, C. Marinescu," PMSG Wind Turbine System for Residential Applications", SPEEDAM 2010 International Symposium on Power Electronics, Electrical Drives, Automation and Motion, 2010, pp.772 – 777.

[75] Kleber Oliveira, João Afonso, Marcelo Cavalcanti. Multilevel Inverter for Grid-Connected Photovoltaic Systems with Active Filtering Function. 4th Doctoral Conference on Computing, Electrical and Industrial Systems (DoCEIS), Apr 2013, Costa de Caparica, Portugal. pp.289-298.

[76] V. Fernão Pires, J. F. Martins, D. Foito and Chen Hão,"A Grid Connected Photovoltaic System with a Multilevel Inverter and a Le-Blanc Transformer", Int. Journal of Renewable Energy Research, Vol.2, No.1, 2012, pp. 84-91.

[77] Muhammad Bilal Satti, Ammar Hasan and Mian Ilyas Ahmad," A New Multilevel Inverter Topology for Grid-Connected Photovoltaic Systems", International Journal of Photoenergy, Volume 2018, pp. 1-10.

[78] K.S. Srikanth," A Three Phase Multi Level Converter for grid Connected PV System", International Journal of Power Electronics and Drive System (IJPEDS), Vol. 5, No. 1, July 2014, pp. 71-75.

[79] Anirudh Budnar Acharya, Mattia Ricco, Dezso Sera , Remus Teodorescu and Lars Einar Norum ," Arm Power Control of the Modular Multilevel Converter in Photovoltaic Applications", Energies 2019, 12, 1620, pp.1-24.

[80] Cristian Verdugo, Samir Kouro, Christian A. Rojas, Marcelo A. Perez, Thierry Meynard and Mariusz Malinowski," Five-Level T-type Cascade Converter for Rooftop Grid-Connected Photovoltaic Systems", Energies 2019, 12, 1743, pp. 1-20.

[81] R. Lasseter, P. Paolo, "MicroGrid: a conceptual solution", IEEE Annual Power Electronics Specialists Conference, pp. 4285-4290, June 2004.

[82] R. Lasseter, "MicroGrids", IEEE Power Eng Soc Transm Distrib Conf, pp. 305-308, 2002.

[83] Marnay Chris, Venkataramanan Giri, "Microgrids in the evolving electricity generation and delivery infrastructure", IEEE Power Engineering Society General Meeting, pp. 18-22, 2006.

[84] Pecas Lopes JA, Moreira CL, Madureira AG "Defining control strategies for MicroGrids islanded operation" IEEE Transaction Power System, Vol. 21, pp. 916-924, 2006.

[85] S. Obara, "Analysis of a fuel cell micro-grid with a small-scale wind turbine generator", Int. Journal of Hydrogen Energy, Vol. 32, pp. 323 – 336, 2007.

[86] A. Chimtavee, N. Ketjoy, K. Sriprapha, S. Vaivudh, "Evaluation of PV Generator Performance and Energy Supplied Fraction of the 120 kWp PV Microgrid System in Thailand", Energy Procedia, Vol. 9, pp. 117 – 127, 2011.

[87] B. Zhao, X. Zhang, J. Chen, "Integrated Microgrid Laboratory System", IEEE Transaction on Power System, Vol. 27, pp. 2175-2185, 2012.

[88] L. Xu, D. Chen, "Control and Operation of a DC Microgrid with Variable Generation and Energy Storage", IEEE Transaction on Power Delivery, Vol. 26, pp. 2513-2522, 2011.

[89] Jong-Yul Kim, Jin-Hong Jeon, Seul-Ki Kim, Changhee Cho, June Ho Park, Hak-Man Kim, Kee-Young Nam, "Cooperative Control Strategy of Energy Storage System and Microsources for Stabilizing the Microgrid during Islanded Operation", IEEE Transaction on Power Electronics, Vol. 25, pp. 3037-3048, 2010.

[90] A. Elmitwally, M. Rashed, "Flexible Operation Strategy for an Isolated PV-Diesel Microgrid without Energy Storage", IEEE Transaction on Energy Conversion, Vol. 26, pp. 235-244, 2011.

[91] Sungwoo Bae, Alexis Kwasinski, "Dynamic Modeling and Operation Strategy for a Microgrid With Wind and Photovoltaic Resources", IEEE Transaction on Smart Grid, Vol. 3, pp. 1867-1876, 2012.

[92] Lin Ye, Hai Bo Sun, Xu Ri Song, Li Cheng Li, "Dynamic modeling of a hybrid wind/solar/hydro microgrid in EMTP/ATP", Renewable Energy, Vol. 39, pp. 96-106, 2012.

[93] N. Eghtedarpour, E. Farjah, "Control strategy for distributed integration of photovoltaic and energy storage systems in DC micro-grids", Renewable Energy, Vol. 45, pp. 96-110, 2012.

[94] Dulal Manna , Swapan K. Goswami and Pranab Kumar Chattopadhyay," Optimisation of droop coefficients of multiple distributed generators in a micro-grid", IET Gener. Transm. Distrib. Vol. 12 Iss. 18, pp. 4108-4116, 2018.

[95] Morad M. A. Abdelaziz, , Hany E. Farag, , Ehab F. El-Saadany, and Yasser Abdel-Rady I. Mohamed," A Novel and Generalized Three-Phase Power Flow Algorithm for Islanded Microgrids Using a Newton Trust Region Method", IEEE TRANSACTIONS ON POWER SYSTEMS, Vol. 28, pp. 190-201,2012.

[96] Jiahui Zhua, Xiaodong Zhenga, Ming Qiua, Zhipeng Zhangb, Jianwei Lib and Weijia Yuanb," Application Simulation of a Resistive Type Superconducting Fault Current Limiter (SFCL) in a Transmission and Wind Power System", Energy Procedia, Vol. 75, 2015, pp. 716 – 721.

[97] Jia, J., Yang, G., & Nielsen, A. H. (2017). A Review on Grid-connected Converter Control for Short Circuit Power Provision under Grid Unbalanced Faults. IEEE Transactions on Power Delivery, Vol. 33, No. 2, pp. 649 - 661. https://doi.org/10.1109/TPWRD.2017.2682164

[98] Aazim Rasool, Xiangwu Yan, Haaris Rasool, Hongxia Guo and Mansoor Asif," VSG Stability and Coordination Enhancement under Emergency Condition", Electronics, Vol. 7, No. 202, pp. 1-18, 2018.

[99] R. Caldon, M. Coppo, A. Raciti, R. Sgarbossa and R. Turri,"Modeling the Control of Islanded Networks Supplied by Inverters: the Case of MV and LV Systems", AEIT Annual Conf. 2013, 3-5 Oct. 2013, Mondello, Italy, pp. 1-5.

[100] Longchang Wang, Houlei Gao and Guibin Zou," Modeling methodology and fault simulation of distribution networks integrated with inverter-based DG", Protection and Control of Modern Power Systems, Vol. 2, No.31, pp. 1-9, 2017.

[101] Ali Mekkaoui, Mohammed Laouer and Younes Mimoun," Modeling and simulation for smart grid integration of solar/wind energy", Leonardo Journal of Sciences, Iss. 30, January-June 2017 p. 31-46.

[102] S. Sathish Kumar, B.Swapna and Dr.C.Nagarajan," Modeling and Control for Smart Grid Integration with MPPT of Solar/Wind Energy Conversion System", International Journal of Innovative Research in Science, Engineering and Technology, Vol. 3, Special Issue 1, February 2014, pp. 920-929.

[103] Dr.V.Jayalakshmi and Sujeet Kumar," Simulation for Smart Grid Integration of Solar/Wind Energy Conversion System", International Journal of Pure and Applied Mathematics, Vol. 119, No. 12, 2018, pp. 7897-7910.

[104] Chee Lim Nge, Ole-Morten Midtgård and Lars Norum," PV with Battery in Smart Grid Paradigm: Price-Based Energy Management System", 2012 38th IEEE Photovoltaic Specialists Conference, 2012, pp. 575-579.

[105] Piyush R. Patel and Mr. N.K.Singh," Modelling and Control for Smart Grid Integration of Solar/Wind Energy Conversion System", International Journal for Technological Research in Engineering Vol. 2, Iss. 2, Oct. 2014, pp. 128-134.

[106] Ibrahim Benabdallah, Abeer Oun and Adnène Cherif," Grid Connected PV Plant based on Smart Grid Control and Monitoring", (IJACSA) International Journal of Advanced Computer Science and Applications, Vol. 8, No. 6, 2017, pp. 299-306.

[107] Abdel-Salam M., Ahmed A., Ziedan H., Kamel R., Sayed Kh., Amery M., and Swify M., El-kishky H. and Khalaf M. Adaptive and Intelligent Protection System for Micro Grid Operates In Both Grid Connected and Islanding Modes.

35th International Telecommunications Energy Conference (INTELEC), Hamburg, Germany, October 2013, pp. 1-6.

[108] Paulo F. T., Hailian X. K. and Kungl T. H.Wind Farm in Weak Grids Compensated with STATCOM. Proceedings of the Nordic wind power conference, Sweden, 2005, Topic 7.

[109] A. Delavari, I. Kamwa and A. Zabihinejad, 2016, "A Comparative Study of Different Multilevel Converter Topologies for High Power Photovoltaic Applications". 7thPower Electronics, Drive Systems &Technologies Conference (PEDSTC 2016), Iran University of Science and Technology, Tehran, Iran.

[110] Yousef Firouz, Mohammad TavakoliBina andBahmanEskandari, 2014, ” Efficiency of three-level neutral-point clamped converters: analysis and experimental validation of power losses, thermal modelling and lifetime prediction”, IET Power Electron., Vol. 7, No. 1, pp. 209–219.

[111] XinboCai, Zhenbin Zhang, Zhe Chen and Ralph Kennel, 2016,” DC-bus Voltage Balancing for Three-level NPC Inverter Using Deadbeat Controller”,2016 IEEE 8th International Power Electronics and Motion Control Conference IPEMC-ECCE Asia, pp. 1-6.

[112] M. Liserre, F. Blaabjerg, and S. Hansen, "Design and control of an LCL filter based three-phase active rectifier". IEEE Transactions on Industry Applications, Vol. 41, No. 5, pp. 1281 - 1291, 2005.

[113] B. Bolsens, K. Brabandere, J. Keybus, J. Driesen, R. Belmans, "Model-based generation of low distortion currents in grid-coupled PWM inverters using an LCL output filter", IEEE Transactions on Power Electronics, Vol. 21 , No. 4, pp. 1032 - 1040 , 2006.

[114] H. Cha and T-K. Vu, "Comparative analysis of low-pass output filter for single-phase grid-connected photovoltaic inverter", IEEE Applied Power Electronics Conference and Exposition (APEC), Palm Springs, CA, USA, pp. 1659-1665, 2010.

[115] Muhammad H. Rashid, 2001,"Power Electronics Handbook", Academic Press.

[116] Jackson John Justo, Francis Mwasilu, Ju Lee and Jin-Woo Jung, "AC-microgrids versus DC-microgrids with distributed energy resources: A review", Renewable and Sustainable Energy Reviews, Vol. 24, 2013, pp. 387–405.

[117] A. H. KasemAlaboudy, Member, IEEE, H. H. Zeineldin, Member, IEEE, and James L. Kirtley, Jr., Fellow, IEEE," Microgrid Stability Characterization Subsequent to Fault-Triggered Islanding Incidents", IEEE TRANSACTIONS ON POWER DELIVERY, VOL. 27, NO. 2, APRIL 2012, pp. 658-669.

[118] SrikanthKotra, Student Member, IEEE, Mahesh K. Mishra, Senior Member, IEEE, NakkaPruthviChaithanya," Design and Small Signal Analysis of DC Microgrid with Hybrid Energy Storage System", 2017 IEEE PES Asia-Pacific Power and Energy Engineering Conference (APPEEC), 2017, pp. 1-6.

[119] M. Reza Nassaj, SamanMehrnia, Hassan Rastegar and MehrdadAbedi," Improving the response transient and dynamic stability using voltage-based droop control in an islanded microgrid equipped with energy storage", 2017 Smart Grid Conference (SGC), pp. 1-7.

[120] Shivam and RatnaDahiya," Stability analysis of islanded DC microgrid for the proposed distributed control strategy with constant power loads", Computers and Electrical Engineering, 2018, pp.1–12.

[121] Shan Yang and Xiangqian Tong," Integrated Power Flow and Short Circuit Calculation Method for Distribution Network with Inverter Based Distributed Generation", Mathematical Problems in Engineering, Vol. 7, 2016, pp. 1-10.

[122] Hanmei Peng, Min Su, Shuaihu Li , and Canbing Li," Static Security Risk Assessment for Islanded Hybrid AC/DC Microgrid", IEEE Access, Vol. 7, pp. 37545-37554, 2019.

Appendix A. Simulation Circuits

A.1 PMSG wind turbine connected to grid

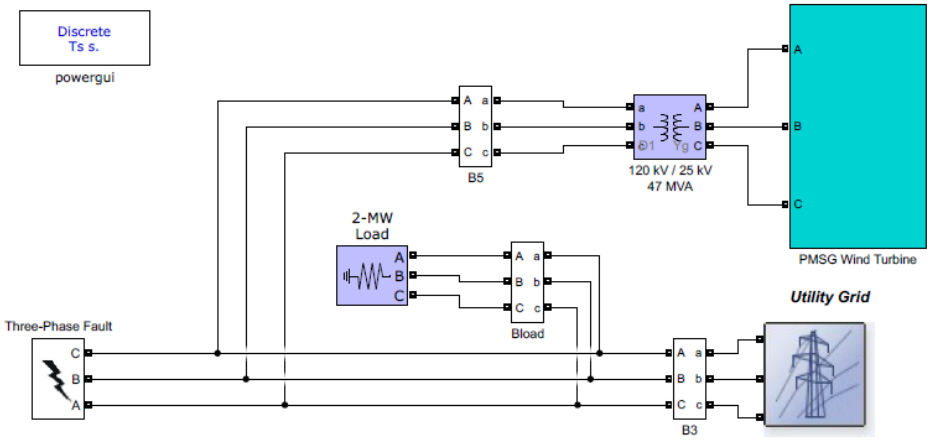

Fig. A.1 ─ Matlab simulated circuit of PMSG wind turbine connected to grid

A.2 Three-phase-to-ground fault of AC Mcrogrid.

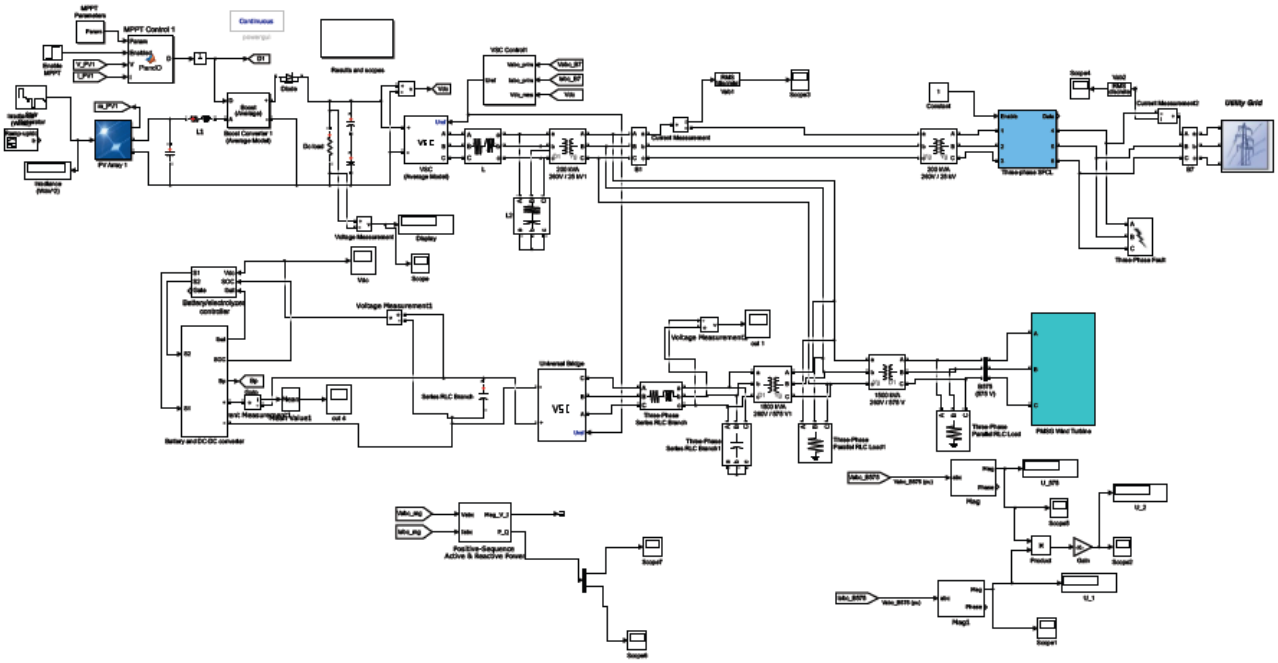

Fig. A.2 ─ Matlab simulated circuit of Three-phase-to-ground fault of AC Mcrogrid

A.3 Three-phase-to-ground fault of DC Mcrogrid

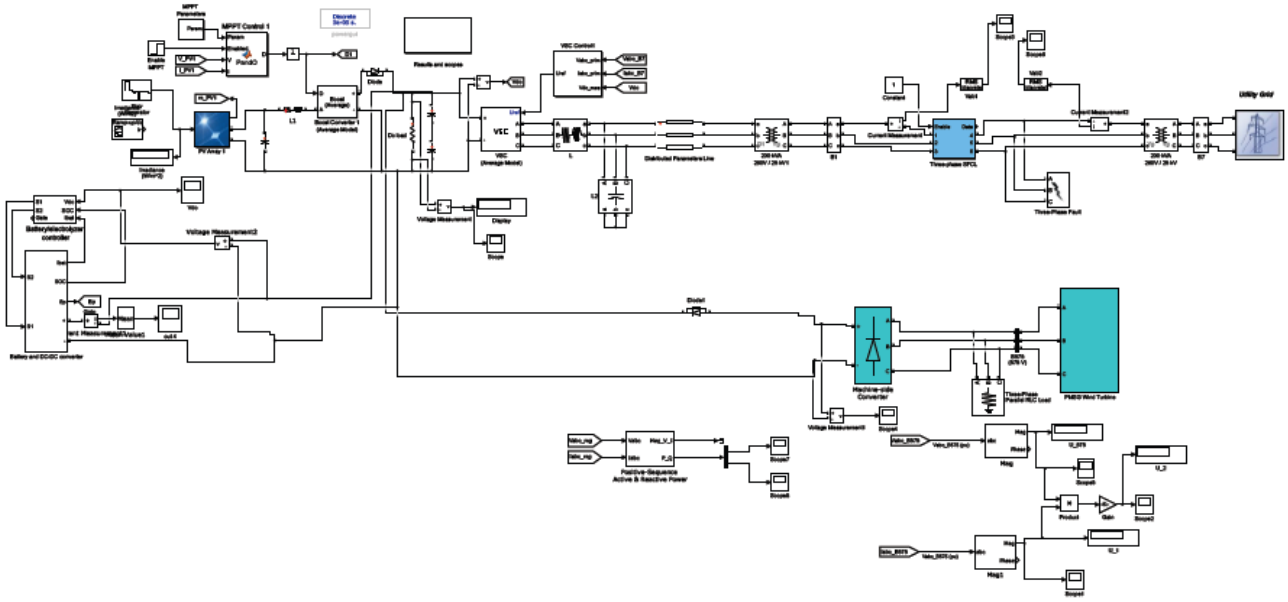

Fig. A.3 ─ Matlab simulated circuit of Three- phase- to- ground fault of AC Mcrogrid

A.4 MATLAB program code of the short circuit current calculation of grid-connected Microgrid

```
Vf=Vm;
nbus=38;
If=zeros(nbus,nbus);
nl = linedata(:,1); nr = linedata(:,2); R = linedata(:,3);
X = linedata(:,4);
nf = input('Enter Faulted Bus No. -> ');
Zf = input('complex form (for bolted fault enter 0). Zf = ');
nc = length(linedata(1,:));
  if nc > 4
  BC = linedata(:,5);
  elseif nc ==4, BC = zeros(length(linedata(:,1)), 1);
```

```
  end
  nc1 = length(linedata(:,1));
zline=zeros(nc1,nc1);
for r=1:nc1
    zline(nl(r),nr(r))=R(r)+sqrt(-1)*X(r);
end
ZB = R + j*X;
nbr=length(linedata(:,1)); nbus = max(max(nl), max(nr));
for n=1:nbus
    if n>=34
        Vf(n)=Vm(n);
    end
end
Vf1=Vf;Vf0=Vf;If1=If;
while(100)
    for n = 1:nbus
    if n==nf
        Vf(nf)=If(nf,nf)*(Zf);
    else
    Vf(n) = Vf0(n)*(1- ((Zbus(n,nf))/(Zf + Zbus(nf,nf))));
    Vfm = abs(Vf(n)); angv=angle(Vf(n))*180/pi;
   fprintf('   %4g',  n), fprintf('%13.4f', Vfm),fprintf('%13.4f\n', angv)
    end
end
fprintf('  \n')

fprintf('Line currents for fault at bus No.  %g\n\n', nf)
```

```
fprintf('    From     To    Current    Angle\n')
fprintf('    Bus      Bus   Magnitude  degrees\n')

 for I = 1:nbr
        m=nl(I);l=nr(I);
           if l>=34
           if abs(Vf(l))>=0.9
              Id=Pg(l)/abs(Vf(l));
              Iq=Qg(l)/abs(Vf(l));
              If(m,l)=Id+Iq*sqrt(-1);
           elseif abs(Vf(l))<=0.9|abs(Vf(l))>=0.4
                 Id=Pg(l)/abs(Vf(l));
                 Iq=2*(1-abs(Vf(l)))*1.5;
                 If(m,l)=Id+Iq*sqrt(-1);

           elseif abs(Vf(l))<=0.4
                 Id=0;
                 Iq=2;
                  If(m,l)=Id+Iq*sqrt(-1);
           end
             else, If(m,l)= (Vf(m)-Vf(l))/zline(m,l);
           end
        If(l,m)=If(m,l);
 end
 If(nf,nf)=0;
 for kk=1:nbus
    if  kk==nf
```

```
        If(nf,nf)=If(nf,nf)+0;
    else
        If(nf,nf)=If(nf,nf)+If(nf,kk);
    end
end
  dV=abs(Vf1)-abs(Vf);
  dI=abs(If1)-abs(If);
    errorV=max(abs(dV));
 errorI=max(abs(dI));
  if abs(errorV<=0.00001) & abs(errorI)<=0.00001
     break
 end
 Vf1=Vf;If1=If;
end
Ifm = abs(If(nf,nf)); Ifmang=angle(If(nf,nf))*180/pi;
fprintf('Total fault current = %8.4f per unit \n\n', Ifm)
fprintf('Bus Voltages during fault in per unit \n\n')
fprintf('    Bus     Voltage       Angle\n')
fprintf('    No.     Magnitude     degrees\n')
 for I=1:nbr
     m=nr(I);l=nl(I);
     Ilf(I)=If(m,l);
 End
```

A.5 MATLAB program code of the short circuit current calculation of isolated Microgrid

```
Vf=Vm;
nbus=38;
If=zeros(nbus,nbus);
nl = linedata(:,1); nr = linedata(:,2); R = linedata(:,3);
X = linedata(:,4);
nf = input('Enter Faulted Bus No. -> ');
Zf = input('complex form (for bolted fault enter 0). Zf = ');
nc = length(linedata(1,:));
 if nc > 4
 BC = linedata(:,5);
 elseif nc ==4, BC = zeros(length(linedata(:,1)), 1);
 end
ZB = R + j*X;
nbr=length(linedata(:,1)); nbus = max(max(nl), max(nr));
for n=1:nbus
   if n>=34
      Vf(n)=Vm(n);
   end
end
 Vf1=Vf;Vf0=Vf;If1=If;
while(10000)
for n = 1:nbus
   if n==nf
      Vf(nf)=If(nf,nf)* (Zf)
   else
```

```
    Vf(n) = Vf0(n)*(1- Zbus(n,nf)/(Zf + Zbus(nf,nf)));
    Vfm = abs(Vf(n)); angv=angle(Vf(n))*180/pi;
   fprintf('   %4g',  n), fprintf('%13.4f', Vfm),fprintf('%13.4f\n', angv)
    end
end
 fprintf('  \n')
fprintf('Line currents for fault at bus No.  %g\n\n', nf)
fprintf('     From      To     Current     Angle\n')
fprintf('     Bus       Bus    Magnitude   degrees\n')
for n= 1:nbus
    for I = 1:nbr
        m=nr(I);l=nl(I);
        if l>=34|m>=34
           if l>=34
           if abs(Vf(l))>=0.9
              Id=Pgen(l)/abs(Vf(l));
              Iq=Qgen(l)/abs(Vf(l));
              If(m,l)=Id+Iq*sqrt(-1);
           elseif abs(Vf(l))<=0.9|abs(Vf(l))>=0.4
                 Id=Pgen(l)/abs(Vf(l));
                  Iq=2*(1-abs(Vf(l)))*1.5;
                  If(m,l)=Id+Iq*sqrt(-1);
                  if abs(If(m,l))>2
                     If(m,l)=2*cos(Iq/1.5)+2*sin(Iq/1.5)*sqrt(-1);
                  end
           elseif abs(Vf(l))<=0.4
                  Id=0;
```

```
            Iq=1.5;
            If(m,l)=Id+Iq*sqrt(-1);
        end
        elseif m>=34
        if abs(Vf(m))>=0.9
           Id=Pgen(m)/abs(Vf(m));
           Iq=Qgen(m)/abs(Vf(m));
           If(m,l)=Id+Iq*sqrt(-1);
        elseif abs(Vf(m))<=0.9|abs(Vf(m))>=0.4
             Id=Pgen(m)/abs(Vf(m));
            Iq=2*(1-abs(Vf(m)))*1.5;
            If(m,l)=Id+Iq*sqrt(-1);
            if abs(If(m,l))>2
               If(m,l)=2*cos(Iq/1.5)+2*sin(Iq/1.5)*sqrt(-1);
            end
        elseif abs(Vf(m))<=0.4
            Id=0;
            Iq=1.5;
            If(m,l)=Id+Iq*sqrt(-1);
        end
        end
        If(l,m)=If(m,l);
      end
   end
end
for n= 1:nbus
    for I = 1:nbr
```

```
      if nl(I) == n | nr(I) == n
        if nl(I) ==n       k = nr(I);
        elseif nr(I) == n  k = nl(I);
        end
        if (nl(I)<34 & nr(I)<34)
        If(n,k)= (Vf(n) - Vf(k))/ZB(I)+BC(I)*Vf(n);
           Ilf(I)=If(n,k);
        end
         end
      end
    end

If(nf,nf)=0;
 for kk=1:nbus
     if  kk==nf
        If(nf,nf)=If(nf,nf)+0;
     else
         If(nf,nf)=If(nf,nf)+If(nf,kk);
     end
 end
   dV=abs(Vf1)-abs(Vf);
   dI=abs(If1)-abs(If);
     errorV=max(abs(dV));
  errorI=max(abs(dI));
  if abs(errorV<=0.00001) & abs(errorI)<=0.00001
      break
  end
```

```
  Vf1=Vf;If1=If;
end
Ifm = abs(If(nf,nf)); Ifmang=angle(If(nf,nf))*180/pi;
fprintf('Total fault current = %8.4f per unit \n\n', Ifm)
fprintf('Bus Voltages during fault in per unit \n\n')
fprintf('     Bus     Voltage       Angle\n')
fprintf('     No.     Magnitude     degrees\n')
  for I=1:nbr
      m=nr(I);l=nl(I);
      Ilf(I)=If(m,l);
  End
```

Appendix B. Published Papers

[1] Aref M., Oboskalov V.P., "Steady-State and Dynamic Performance of Large Scale Fixed-Speed Wind Farms Connected to an Electric Grid as Influenced by Grid Strength", IV Russian youth scientific school-conference "ENERGY, ELECTROMECHANICS AND ENERGY EFFICIENT TECHNOLOGIES WITH THE EYES OF YOUTH, 1-3 Nov., 2016, Tomsk, pp. 196-199.

[2] Aref M., Oboskalov V.P., "Modeling And Analysis of Grid Connected PMSG Wind Turbine For Steady State and Transient Behavior of Different Fault Time", IV Russian youth scientific school-conference "ENERGY, ELECTROMECHANICS AND ENERGY EFFICIENT TECHNOLOGIES WITH THE EYES OF YOUTH, 1-3 Nov., 2016, Tomsk, pp. 188-191.

[3] Aref M., Ahmed E., Oboskalov V.P, "Modelling and Simulation MPPT of PV System With Three-phase Three-level Converter", IV Russian youth scientific school-conference "ENERGY, ELECTROMECHANICS AND ENERGY EFFICIENT TECHNOLOGIES WITH THE EYES OF YOUTH, 1-3 Nov., 2016, Tomsk, pp. 191-195.

[4] М. АРЕФ, В. П. ОБОСКАЛОВ. Схема защиты ветряного PMSG генератора, работающего на централизованную электрическую сеть // Эффективное и качественное снабжение и использование электроэнергии 6-я международная н/пр конференция ЭКСИЭ-06, Екатеринбург 2017, с. 246-250.

[5] Mahmoud Aref, Vladislav Oboskalov, Anatolijs Mahnitko and Renata Varfolomejeva, "Protection Design Scheme of Grid Connected PMSG Wind Turbine", in 58th International Scientific Conference on Power and Electrical Engineering of Riga Technical University (RTUCON), Riga, Latvia, 12-13 Oct. 2017, pp. 1-6.

[6] Ареф М., Удинцев В.Н. и Обоскалов В.П, “Цифровое управление трехфазным трехуровневым инвертором для солнечных батарей”, журнал Промэнергетика, с.50-58.

[7] Mahmoud Aref, Amir Abdelmeneam, Vladislav Oboskalov and Anatolijs Mahnitko, "Transient analysis of AC and DC microgrid with effective of SFCL", in 59th International Scientific Conference on Power and Electrical Engineering of Riga Technical University (RTUCON), Riga, 12-13 Nov. 2018, Riga, Latvia, Latvia, pp. 1-6.

[8] Mahmoud Aref, Ismaiel Ahmed, Vladislav Oboskalov, and Anatolijs Mahnitko, "Microcontroller Look-up Table of Digital Control MPPT of PV System", in 59th International Scientific Conference on Power and Electrical Engineering of Riga Technical University (RTUCON), Riga, 12-13 Nov. 2018, Riga, Latvia, pp. 1-5.